STAFF Spectrum Analyser

Conversion of the Science Data to Physical Units

C.C. Harvey, M. Belkacemi,
R. Manning, F. Wouters, Y. de Conchy

Bars indicate changes since Issue 5, Rev. 6, dated June 26, 1998

Contents

List of Figures

List of Tables

Document Status Sheet			
1. Document Title: **STAFF-SA Science Data**			
2. Document Reference Number: **OBSPM–TN–0001**			
3. Issue	4. Revision	5. Date	6. Reason for Change
0	4	May 30, 1994	Document brought under control
1	0	October 20, 1994	Section 2.1, conversion to physical units Section 2.1, calibration of AGC Section 2.1, correction d'une erreur de frappe Section 4.1, correction of eq. 11 Section 6, first half-page completely rewritten Table 3, minor corrections to entries for $B(f_n)$, $G_i^m(f, A)$, and $P_i^m(f_n)$ Section 7.1.2, minor typographic corrections Section 8.3.2 major clarification, with reference to the new Appendix 2
2	0	November 4, 1994	Separation of calibration issues to document OBSPM–TN–0005 Section 1, new section Section 1.1, additional explanation Section 2.1, new definition of $Q_i^m(A_i^m)$ Section 5.1, new definitions of N_{ij}^n and R^n Section 5.1.1, new section Section 6, eq. 34 modified Section 6, eq. **??** disappeared with Version 4 (see note at beginning of Section 6) Table (now 3 and 4, updated Appendix 1 is new
2	0	December 2, 1994	Sect. 2.1, clarifications Eqs. 11 and 13 are new Typos corrected in eqs. 28 and 29 Tables 3 and 4, new column with units
2	3	February 2, 1995	$R^n \rightarrow H^n$ throughout $A_i^{mn} \rightarrow R_i^{mn}$ throughout α_B and α_E added to eqs. 10
2	4	March 22, 1995	Eq. 32 added for completeness New section 6.3 Corrections to units of G, H and R in Table 3

Document Status Sheet			
1. Document Title: **STAFF-SA Science Data**			
2. Document Reference Number: **OBSPM–TN–0001**			
3. Issue	4. Revision	5. Date	6. Reason for Change
3	0	May 30, 1995	New section (4.2) concerning coordinate systems Section 9.2, new discussion of spin phase Section 10, two new computational steps Appendix 2, clearer definition of ϕ
3	1	June 7, 1995	Introduction of eqs. 23
3	2	July 20, 1995	Complete revision of Appendix 2
4	0	November 6, 1995	Revised Appendix 2 used to update entire document **without use of change bars**. Completely rewritten chap. 6 including sect. 41, new sect. 9.3, substantially modified sects. 4.4, 9.2, and 10, simplified sect. 2.3.
4	1	November 13, 1995	Subscripts m and n replaced by k and ℓ Appendix D, discussion of separation of variables.
4	2	February 15, 1996	Clearer definition of ϵ_i (eq. 27) Inclusion of Δ_{1i} in eq. 26 New section 7.2 Explicit equations for Δ_{ij} in Appendix B Exact solution moved to Appendix C
4	3	March 3, 1996	Numerous corrections to equations Appendix B
4	4	April 17, 1996	New sections 7.2, 9.2.1 and 9.4 Improvements to Fig. 1 Eq. 6 added for clarification Minor corrections sect. 3.1, including eq. 17 Much new material in Sect. 7.1, including Table 5 and Fig. 6 Correction of eq. 57 Proof of convergence added to sect. 9.3 Corresponding corrections to Chap. 10
4	5	May 1, 1996	New section 9.5 and corresponding modification of Chap. 10 New section heading 6.1.1

Document Status Sheet			
1. Document Title: **STAFF-SA Science Data**			
2. Document Reference Number: **OBSPM–TN–0001**			
3. Issue	4. Revision	5. Date	6. Reason for Change
5	0	May 27, 1996	Discussion of e-mode logical instruments in sect. 9.5.2 New sect. 9.5.4 Correction to sect. 8: co-ordinate system when despin OFF
5	1	7 February 1997	First version produced under UNIX Corrections to eqs. **??** (removed at Version 5.4), 64 and 71
5	2	January 4 1998	Corrections to several internal and external cross-references Modifications to sect. 9.3 New sect. 9.3.1
5	3	January 25, 1998	Corrections to internal cross-references Unnumbered equation before eq. 63 corrected as was eq. 64 in revision 5.1 New test for despin OFF in Section 10, and corresponding new procedure *still to come* Explanation in Section 6.3 of why $S_p^m(A_p^m)$ is complex
5	4	11 February 1998	Document upgraded to LaTeX 2 Sections 7.1 and 7.2 placed in new Section 7 Despin "OFF promoted to new Section 8 Generalisation of Section 8 to $\phi_c \neq 0$
5	5	14 June 1998	Introduction, new paragraph near start Section 4.2, cross-ref. to CWD-OBSPM-DD-002 Appendix A.2, references to eq. 26 Correction to eq. 47 (ϕ replaced by ϕ_c) Insertion of (incomplete) eq. 50 Linearity of eq. 50 noted when $\phi_c = 0$ Last paragraph of Section 8 modified Complete modification of Section 9.3.1 Corrections to eq. 91 et seq. to end of section Attempt to improve Fig. 3
5	6	26 June 1998	In Section 9.3.1 changes to eqs. 59 and 60 and the test for convergence

Document Status Sheet			
1. Document Title: **STAFF-SA Science Data**			
2. Document Reference Number: **OBSPM–TN–0001**			
3. Issue	4. Revision	5. Date	6. Reason for Change
6	0	August 8, 1998	Modification to calibration model to take account of what was thought to be "Receiver noise due to strapped spin-plane AGCs"
6	1	January 24, 1999	Accumulated corrections
7	0	March 19	Abandon of "Receiver noise due to strapped spin-plane AGCs" which turned out to be cross-talk. All other modifications in Version 6 are carried forward, as follows : Factor of 1.024 introduced into eq. 1 New caption for Table 1 Explanation of last column of Table 1 in Section 3 New Section 4.6 Table 3 split into Tables 3 and 4 Reorganisation of Chapter 6.1.1 Section 9.3.1, "*The treatment of sub-matrices*" re-organised in accordance with Fig. 6 Other minor improvements to text
7	1	April 13, 1999	Revision of cross-references to notes TN–0005 and TN 0006 Table 7: corrections to Column 5, "Determined"
7	2	July 5, 2000	Sect. 3, first paragraph: last sentence added Sect. 5.1.1, last sentence: reference changed Sect. 9.3.1: clarification of text. Suggested modifications are hidden in the LaTeX, awaiting validation Correction to eq. 64 (this equation was modified for Issue 5 Rev 1, but the wrong pair of indices where exchanged) New Section 12
7	3	November 19, 2000	Sect. 3, paragraph 2, note on flash converter timing
7	4	November 13, 2001	New Sect. 2.2 to explain spin-plane AGC New Sect. 4.1 concerning factor $\sqrt{2}$

Document Status Sheet			
1. Document Title: **STAFF-SA Science Data**			
2. Document Reference Number: **OBSPM–TN–0001**			
3. Issue	4. Revision	5. Date	6. Reason for Change
6	5	February 3, 2004	Section 4 largely rewritten for clarification
			Section 4.2, clarifications to last two paragraphs
			New Section 4.3
			New Figure 4
			Appendix A, multiple clarifications connected to Section 4
		March 24, 2004	

1 Introduction

This document describes the STAFF Spectrum Analyser hardware and the calibration model used to convert the data from the telemetry to physical units.

This document started life as a description of the calibration model. But as this cannot be described without a description of the experiment, the latter was added as and when required. Three and a half years and six issues after the first release, it is evident that the present document would be much easier to read if it were to be completely rewritten, and split into two: the instrument description, and the calibration model. [5]

The activity associated with the calibration of the data falls into four parts:

1. **The calibration model.** The calibration model is a combination of mathematical algorithms and tables of coefficients used by those algorithms. [7]

2. **Routine Processing.** The application of the routine calibration procedure to the data. This must be performed every time data is processed for physical use. It will be performed at all WEC sites (including CTM and JSOC).

3. **Update of Calibration Coefficients.** The coefficients used for the routine processing may change with time during the life of the mission, and so must be updated periodically. These updates must be implemented at all sites operating the WEC software.

4. **Determination of the Calibration Coefficients** used by the calibration procedure. The initial set of coefficients will be derived from measurements performed in the laboratory before launch. Subsequently, these coefficients will be verified periodically using the experiment internal calibration cycle, which will be performed regularly throughout the mission. Whenever any significant change is detected an updated set of calibration coefficients will be issued.

The present document treats the first two of the above four chapters. It describes the instrument, the calibration model, and the application of the calibration coefficients to the data. A separate document, ref. OBSPM–TN–0005, describes the procedures to determine and update of the calibration coefficients.

There are numerous cross-references between these two documents, both of which are susceptible to frequent revision. Accordingly, Appendix A of each document provides a table of cross-references between the documents. In this document, all references such as to section (5a) or equation (5x) refer to ref. OBSPM–TN–0005 refer to Appendix A of this paper. By cross-reference to Appendix A of the companion paper OBSPM–TN–0005, it is possible to locate the desired equation, figure, section or chapter. The Appendix A of each paper is derived using the same LaTeX file, but handling it differently, in the two papers. Thus it is possible to manage inter-paper cross-references in an automatic and coherent manner. [18]

1.1 Instrument Description

The STAFF Spectrum Analyser has five input channels, which are connected to five different sensors. It makes estimations of the cross-spectral power density at 27 frequencies, arranged in three bands which are conventionally denoted A, B and C. We denote

$$\begin{array}{llll} \text{the} & 5 & \text{input signals by} & x_i \quad \text{for} \quad 1 \le i \le 5, \quad \text{and} \\ \text{the} & 27 & \text{output frequencies by} & f_{mn} \quad \text{for} \quad 1 \le m \le 3, \quad 0 \le n \le 8 \end{array}$$

Thus there are $5 \times 5 \times 3 \times 9 = 675$ different output channels representing

$$< \overline{x}_i \overline{x}_j^*(f_{mn}) > .$$

This is 5×5 Hermitian (*i.e.*, 5 real diagonal elements, 10 complex off-diagonal ones) cross-spectral power density matrix of the fluctuations in the ambient medium, at frequency f_{mn} ; such matrices are calculated at each of 27 frequencies f_{mn}. The instrument generally telemeters the diagonal ($i = j$) elements of the matrix more rapidly than the off-diagonal ($i \neq j$) elements.

The centre frequencies of the 27 output channels are distributed logarithmically, and each channel has a passband proportional to its centre frequency.

The separation into bands A, B and C is performed by the analogue part of the receiver. Inside each band m further separation into 9 narrower frequency bands is performed by the digital part of the receiver; for this, the same numerical algorithm is executed in band m at a speed proportional to 2^{3m}. The precise centre frequencies are given by the expression, (*Label* **fdef**)

$$f_{mn} = \frac{1000}{1024} \times 2^{3m} \times 2^{(2n+1)/6} \; ; \tag{1}$$

[3] the 27 frequencies are shown in Table 1. The last column indicates the number of waveform samples used to calculate each elementary cross-spectral matrix.

The receivers of bands A, B and C each have their own automatic gain control (AGC). The AGC control voltage in telemetered to the ground; this gives an estimate of the root mean square electric field in the frequency band determined by the pre-converter (analogue to digital) filters. These bands are indicated in the last line of Table 1. For reasons of phase stability, the analogue passband is much wider than the band analysed by the digital filter; therefore, there is considerable frequency overlap. [6]

The calibration model of the STAFF Spectrum Analyser is rather complicated. All data is integrated over a significant part of one satellite spin period; therefore the data is de-spun before being analysed digitally. The de-spin is digital, being performed after the analogue/digital conversion of the signal, and consequently after the analogue receivers. Thus, even the diagonal elements of the cross-spectral matrix (the power spectra) of the spin plane components are derived using data from two different analogue receivers (because the receivers measuring B_y and B_z at one instant will be measuring respectively B_z and $-B_y$ one quarter of a spin later). The off-diagonal elements of the cross-spectral matrices depend upon signals from two directions in inertial space, which are correlated against each other. When one of the signals used for this correlation is along the spin axis (B_x is the only axial component), the final output depends upon data from three analogue receivers (one axial and two spin-plane). Otherwise, the output depends upon data from either two (electric/electric or magnetic/magnetic) or four (two electric and two magnetic) analogue receivers. [10]

Such complexity calls for careful calibration methodology. Calibration falls into two distinct parts: calibration of the analogue receivers, and calibration of the digital receiver. The interface between the two is the analogue to digital converter.

(*Label* **Table1**)

Figure 2 is a schematic representation of the STAFF-SA instrument. The figure shows the principal components of the instrument, the symbols used to denote the quantities of physical interest passing from one component to the next, and the relationship between these different quantities. This diagram will be explained in detail in the following sections. The significance of the different symbols is summarised in Tables 3 and 4.

The calibration procedure concerns the overall spectrum analyser. The analogue contribution contains a greater number of parameters, which may be expected to require updates during the course of the mission. The digital part contains fewer parameters, and is stable over the lifetime of the mission.

The analogue transfer functions also convert to physical units; the RMS input signals measured within each of the the pre-converter passbands (band A, B or C) are returned respectively in nT and V/m for the magnetic and electric sensors. After spectral analysis, the units of the

Band	A	B	C	Number
Range	8 – 64	64 – 512	512 – 4096	of
	$m = 1$	$m = 2$	$m = 3$	samples
n=0	8.7692	70.1539	561.2310	240
1	11.0485	88.3883	707.1068	192
2	13.9203	111.3623	890.8987	154
3	17.5385	140.3078	1122.4620	122
4	22.0971	176.7767	1414.2136	98
5	27.8406	222.7247	1781.7974	78
6	35.0769	280.6155	2244.9241	62
7	44.1942	353.5534	2828.4271	50
8	55.6812	445.4494	3563.5949	40
$f_{\rm sampling}$	250.0000	2000.0000	16000.0000	n/a

Table 1: The Central Frequencies (in Hz) of the 27 Passbands. The last line indicates the sampling frequency, and the last column indicates the number of data samples (out of the 240) in each window used to calculate the spectral estimates (see Section 3).

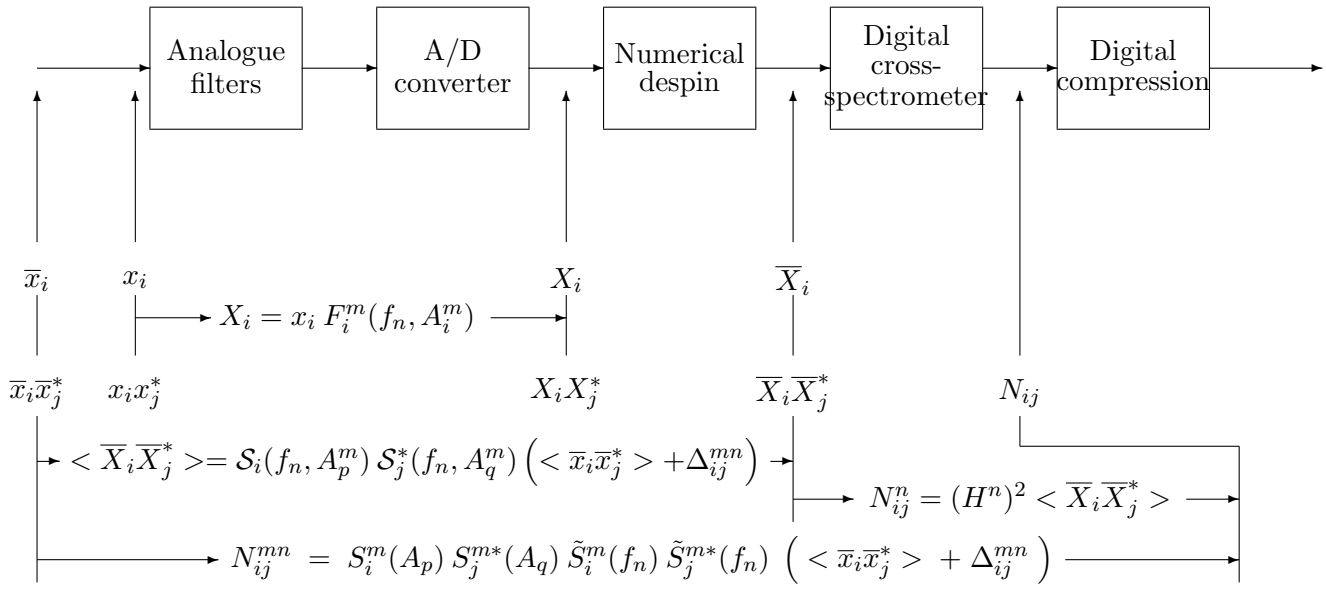

Figure 1: Schematic Representation of the Spectrum Analyser showing Signals and their Relationships. In these equations p and q are defined by eq. 36, and there is summation over neither i, j nor p, q.

spectral estimates are $\mathrm{nT}^2\,\mathrm{Hz}^{-1}$, $(\mathrm{V/m})^2\,\mathrm{Hz}^{-1}$ or $\mathrm{nT}\,(\mathrm{V/m})\,\mathrm{Hz}^{-1}$ respectively for the magnetic, and electric and cross spectra. [2] Note that the experiment actually measures the electric potential difference between the two spheres of the double sphere electric dipole antenna. To determine the electric field strength in V/m requires knowledge of the effective electrical length of the antenna. For the purpose of calculation, this is assumed to be equal to the geometrical distance between the two antennas. It must be remembered that this is an assumption which may be seriously wrong, especially near characteristic frequencies of the ambient medium. [10]

1.2 The Analytic Signal

For the STAFF-SA instrument, we are concerned by both the magnitude and also the phase of the instrument response. Therefore, instead of using the gain expressed in deciBels, we will use the transfer function of the analogue receivers, which is the ratio, in general complex, of the output (to the A/D converter) with respect to the input signal, (*Label* **defF**)

$$F(f) = \frac{\text{output signal}}{\text{input signal}} \tag{2}$$

where "signal" implies the analytic signal (D. Gabor, *Jour. Inst. Electr. Engrs.*, **93**, 429, 1946), defined by (*Label* **AS**)

$$X(t) = 2\int_0^\infty \tilde{x}(f)e^{2\pi i f t}df. \tag{3}$$

where $\tilde{x}(f) = \int_{-\infty}^{\infty} x(t)e^{-2\pi i f t}dt$ is the Fourier transform of the true signal $x(t)$. When $x(t)$ is real, there is a simple relationship between $x(t)$ and $X(t)$ (see, for example, Born M. and E. Wolf, Principles of Optics, Pergamon, 1964, Chapter 10, section 10.2): [2]

$$x(t) = \mathcal{R}e\{X(t)\} \quad \text{and} \quad X(t) = x(t) + \frac{i}{\pi}\int_{-\infty}^{\infty} \frac{x(t')}{t'-t}dt'. \tag{4}$$

This well-known definition is repeated here because most of the STAFF-SA transfer functions are complex, and it is important to be clear about the sense of the corresponding phase changes. In particular, from eq. 2, if the argument of F lies in the range

$$0 < \tan^{-1}\left(\frac{\mathcal{I}m\{F\}}{\mathcal{R}e\{F\}}\right) < \pi\ ,$$

then the phase of the output signal leads (is in advance with respect to) the phase of the input signal. The gain G in dB can always be obtained from the analogue transfer function,

$$G = 10\log_{10}(FF^*)\ ; \tag{5}$$

but the converse is not true, because G contains no phase information.

2 The Analogue Receivers

The analogue circuit is represented schematically in Fig. 3; there are 15 analogue receivers. Calibration involves, for each of these 15 receivers, the determination of its transfer function as a function of frequency and the telemetered AGC output. The analogue receiver transfer function has very little variation within its useful passband and the variation of the relative calibration with frequency is not expected to change significantly during the mission. The calibration of the magnitude of transfer functions all receivers within each band is verified during each in-flight calibration cycle.

Across the interface between the analogue and the digital parts of the STAFF Spectrum Analyser there pass 15 analogue waveform signals and 9 analogue AGC signals. The waveform outputs each come from a separate dedicated receiver, and so each receiver can be identified by the waveform signal X_i^m which it produces. Here m denotes one of 3 possible bands (A, B or C), and i denotes the field component which it measures, from the 5 possibilities

$$B_x,\ B_y,\ B_z,\ E_y \text{ or } E_z\ .$$

The AGCs of the spin-plane electric and magnetic components (E_y and E_z. B_y and B_z) are tied together, so that the corresponding waveform inputs may be despun digitally without having to allow for different gains of the corresponding y and z analogue channels. Therefore there are only 9 AGC outputs,

$$A^1_{Bx},\ A^2_{Bx},\ A^3_{Bx},\ A^1_{Bs},\ A^2_{Bs},\ A^3_{Bs},\ A^1_{Es},\ A^2_{Es},\ A^3_{Es}$$

Each analogue waveform output is sampled at approximately four times the highest frequency analysed digitally (twice the Nyquist frequency), as described in Section 3. [2]

2.1 The Analogue Transfer Functions

(*Label* **ATF**)

The analogue transfer function F includes all effects of the analogue receivers; it is convenient to let it include also the (small) phase factor a defined by eq. 17 below, to account for the effect of non-simultaneous sampling of the outputs of the different analogue receivers.

As there are 15 analogue receivers per instrument, we have 15 transfer functions per instrument. (Furthermore, there are 6 instruments: 1 engineering model, 4 flight models, and 1 spare.) We will denote the transfer function of the receiver producing the X_i^m output by $F_i^m(f, A)$; thus the analytic signal X_i at the output from analogue receiver i of band m is related to the signal x_i at the input by (*Label* **ATF1**)

$$X_i = x_i\, F_i^m(f, A)[3]\ ; \tag{6}$$

The $F_i^m(f, A)$ [4]are functions of frequency f and of the corresponding AGC output A. For the x-components the transfer functions are thus (*Label* **ATF2**)

$$F^m_{Bx}(f, A^m_{Bx}),\ \text{ for } m = A, B \text{ or } C, \tag{7}$$

while for the spin-plane components they are (*Label* **ATF3**)

$$F^m_{By}(f, A^m_{Bs}),\ \ F^m_{Bz}(f, A^m_{Bs}),\ \ F^m_{Ey}(f, A^m_{Es}),\ \ F^m_{Ez}(f, A^m_{Es}),\ \text{ for } m = A, B \text{ or } C. \tag{8}$$

Note that these functions F_i^m are all complex, that is, they include the correction for the amplitude *and the phase* of the analogue receiver. The functions $F_i^m(f, A_i^m)$ need to be evaluated at only the nine frequencies (per band) f^n defined by the central frequencies of the channels of the digital spectrum analyser (see chapter 5). [2]

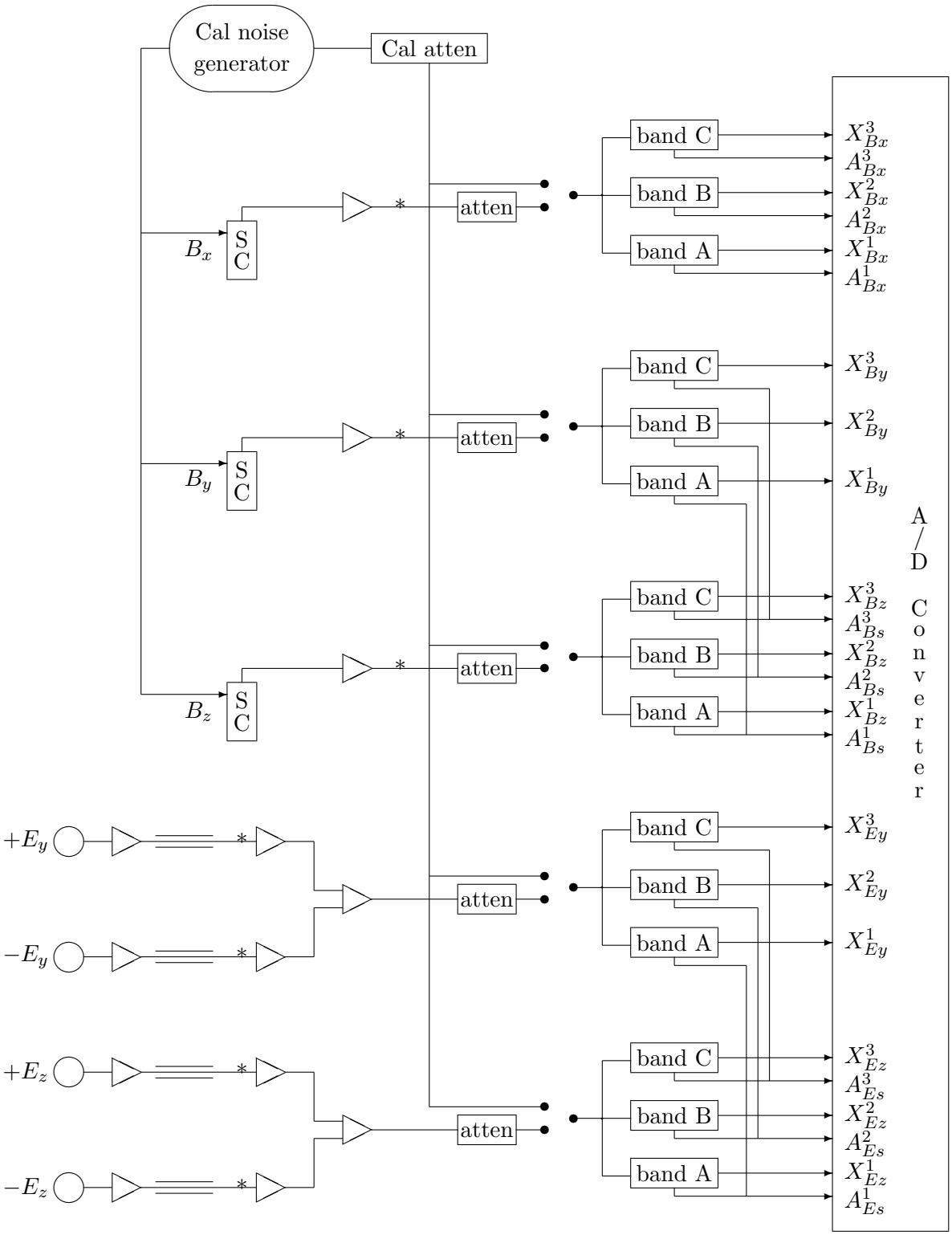

* Points at which laboratory calibration signals are injected

Figure 2: The Analogue Part of the Receiver

2.2 The Spin-Plane AGC

[3]

The digital cross-spectrum analyser requires that

- the AGC does not vary rapidly compared to the integration time,

and the numerical despin algorithm requires that

- the AGCs of y and z receivers be the same.

Therefore the magnetic and electric pairs spin-plane receivers have

- their AGCs strapped together so as to use a common control potential, and
- this common AGC potential is determined independently of spacecraft spin phase.

This is achieved by using the total spin-plane power $|B_{yy}|^2 + |B_{zz}|^2$, which is independent of the orientation of the antennas about the x-axis. Besides enabling numerical despin to be performed, the strapping together of the spin-plane AGCs in this way allows the calibration model to be simplified by use of eqs. 23 and 24, [2] so as to treat the difference between the y and z-receivers as a small parameter. This is further developed in Chapter 6.

Laboratory experiments and in-flight measurements (see Section 4.1 and e-mail dated 2001/09/28) have shown that the spin-plane AGC value B_s is determined by the total spin-plane power in the receiver passband, not the mean power (which could alternatively have been used). Thus when signals with identical spectra are applied to the three magnetic input channels, the spin-plane AGC potential corresponds to a greater attenuation than does the axial AGC ; hence the waveform signal applied to the A/D converter is approximately 3 dB greater for B_x than for the two spin-plane components. Use of $\frac{1}{2}(|B_{yy}|^2 + |B_{zz}|^2)$ to determine the spin-plane AGC level would have avoided this difference, and its associated differences of digital saturation level and digitisation noise.

Note that all the $F_i^m(f, A)$ are single-valued functions of the corresponding AGC level A. On the other hand, the spin-plane AGC value A_{Bs}^m depends upon the two inputs x_{By}^m and x_{Bz}^m (and similarly for A_{Bs}^m); therefore the integrated power of the separate input signals x_{By}^m and x_{Bz}^m are NOT single-valued functions of A_{Bs}^m; nevertheless, the ratio of the output waveform to the input waveform is a single-valued function of A for all 15 analogue receivers, that is, **all** the functions $F_i^m(f, A)$ (eq. 2) are single-valued functions of the corresponding A. [6]

2.3 Separation of Variables for the Axial Component, B_x

We treat the spin-plane components in a way which is physically equivalent (*i.e.*, the physical approximation is of the same nature) but chosen so as to simplify the effects introduced by the despin algorithm. Therefore the separation of the variables of the spin plane transfer functions is postponed until Section 6.1.1. [4]

It is convenient to assume that the frequency-dependent and the AGC-dependent variations of the analogue transfer function can be separated; that is, $F_i^m(f^n, A_i^m)s$ can be written in the form (*Label* **FPQ**)

$$F_i^m(f^n, A_i^m) = P_i^m(f^n) \times Q_i^m(A_i^m), [2] \tag{9}$$

where the $i \times m \times n = 5 \times 3 \times 9 = 135$ complex coefficients $P_i^m(f^n)$ represent the relative amplitudes and the phase shifts for the 9 values of f^n of channel i and band n, [2] and the $i \times m = 5 \times 3 = 15$ complex functions Q_i^m represent the variation of the receiver amplitudes and phase shifts with AGC output.

When $F_i^m(f^n, A_i^m)$ is written in the form of eq. 9, $P_i^m(f^n)$ and $Q_i^1(A_i^m)$ are not uniquely defined; we can multiply Q by some arbitrary factor, while dividing P by the same factor. This allows a useful physical meaning to be attached to $Q_i^m(A_i^m)$; we define the function Q_i^m to be the calibration function relating the AGC signal to the axial or gyrotropic spin-plane root mean square noise (in nT or V/m) in the band of frequencies defined by the analogue filters (*i.e.*, the

low-pass anti-Nyquist filter and the high-pass anti-saturation filter). The bands are indicated in the last line of Table 1. In this way the tables $Q_i^m(A_i^m)$ constitute the calibration tables for the AGC outputs; these will be used for estimating the quality of the scientific output. [6] [8]

More precisely, $Q_{Bx}^m(A_{Bx}^m)$ is defined so that when white noise of spectral density ρ_m (in $\mathrm{nT^2\,Hz^{-1}}$) in band m is applied [2] to the B_x sensor, [2] (*Label* **defQ1**)

$$\rho_m = |Q_{Bx}^m(A_{Bx}^m)|^{-2} \text{ .[3][3]} \tag{10}$$

The AGCs A_{Bx}^m are measured in telemetry units, $0 \leq A_{Bx}^m \leq 255$. In general the Q_{Bx}^m are complex, but we specify that, for some reference value A_{ref} of the AGC outputs A_{Bx}^m (*Label* **defQ2**)

$$Q_{Bx}^m(A_{\mathrm{ref}}) \text{ is real and positive} \tag{11}$$

A_{ref} is chosen to be neither close to receiver saturation nor close to the noise level; the optimum choice of A_{ref} is discussed in paper TN–0005. [7] Eqs. 10 and 11 uniquely define all 3 functions Q_{Bx}^m for the AGC level A_{ref}. The seemingly "inverse" definition of eq. 10 is a consequence of eqs. 2 and 9; it would have been possible to write $F = P \div Q$ instead of $F = P \times Q$ in eq. 9.

The separation of eq. 9 is a mathematical artefact, to which we try to attach physical meaning: the conversion to physical units is assured by Q_{Bx}^m , while P_{Bx}^{mn} is a multiplicative factor which takes into account the amplitude and phase variation of analogue receiver m, i across its passband. [11]

2.4 Definition of the $P_{Bx}^m(f^n)$ Functions

Having defined the 3 $Q_{Bx}^m(A_{\mathrm{ref}})$ (*i.e.*, for the particular value $A = A_{\mathrm{ref}}$), the 3 (complex) functions $P_{Bx}^m(f^n)$ are then uniquely defined by eq. 9. For each of the 3 receivers and each of the 9 frequencies f^n, $(0 \leq n \leq 8)$, $F_{Bx}^m(f^n, A_{Bx}^m)$ is the complex transfer function defined by eq. 2; thus (*Label* **defP**)

$$P_{Bx}^m(f^n) = \frac{F_{Bx}^m(f^n, A_{\mathrm{ref}})}{Q_{Bx}^m(A_{\mathrm{ref}})} = \frac{X_{Bx}(f^n)}{x_{Bx}(f^n)} \times \sqrt{\rho}_m \text{ for AGC output } A_{\mathrm{ref}} \text{ .} \tag{12}$$

The units of P are the inverse of those of Q. [27] Since $|x_{Bx}|^2 = \rho_m$, if it were not for the phase information included in the definition of $P_{Bx}^m(f^n)$, eq. 12 would be much more simple, namely (*Label* **defmP**)

$$|P_{Bx}^m(f^n)| = \text{value of } |X_{Bx}(f^n)| \text{ for AGC output } A_{\mathrm{ref}} \text{ .[4]} \tag{13}$$

In reality, the calibration coefficients $P_{Bx}^m(f^n)$ are determined simultaneously with the digital calibration coefficients H^n (introduced in section 5.1), in the form of the function $\tilde{S}_{Bx}$ (see eq. 36). The determination of the entire set of calibration coefficients is described at length in the document TN–0005. [3] [3]

2.5 Definition of the Q_{Bx}^m Functions

Finally, by varying the input noise level ρ, it is possible to determine the variation of the 3 functions $Q_{Bx}^m(A_{Bx}^m)$ in terms of the 3 AGC values A_{Bx}^m, using eqs. 9 and 12; [2] thus

$$Q_{Bx}^m(A_{Bx}^m) = \frac{F_{Bx}^m(f^n, A_{Bx}^m)}{P_{Bx}^{mn}} = \frac{F_{Bx}^m(f^n, A_{Bx}^m)}{F_{Bx}^m(f^n, A_{\mathrm{ref}})}\, Q_{Bx}^m(A_{\mathrm{ref}}) \tag{14}$$

$$= \frac{\text{phase factor for AGC } A_{Bx}^m}{\text{phase factor for AGC } A_{\mathrm{ref}}} \times \frac{|F_{Bx}^m(f^n, A_{Bx}^m)|}{|F_{Bx}^m(f^n, A_{\mathrm{ref}})|} \times Q_{Bx}^m(A_{\mathrm{ref}}) \tag{15}$$

where "phase factor" is $F/|F| = e^{i\,\text{phase}-\text{shift}}$ of the transfer function of receiver i of band m. [4]

For the axial component B_x, from eqs. 10 and 14

$$\sqrt{\rho}_m = \frac{|F^m_{Bx}(f^n, A_{\text{ref}})|}{|F^m_{Bx}(f^n, A^m_{Bx})|}\,\frac{1}{Q^m_{Bx}(A_{\text{ref}})}$$

so that eq. 15 yields [3] (*Label* **defQ5**)

$$Q^m_{Bx}(A^m_{Bx}) = \frac{\text{phase factor for AGC } A^m_{Bx}}{\text{phase factor for AGC } A_{\text{ref}}} \times \frac{1}{\sqrt{\rho}_m \text{ for AGC output } A^m_{Bx}}\ . \tag{16}$$

2.5.1 The phase of the Q^m_{Bx} functions

The functions Q^m_{Bx} may not need to be complex, the receiver phase may be found not to change significantly with AGC level; that is, the functions $Q^m_{Bx}(A^m_{Bx})$, defined to be real [10] for $A^m_{Bx} = A_{\text{ref}}$, may for all practical purposes be considered real for all values of A^m_{Bx}. Although this still *November 1994* [2] seems to be the case, it may be better to design the system to allow for complex $Q^m_{Bx}(A^m_{Bx})$.

However, we may note that the absolute variation of phase with AGC level cannot be verified by the in-flight calibration procedure. Although this procedure does vary the input signal level, it does so simultaneously for all input channels. Thus the relative phases between the channels are checked at different signal levels, but any variation of phase with AGC level which affects all channels in the same way will not be calibrated in-flight. [5]

So, if laboratory measurements show that $Q^m_{Bx}(A^m_{Bx})$ can be taken as real, there is no need to forsee complex values; once launched, no change of the imaginary part of $Q^m_{Bx}(A^m_{Bx})$ can be detected via the calibration data. [3]

2.6 Discussion

In section 6.1.1 we will also separate (eq. 35) the variables for linear combinations (defined by eqs. 23 and 23) of the spin-plane transfer fucntions. These separations perfromed later are similar in principle to that performed for the axial components in section 2.3.

This separation of variables has several advantages:

- If the calibration information is provided in tabular form, the total number of calibration coefficients (required for the analogue receiver calibration) is $15 \times (9 + 256) = 3975$ (complex) words, instead of the $15 \times 9 \times 256 = 34560$ (complex) words which would be required without any separation of variables.

- The coefficients P^{mn}_{Bx} are relatively stable in time; nevertheless, they are verified by the in-flight calibration procedure (see section ref. 1009 of Appendix 1).

- The coefficients P^{mn}_{Bx} can be combined with similar coefficients defined for the digital part of the calibration procedure (see eq. 36).

- The separation of variables can be done in such a way as to obtain a simple expression to estimate the spectral density in physical units using only the AGC data. [2]

3 The Analogue to Digital Converter

(*Label* **ADC**)

A single analogue to digital "flash" converter is employed. This samples the various analogue channels cyclically, according to a sequence piloted by the microprocessor of the digital analyser. The converter samples the signal in the range $0-5.12\,\mathrm{V}$ and converts it to an 8-bit digital output whose 256 steps each represent an increment of 20 mV.

A diagram of the digital part of the receiver is shown in Fig. 5. The timing of the sampling is controlled by interrupts from the processor, which occur at a frequency of 16 kHz (see Ref. 1). The flash converter works rapidly enough to be able to make several samples between two interrupts. The sampling sequence can be summarised by

$$(W^C \text{ times } 8 \text{ then } W^B) \text{ times } 8 \text{ then } W^A \ ,$$

where W^m represents the sequential sampling of the 5 waveform outputs from the analogue receivers of band A, B or C,

$$W^m = W^m_{Bx},\ W^m_{By},\ W^m_{Bz},\ W^m_{Ey},\ W^m_{Ez} \ .$$

This sampling of the 5 inputs is repeated 8 times, then the 5 outputs from receivers of band B are sampled once each, in the same order. This whole procedure is then repeated 8 times, and then the analogue outputs from the receivers A are sampled, once each. And so on. Note that the flash converter operates fast enough ($\simeq 1.5\ \mu$s) for the 5 (Band C) + 5 (Band B) + 5 (Band A) = 15 samples to be obtained in $15 \times 1.5 = 22.5\ \mu$s, which is well within the interval $1/16000 = 62.5\ \mu$s at which the band C waveform is sampled ; the band C waveform data samples are uniformly spaced, despite the cyclically varying load on the flash converter. [4]

The sampling of the AGC outputs is interleaved with the sampling of the waveform signal. In each band, 240 waveform samples are required to compute one elementary spectrogram in the lowest frequency channel. Fewer samples are required at the other frequencies, as indicated in the last column of Table 1. [2] After each acquisition of 240 samples in band C (*i.e.*, after the acquisition of 240 ($\times 5$) band C data samples), the 3 band C AGCs are sampled. Similarly, after acquisition of 240 band B waveform samples, the three band B AGCs are sampled. And the same for the AGCs of the band A.

The different waveform signals are sampled at respectively 16 kHz, 2 kHz and 250 Hz in bands C, B and A. Therefore, the 240 waveform samples in each of 5 channels, and the corresponding 3 AGC samples are obtained in

15 ms for band C,
120 ms for band B,
960 ms for band A.

The STAFF Spectrum Analyser data acquisition interval in normal mode is 1 s for the auto-spectra, and 4 s for the cross-spectra. Therefore, the data must be de-spun to an inertial co-ordinate system before integration. De-spin is effected numerically. Tables of *cosine* and *sine* coefficients are obtained by dividing the full 360° of rotation into 256 sectors of 1.41° each. The waveform data acquired in bands A and B are de-spun immediately after A/D conversion. For band C, during the 15 ms required to acquire the 240 data samples for one elementary cross-spectral matrix, the satellite has rotated through only 1.35°, which is below the precision of the de-spin algorithm; therefore the cross-spectral matrix is computed using the raw data, and the resulting elementary cross-spectral matrix is de-spun before being transferred to the accumulator, as shown in Figure 5.

The elementary cross-spectral matrices in the inertial co-ordinate system are accumulated during the required integration time. The AGCs are accumulated over the same time interval.

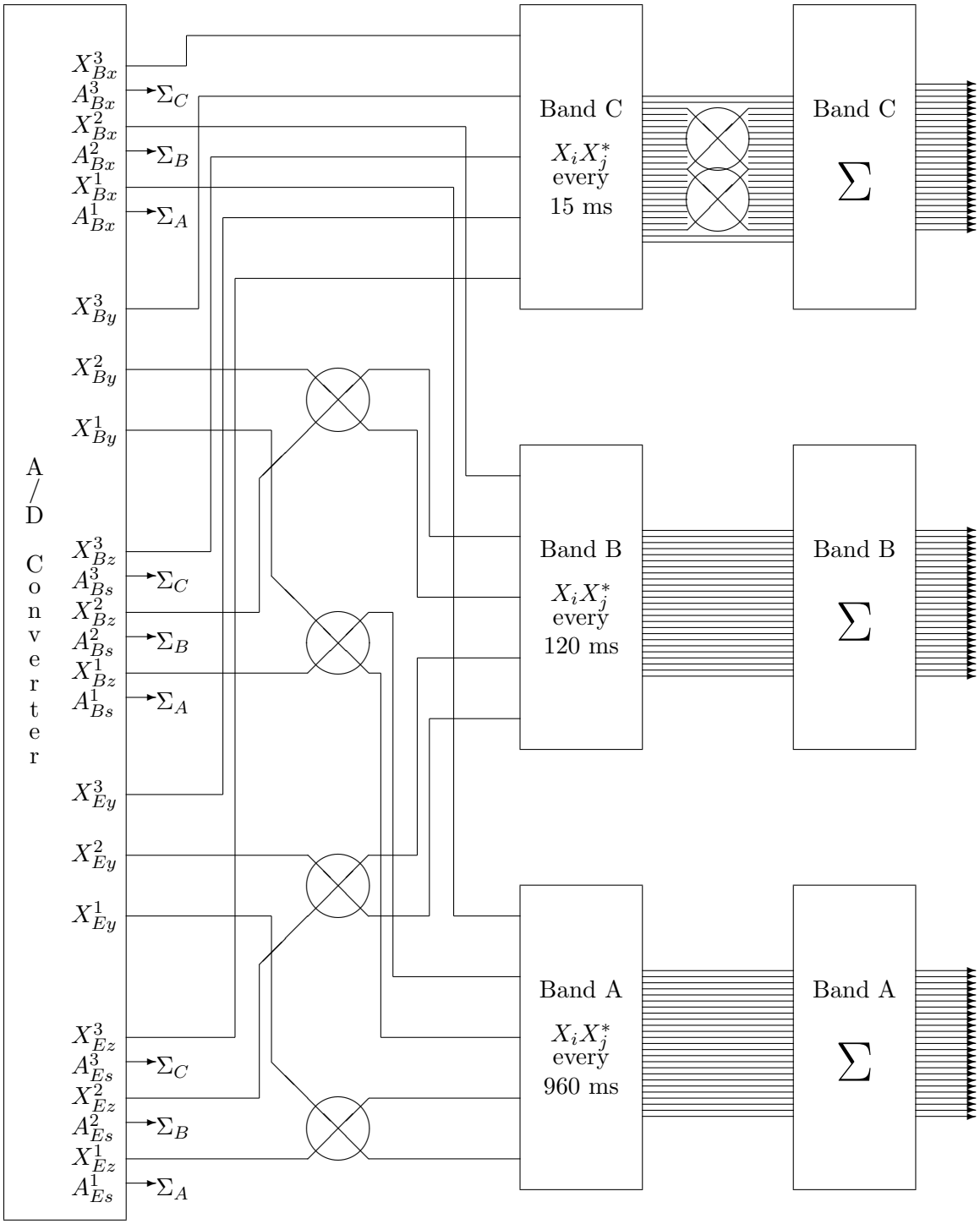

Figure 3: The Digital Part of the Receiver

3.1 Effects of Non-Simultaneous Sampling of the Analogue Channels

(*Label* **NSSAC**)

As there are 5 inputs (values of i), the converter has to take 5, 10 or 15 samples (depending upon whether band C, C+B, or C+B+A are to be sampled) in $1/16\,000 = 62.5\,\mu$s. The 5 inputs i are sampled sequentially, and the [3] delay between samples is $\Delta t \simeq 1.5\,\mu$s. This delay causes an additional relative phase shift between the digitised data from the different input channels.

The phase factor a by which the analogue transfer function (eq. 6) must be multiplied to obtain the transfer function of eq. 20 (both are functions of channel i, band m and frequency n) is (*Label* **NSSAC1**)

$$a_j^{mn} = \exp\{\sqrt{-1}\ \times 2\pi f_{mn} \times \Delta t \times i\} \tag{17}$$

where the frequencies f_{mn} are given by eq. 1 and $\Delta t = 1.5\ 10^{-6}$. For the highest frequency ($n = 9$ of band $m = 3$), the phase shift of B_z ($i = 5$) with respect to E_x ($i = 1$) amounts to 7.9°; [5] it is small, but not negligible.

In any case, the sampling procedure has been implemented such that this phase shift simply adds to the phase of the corresponding analogue receiver; it may be [2] treated as part of the analogue transfer function (see sections 2.1 and 6).

4 The De-Spin Algorithm

(*Label* **CDS**)

The de-spin algorithm rotates the outputs X_i and X_j of all pairs i and j of spin-plane analogue receivers (i.e., all channels for which $j - i = 1$ and $j + i = 5$ or 9) to an inertial co-ordinate system $\overline{X}_i$ and $\overline{X}_j$, ready for input to the digital spectrum analyser; (*Label* **despin**)

$$\left.\begin{array}{rcl} \overline{X}_i & = & X_i \cos\phi' - X_j \sin\phi' \\ \overline{X}_j & = & X_i \sin\phi' + X_j \cos\phi' \end{array}\right\} \tag{18}$$

where ϕ' is the angle through which the spacecraft has rotated since the time $T_{\rm SRP}$ of the Sun Reference Pulse. The $\overline{X}_i$-axis of the inertial system thus lies in the plane of the WEC y-axis at time $T_{\rm SRP}$. The different receivers will, in general, have transfer functions which differ in both amplitude and phase. As the satellite rotates, the sensor and analogue receiver which measure the spin-plane field component $B_y = \overline{B}_y$ when $\phi' = 0$ will measure $B_y = \overline{B}_z$ one quarter of a spin (*i.e.* $\simeq$ 1 s) later, while the sensor measuring $B_z = \overline{B}_z$ when $\phi' = 0$ will measure $B_z = -\overline{B}_y$; and so on. The effect of this is that the spin phase enters into the analogue transfer functions.

Although the relatively simple concept of the elementary analogue transfer function of Eq.6 disappears with de-spin, we will show (Appendix A, pages 55 *et seq.*) that after averaging the instantaneous cross-spectral matrix over the integration time of the digital spectrum analyser (which is an appreciable fraction of, or even comparable with, the spin period), there remains a well-defined relation between the cross-spectral matrix of the fluctuations in the ambient medium and the cross-spectral matrix of the signals at the output of the despin ; the latter is, of course, what the digital analyser determines. This relatively complicated transfer function can be determined, and its effects subsequently corrected during data analysis (provided that we manage to avoid one (highly unlikely) singular condition, as described in section 9.2).

4.1 The Factor $\sqrt{2}$

[3]

Despin was not thoroughly tested before launch, due to the practical difficulty of performing tests using stimuli which are spin modulated in synchronisation with the Sun pulses. In flight, data is normally taken with the despin algorithm ON, while the in-flight internal calibration cycle is normally executed with the despin OFF in order to calibrate separately the two spin-plane receivers.

On 2000 October 11 two calibration cycles were executed consecutively, the first with the despin algorithm ON and the second with it OFF. Analysis of the data (see e-mail dated 2001/09/30) shows that when an identical (phase coherent) signal is applied to all inputs :

- When the on-board despin is **OFF** :

  the AGC level for the axial receiver signal is significantly less than for the (combined) spin-plane receivers, by 8, 10 and 5 (decompressed telemetry units) respectively in bands A, B and C (for reasons explained in Section 2.2) ; and the

  spectral power density (output from the digital analyser, converted to physical units) is essentially the same in the axial and the two spin-plane autospectral channels.

- When the on-board despin is **ON** :

  the AGC levels remain unchanged with respect to despin OFF, in conformity with the AGC being determined before the despin. The

spectral power density (in physical units) remains unchanged along the spin axis, but the two spin-plane components each decrease by a factor of approximately 2 compared to despin OFF.

Detailed examination of the telemetry data (see e-mail of 2001/09/28) shows that the spin-plane digital telemetry, after logarithmic decompression, decreases by a factor of approximately 2 when the despin algorithm is ON (compared to despin OFF). This is true for both band B (for which the waveform data is continuously despun) and band C (for which the elementary cross-spectral matrices are despun before being integrated). The most probable explanation is that the coefficients used in the despin algorithm are not $\cos\theta$ and $\sin\theta$, but $\frac{1}{\sqrt{2}}\cos\theta$ and $\frac{1}{\sqrt{2}}\sin\theta$. The origin of this factor of $\sqrt{2}$ is not understood, but it is "compatible" with the use of $|B_{yy}|^2 + |B_{zz}|^2$ instead of $\frac{1}{2}(|B_{yy}|^2 + |B_{zz}|^2)$ to determine the AGC signal as explained in Section 2.2 – provided it is remembered that despin is **not** used during calibration !

In summary : a correction must be applied before data obtained with the **on-board despin algorithm ON** is converted into physical units. This correction consists simply of multiplying the spin-plane numerical data (*i.e.*, the telemetry data after decompression) by a factor of 2.

The onboard software must be analysed to confirm this tentative explanation !

4.2 The STAFF-SA Inertial Co-ordinate System

The angle ϕ used in eq. 18 is determined internally (aboard the spacecraft) by the STAFF Spectrum Analyser. Therefore the coordinate system in which the field components $\overline{X}_i$ are delivered is effectively hard-wired aboard the spacecraft.

The angle ϕ is determined using the Sun pulse and the Sun clock delivered to STAFF by the Digital Wave Processor (DWP) experiment. DWP supplies services for the Wave Experiment Consortium (WEC), in particular serving as the on-board Data Processing Unit for WEC and managing most of the interfaces between WEC and the various satellite sub-systems. **We assume that the Sun pulse and the Sun clock signals are delivered the STAFF Spectrum Analyser immediately they are received by DWP from the spacecraft** (*i.e.,* with negligible time delay).

The different co-ordinate systems discussed in this document are fully defined in the document Ref. 2. [3]

The spacecraft mechanical-build coordinate system was defined by ESTEC during construction of the spacecraft; in the "Data Delivery Interface Document", (DDID, Ref. **??** it is called the "body build" system. This same ESOC document defines attitude system with its axes aligned with the mechanical build axes, but permuted cyclically so that the spacecraft spins about an axis close to the attitude O3 axis. The spacecraft Spin Reference coordinate system is defined in terms of the principle moments of inertia of the spacecraft (after deployment of the booms). The spacecraft spins about the Spin Reference system O3 axis, which is close to the mechanical-build O1 axis. The spacecraft Sun Reference Pulse (SRP) occurs 26.2° before the meridian plane containing O1 axis of the of Spin Reference system sweeps through the solar direction; this value has been obtained from Iannis Dandouras (private communication, 1995 March 14). This implies that each time the SRP is received the spacecraft Spin Reference sytem O1 axis (which is close to the mechanical build Oy axis) has a spin phase angle of $360° - 26.2° = 333.8°$ with respect to the despun satellite coordinate system (see Ref. 2. [27]

Furthermore, it must be remembered that the WEC co-ordinate system is offset by 45° from the spacecraft mechanical build system. Therefore, the SRP occurs when the WEC E_y-axis (*i.e.*, the E_y long-wire antenna) has a spin phase of

$$\phi_0 = 45° - 26.2° = 18.8°$$

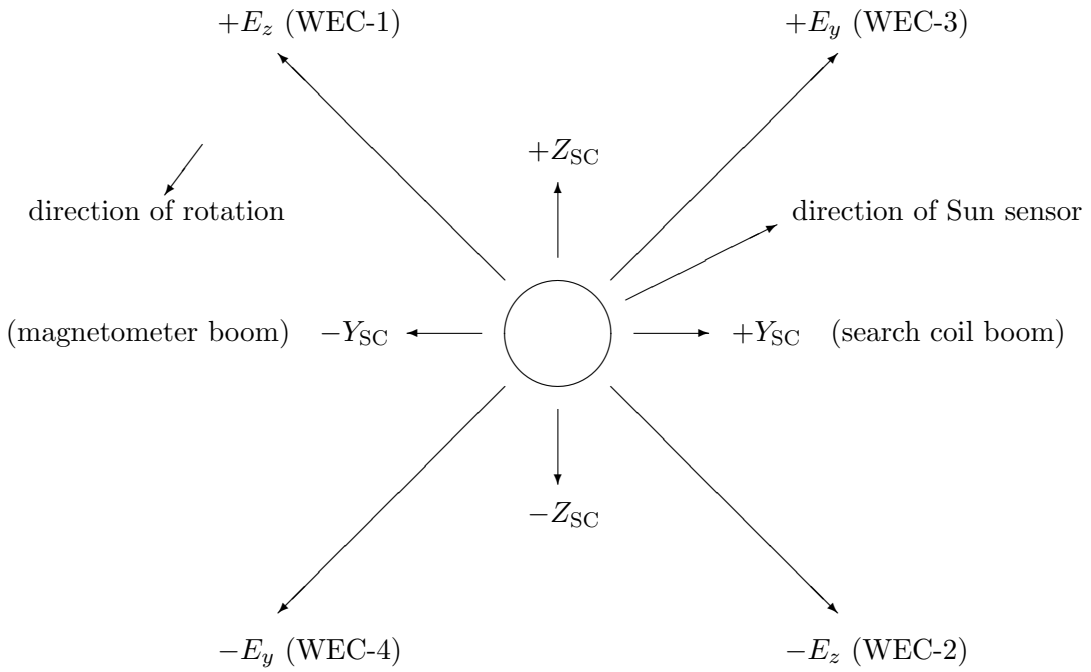

Figure 4: Spin-plane axes of spacecraft and of WEC *(after Fig. 2.1.1.b of EID Part A)*

(in the direction of increasing ϕ) from the plane $\phi = 0$ of the despun satellite co-ordinate system ; that is, the meridian plane containing the WEC E_x sensor sweeps through the solar direction 18.8° **before** the SRP. The geometrical mounting and electrical connections are discussed further in Section 4.3.

Finally, the field components $\overline{X}_i$, and hence the cross-spectral tensor $< \overline{X}_i \overline{X}_j^* >$ derived by the STAFF Spectrum Analyser, are delivered (by the telemetry) in an inertial coordinate system with its Ox axis parallel to the O3 axis of the despun satellite system and its Oy axis at longitude $+\phi_0$ in the despun satellite system. This offset ϕ_0 must be corrected during data processing (see Section 9.5)[11].

4.3 Mechanical Matters

The mounting positions the four EFW preamplifiers is shown in the Cluster Experiment Interface Document, Part A, CL-EST-RS-0002/EID A, Issue 2, Rev. 0, dated 1993/06/01. Fig. 2.1.1.b. (shown schematically in Fig. 4) shows the projection of the mounting positions onto the spin plane ; the $+Y$-axis, is is defined by the radial boom supporting the STAFF search coil. The mounting positions of the four EFW preamplifiers, WEC-1, WEC-2, WEC-3 and WEC-4, are shown, and their bodybuild spin plane phase angles are indicated in the second column of the table below. As it rotates in a right-handed sense about the $+X$-axis (see Fig 2.1.1.a), the angle though which the spacecraft spins from the time the $+Y$-axis (search coil boom) crosses a (fixed) meridian to the time the preamplifier crosses the same meridian is shown in the third column of the table below. The last column shows the field measured by the four preamplifiers.

The information in column 4 has been gleaned from "The Spherical Probe Electric Field and Wave Experiment for the Cluster Mission" by Gustafsson *et al.*, in "Cluster : mission

payload and supporting activities", edited by R. Schmidt, ESA SP-1159, March 1993, page 22. It has been confirmed recently in the document "Calibration of the EFW/STAFF Filters" edited by C.C. Harvey, OBSPM-TN-0008, Ed. 1, Rev. 0, dated January 8, 2002, a document was validated by Lenhart Ahlen. The conclusion is that the $+Y$ electric axis crosses any given inertial meridian plane 45° before the spacecraft $+Y$ axis.

Preamplifier	spin plane polar coordinate	s/c rotation between +OY & preamp. crossings of a fixed meridian	Field sensor
WEC-1	135°	225°	+Z
WEC-2	315°	45°	–Z
WEC-3	45°	315°	+Y
WEC-4	225°	135°	–Y
Sun sensor	26.2∘	333.8°	

The last line of the table shows equivalent information for the Sun sensor, as provided by Iannis Dandouras (private communication, March 14, 1995 see Section 4.2). The same information appears in an e-mail received 24-NOV-1994 10:06:49.82 from Per-Arne Linqvist (and is copied in Appendix 2 of the document "WEC/ISDAT Coordinate Transformations", CWD-OBSPM-DD-002, Issue 1, Rev. 7, dated May 3, 2001), where it is written "At the time $T_{\rm SRP}$, the spacecraft phase is $\phi_{\rm SRP}$. At the time t the phase ϕ is given by eq. 3, page 136 of the DDID, Issue 3 (*Label* **sphase**)

$$\phi = \phi_{\rm SRP} + \omega \cdot (t - T_{\rm SRP}) \tag{19}$$

where ω is the spin rate, which may be obtained from the difference between two successive values of $T_{\rm SRP}$ (as described in App I.6.1 of DDID Issue 3). For a higher accuracy, it may be obtained from a group of values of $T_{\rm SRP}$ (as described in App I.6.2 of DDID Issue 3). Nominally, it should be $360°/4$ s^{-1}.

The spin phase $\phi_{\rm SRP}$ at time $T_{\rm SRP}$ is available in the Spacecraft Attitude and Spin Rates (SATT) file on the CD-ROM, as described on pages 76-78 of DDID Issue 2.3 (pages 88-90 of DDID Issue 3). The value in the test CD-ROM is 333.800 degrees, for all four spacecraft (look in the files 940901ga.1a1, .1a2, .1a3, .1a4)." *Perhaps this should be checked using a CD-ROM obtained from Cluster 2 ?*

More recently, the Cluster Data Delivery Interface Document (DDID), CL-ESC-ID- 2001, Issue 3, dated 19 May, 2000 discussed the spin phase. After stating the obvious (page 134) "After several reviews on the definitions and documentation the applicable definitions for the Spin Phase seems not clear", this document gives the following definition (page 135) : "With this consideration, the phase of the SC that Flight Dynamics Attitude Determination will provide is :
'**Rotation angle of the half-plane defined by the $+Z_{\rm SR}$ and $+X_{\rm SR}$ Spin Reference System axes, around the maximum principal axis of inertia ($+Z_{\rm SR}$) from the time when the Sun direction was contained in this plane**'."
Throughout this Technical Note the spin phase thus defined is denoted by ϕ.

4.4 The Effects of Despin

The analogue transfer function F_j expresses the output X_j of the analogue receiver j in terms of the input x_j; it is defined by eq. 2, which may be written (*Label* **defa**)

$$X_j = x_j F_j(f, A) \quad \text{for} \quad 1 \le j \le 5 \quad \text{(no sum over } j\text{)} \; . \tag{20}$$

$F_j(f, A)$ takes into account the gain (amplitude and phase) of the analogue receiver, and also the small offset (essentially the phase correction given by eq. 17) due to the non-simultaneous sampling of the different receivers by the A/D converter.

The digital analyser computes $< \overline{X}_i \overline{X}_j^* >$, which is the cross-spectral matrix averaged over the Spectrum Analyser accumulation interval. This is comparable with the spacecraft spin period and indeed, in the most frequently used mode of operation, it is approximately equal to one spin period. [3] Several other modes of operation with different integration times are possible. We will consider an arbitrary integration period, during which the spacecraft spins through the range (*Label* **defphi**)

$$\phi_1 \leq \phi \ < \phi_2 \ . \tag{21}$$

All parameters determined by the digital spectrum analyser are derived either by autocorrelation or by cross-correlation. The correlation of any signal with an incoherent noise signal tends to zero as the integration time increases. We assume that the integration time is always **long enough** for the the signal and the noise to be treated separately. [4]

Note that this separation of the effects of signal and noise avoids a difficulty inherent in eq. 2 : that random noise cannot be represented by an analytic signal. The concept of the analytic signal is valid only for coherent signals. [4]

We note that during the determination of the auto-spectra and cross-spectra we will need to correlate $\overline{X}_i$ with $\overline{X}_j$ where $\overline{X}_i$ and $\overline{X}_j$ are given by eq. 18. To keep track of the indices it is necessary to introduce k and ℓ [3] defined by (*Label* **defmn**)

$$\left.\begin{array}{lllllllll} k = 5 - i & \text{for} & 2 \leq i \leq 3 & \text{and} & \ell = 5 - j & \text{for} & 2 \leq j \leq 3 & \text{(magnetic sensors)} \\ k = 9 - i & \text{for} & 4 \leq i \leq 5 & \text{and} & \ell = 9 - j & \text{for} & 4 \leq j \leq 5 & \text{(electric sensors)} \end{array}\right\} \text{[3]} \tag{22}$$

Thus in all equations, the value of k to be used is determined by the value of i, and the value of ℓ is determined by the value of j, in conformity with eq. 22; there is no requirement for a similar equation for $i = 1$ or $j = 1$. Note that k and ℓ correspond to the the spin-plane input [2] channels respectively orthogonal to channels i and j. [3]

4.4.1 Despinning the signal

It is shown in Appendix A how eqs. 18 and 20 can be used to derive the instantaneous values of the elements of the cross-spectral matrix $\overline{X}_i \overline{X}_j^*$ in terms of the corresponding elements $\overline{x}_i \overline{x}_j^*$ of the field fluctuations of the ambient medium in an inertial co-ordinate system; the resulting expressions are eqs. 80 and 81.

4.5 The Effect of Numerical Integration

4.5.1 Integrating the signal

The expressions 80 and 81 can be integrated over the duration of the integration period, to yield the output $< \overline{X}_i \overline{X}_j^* >$ in terms of the estimates $< \overline{x}_i \overline{x}_j^* >$ of the mean cross-spectral power of the fields in the ambient medium (which is what we want to determine); the corresponding equations are 83 and 84. [4]

In Appendix A it is found convenient to express the functions F_i and F_j and the homologous functions F_k and F_ℓ in terms of the sum and difference functions (*Label* **defSD**)

$$\left.\begin{array}{rcl} \mathcal{S}_i & = & \frac{1}{2}\,(F_i + F_k) \\ \mathcal{D}_i & = & \frac{1}{2}\,(F_i - F_k) \end{array}\right. \quad \text{and} \quad \left.\begin{array}{rcl} \mathcal{S}_j & = & \frac{1}{2}\,(F_j + F_\ell) \\ \mathcal{D}_j & = & \frac{1}{2}\,(F_j - F_\ell) \end{array}\right\} \ . \tag{23}$$

Thus (*Label* **expSD**)

$$\left.\begin{array}{ccccc} \mathcal{S}_2 & = & \mathcal{S}_3 & = & \mathcal{S}_{Bs} \\ \mathcal{D}_2 & = & -\mathcal{D}_3 & = & \mathcal{D}_{Bs} \end{array}\right. \quad \text{and} \quad \left.\begin{array}{ccccc} \mathcal{S}_4 & = & \mathcal{S}_5 & = & \mathcal{S}_{Es} \\ \mathcal{D}_4 & = & -\mathcal{D}_5 & = & \mathcal{D}_{Es} \end{array}\right\} \quad . \tag{24}$$

The expression for $< \overline{X}_i \overline{X}_j^* >$ in terms of $< \overline{x}_i \overline{x}_j^* >$ and the parameters $\mathcal{S}_i$ and $\mathcal{D}_i$ of eqs. 23 is given by eqs. 83 and 84 of Appendix A. These equations may be written (*Label* **Delta**)

$$< \overline{X}_i \overline{X}_j^* > = \mathcal{S}_i \mathcal{S}_j^* \left(< \overline{x}_i \overline{x}_j^* > + \Delta_{ij} \right) \quad \text{(no sum over } i, j) \tag{25}$$

where Δ_{ij} is a matrix of rather complicated functions derived in Appendix A.2, eqs. 83 and 84, which can be expressed (*Label* **Deltaij**)

$$\begin{aligned} \Delta_{ij}^{mn}(A_{Bs}^m, A_{Es}^m) &= \frac{1}{2}\, \epsilon_i \epsilon_j^* \left[< \overline{x}_i \overline{x}_j^* > + (-)^{(k+\ell)} < \overline{x}_k \overline{x}_\ell^* > \right] \\ &+ m_{2c} \left(\epsilon_j^* + \epsilon_i \right) < \overline{x}_i \overline{x}_j^* > \\ &- m_{2s} \left((-)^\ell \epsilon_j^* \ < \overline{x}_i \overline{x}_\ell^* > + (-)^k \epsilon_i \ < \overline{x}_k \overline{x}_j^* > \right) \\ &+ m_{4c} \frac{1}{2}\, \epsilon_i \epsilon_j^* \left(< \overline{x}_i \overline{x}_j^* > - (-)^{(k+\ell)} < \overline{x}_k \overline{x}_\ell^* > \right) \\ &- m_{4s} \frac{1}{2}\, \epsilon_i \epsilon_j^* \left((-)^\ell < \overline{x}_i \overline{x}_\ell^* > + (-)^k < \overline{x}_k \overline{x}_j^* > \right) , \end{aligned} \tag{26}$$

the m_{nx} being purely geometrical parameters defined by eq. 85, and ϵ_i a set of parameters defined by (*Label* **eps**)

$$\left.\begin{array}{rcccl} \epsilon_1 & = & 0 \, , & & \\ \epsilon_2 = -\epsilon_3 & = & \mathcal{D}_{Bs}/\mathcal{S}_{Bs} & = & \epsilon_{Bs} \, , \\ \epsilon_4 = -\epsilon_5 & = & \mathcal{D}_{Es}/\mathcal{S}_{Es} & = & \epsilon_{Es} \, . \end{array}\right\} \text{[3]} \tag{27}$$

Expressions 25 through 27 are exact; but note that, for simplicity, the superscripts "m" and "n", and the argument "A_p^m" have been dropped from Δ and ϵ in eq. 25; in other words, Δ_{ij} and ϵ_i should be written respectively $\Delta_{ij}^{mn}(A_p^m, A_q^m)$ and $\epsilon_i^{mn}(A_p^m)$ and, for example, the second of eqs. 27 should be written

$$\epsilon_2^{mn}(A_p^m) = \mathcal{D}_{Bs}^{mn}(A_p^m)/\mathcal{S}_{Bs}^{mn}(A_p^m) \ .[2]$$

We may also note that:

- by definition (eqs. 27 and 23), the functions ϵ_i will normally be small;
- when the integration period is an integral number of half spin periods, most of the terms in eq. 26 disappear (see eq. 89).

For these reasons Δ_{ij} will often be rather small, a fact used to simplify the inversion of eq. 25 required to obtain $< \overline{x}_i \overline{x}_j^* >$ (in physical units) from $< \overline{X}_i \overline{X}_j^* >$ (what is actually provided at the spectrum analyser output), as described in section 9.3.

Note that in eq. 25 $\mathcal{S}_i \mathcal{S}_j^*$ and Δ_{ij} are sets of coefficients, not tensors (they have no characteristic properties under rotation; for them, the concept or rotation is meaningless); this explains why the expression "no sum over i, j" appears rather frequently.

4.6 Discussion

The expressions 23 and 24 were first introduced for mathematical convenience, but there is strong physical support for their use: [10]

1. The spin-plane receivers are strapped together in pairs with common AGC outputs. Thus the functions $\mathcal{S}_{Bs}$, $\mathcal{D}_{Bs}$ and $\mathcal{S}_{Es}$, $\mathcal{D}_{Es}$ can be used in place of F_2, F_3 and F_4, F_5 as calibration functions. Indeed, it is useful to do this, because:

2. the functions $\mathcal{S}_{Bs}$ and $\mathcal{S}_{Es}$ are determined (more or less) directly by the in-flight calibration cycle;

3. the functions $\mathcal{D}_{Bs}$ and $\mathcal{D}_{Es}$ cannot be determined by the in-flight calibration cycle. They can be determined from pre-launch laboratory measurements, and should be updated using naturally occurring polarised radio waves observed in the magnetosphere, as described in the document OBSPM–TN–0005.

4. The functions $\mathcal{D}_{Bs}$ and $\mathcal{D}_{Es}$ are, in principle, very small compared to the functions $\mathcal{S}_{Bs}$ and $\mathcal{S}_{Es}$. For many application they can be entirely neglected, which enormously simplifies the equations used to obtain the cross-spectral estimates in physical units, thus saving computational effort.

Further discussion of the merits of the $\mathcal{S}$ and $\mathcal{D}$ functions is provided at the end of Section 8 (page 36). Note that the most likely reason for the functions $\mathcal{D}_{Es}$ to be significantly different from zero is unequal deployment of the two orthogonal spin-plane electric field antennas. Therefore the software required to handle $\mathcal{D}_i$ functions, and preferably also that required to determine the $\mathcal{D}_i$ functions from observations of naturally occurring waves, must be operational before the start of the in-flight experiment check-out. [18]

5 The Digital Analyser

The digital analyser is fundamentally different from the analogue receivers: the analogue receivers are linear, while the digital analyser is not. At frequencies well above the inverse of the AGC response time, the waveform output (to the A/D converter) of each analogue receiver is proportional to the input (eq. 2). This is is not the case for the output from the digital receiver: auto-spectra output varies as the square of the input, while the relation for the cross-spectra is more complicated. [5]

The digital analyser computes (in normal mode) the full 5×5 cross-spectral matrix at the 9 frequencies f^n (per band) of the 5 signals at the input to the A/D converter (*i.e.*, the outputs of the analogue receivers). We now describe how this is done. The output is subsequently compressed and formatted for the digital telemetry, as described in section 5.2

The inverse problem, how the cross-spectral matrix at the input to the A/D converter is recovered from the telemetry data, is treated in section 9.1.

5.1 The Digital Transfer Function

(*Label* **DTF**)

The numerical analyser accepts the five de-spun digital inputs $\overline{X}_i^m$ $(1 \leq i \leq 5)$ in each band m, and computes the full 5×5 Hermitian cross-spectral matrix N_{ij}^{mn} at each of the 9 frequencies f^n; the 27 centre frequencies are listed in Table 1.

The bandpass characteristic for each of the 9 values of n is determined by convolving the incoming data with the appropriate numerical window. The same windowing coefficients are used in all 5 digital input channels; consequently, all five input channels have identical bandpass characteristics. Furthermore, the same coefficients are used in all 3 bands; therefore the bandpass characteristics relative to the sampling frequency are identical from one band to another.

The functions x_i, X_i and $\overline{X}_i$ represent the quasi-monochromatic analytic signal, as defined by eq. 3. The spectrum analyser actually determines the spectral power within a finite bandwidth around the central frequency f^n of each output channel. For output channel n we define $B^n(f)$ to be its spectral bandpass characteristic. $B^n(f)$ has a maximum close to f^n, so that the effective frequency of the output channel is (*Label* **deffn**)

$$f^n = \frac{\int_0^\infty B^n(f)\, f\, df}{\int_0^\infty B^n(f)\, df} \ .[2] \tag{28}$$

while its effective bandwidth is (*Label* **defBn**)

$$W^n = \frac{\int_0^\infty B^n(f)\, df}{B^n(f^n)} \ . \tag{29}$$

[8]

After filtering, correlation and integration, the response of the digital analyser to wideband signals in input channels i and j is (*Label* **DTF1**)

$$N_{ij}^n = \int_0^\infty B^n(f)\overline{X}_i(f)\overline{X}_j^*(f)df = (H^n)^2 < \overline{X}_i\overline{X}_j^* > \ .[2] \tag{30}$$

where (*Label* **defR**)

$$(H^n)^2 = W^n \times B^n(f^n) \tag{31}$$

is the "integrated response" of the digital filter. It is denoted by $(H^n)^2$ to simplify the notation, and in particular to make H^n homogeneous with (of the same dimensions as) $G_i^m(f, A)$ in section 6 (see also Table 3). [2] It can be seen that $< \overline{X}_i\overline{X}_j^* >$ is the mean cross-spectral density in the band of frequencies defined by $B^n(f)$. Eq. 30 is the expression which we will use to relate the output cross-spectral matrix elements to the digital spectrum analyser input. [9]

5.1.1 The digital bandpass characteristics

W^n defined by eq. 29 is the equivalent bandwidth of the digital filter. The different sets of coefficients for the various filter channels are chosen so that W^n is 28.6% of the centre frequency of the corresponding channel,

$$W^n = 0.286\, f^n \quad \text{for all } n\ .$$

The different sets of coefficients used do not yield identically self-similar functions $B^n(f)$ for each value of n. Therefore the functions $B^n(f)$ for the 9 channels have been computed from the known coefficients, verified by direct measurement, and used to compute the corresponding values of H^n via eq. 31, as described elsewhere. It is important to note, however, that the important characteristics (*i.e.*, those used in eq. 30) of the functions $B^n(f)$ are are determined during the calibration of the overall (analogue + digital) receiver, as described in sections ref. 1008 of Appendix 1 and ref. 1015 of Appendix 1. [12]

5.2 Logarithmic Compression of the Digital Output

(*Label* **LCDO**)

The output from the digital analyser consists of a 5×5 Hermitian matrix of words with 16 bits of exponent and 16 bits of mantissa. These words are compressed logarithmically before being sent to the telemetry. Different compression algorithms are used for the diagonal and non-diagonal elements of the cross-spectral matrix. [4]

5.2.1 Diagonal elements

The elements on the leading diagonal are real. They are compressed to a single telemetry word of 8 bits, using 5 bits for the exponent e followed by 3 bits for the mantissa m. The decompression algorithm is given by eq. 51. [2]

5.2.2 Non-diagonal elements

The non-diagonal elements of the cross-spectral matrix are complex. They are first normalised with respect to the diagonal elements within the digital spectrum analyser, (*Label* **defz**)

$$z_{ij} = N_{ij} \Big/ \sqrt{\overline{N}_{ii}\overline{N}_{jj}}\ \ .[2] \tag{32}$$

This normalisation uses values of the diagonal elements accumulated during the same time interval as the non-diagonal elements, but not telemetered to the ground. After normalisation, the values $z = x + iy$ satisfy $|z| \leq 1$. For each element z, one 8-bit telemetry word is used: the most significant four bits are used for the real part, and least significant four bits for the imaginary part. For both parts, the most significant bit is used to indicate the sign ($0 \equiv +$, $1 \equiv -$). The remaining three bits are used to form real integers m_x and m_y in the range $0 \leq m \leq 7$ which indicate the magnitude of x and y, as follows:

$$\left.\begin{array}{rcll} 0 & \leq x < & 2^{-8} & \text{for} \quad m_x = 0 \\ 2^{m_x-9} & \leq x < & 2^{m_x-7} & \text{for} \quad m_x = 1 \\ 2^{m_x-8} & \leq x < & 2^{m_x-7} & \text{for} \quad 2 \leq m_x \leq 7 \end{array}\right\} \tag{33}$$

and similarly for y. The distribution is logarithmic, with a slight modification at the lower end to improve resolution when x or y is near zero. It gives the distribution of samples in the

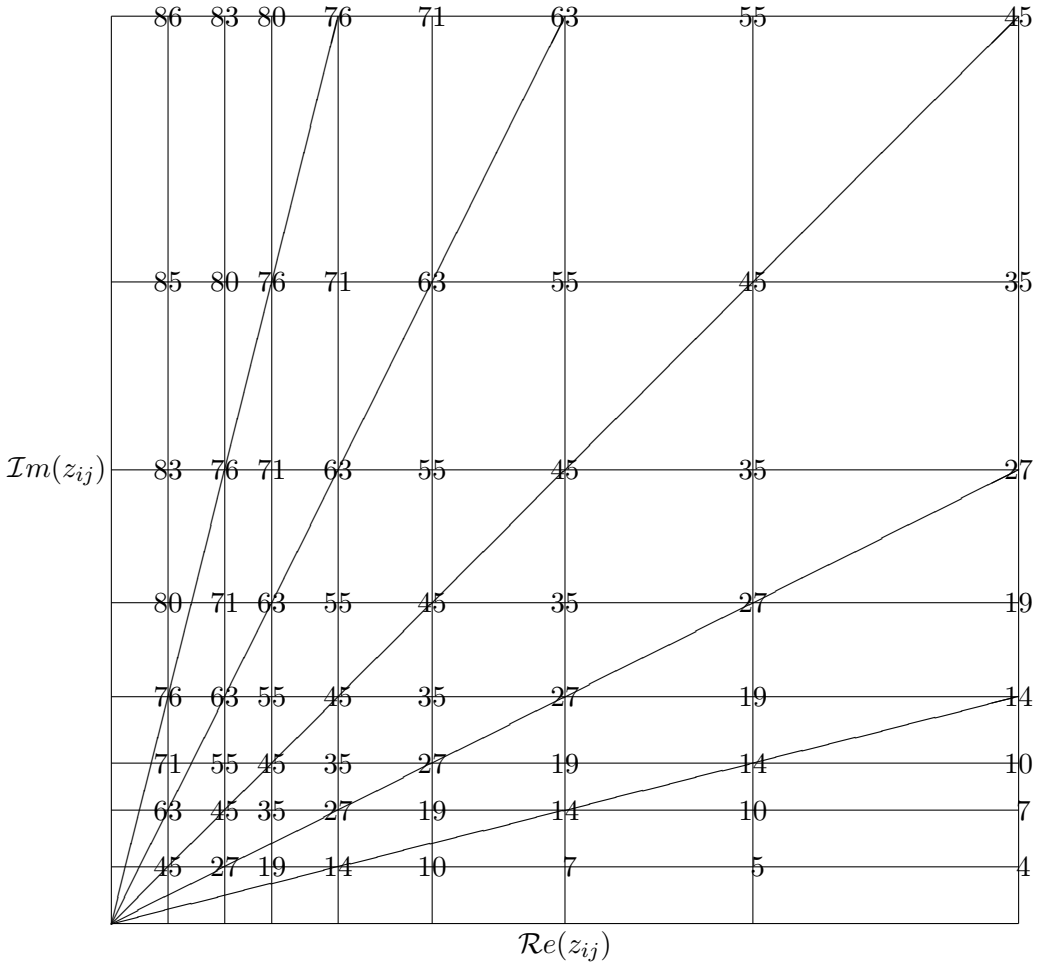

Numbers indicate the phase of the corners of the bins.
The diagonal lines of constant phase are to guide the eye.

Figure 5: Distribution of the 64 sampling bins in the first quadrant of the z_{ij} plane.

m	2^{m-7}	measured
0	<0.00390625	<0.003922
1	<0.015625	<0.015686
2	<0.03125	<0.03529
3	<0.0625	<0.062745
4	<0.125	<0.141176
5	<0.25	<0.250979
6	<0.5	<0.5647
7	<1	<1

Table 2: The Upper Limits of the Digitisation Steps

complex z-plane as shown in Fig. 5; it includes both magnitude and phase information for small $|z|$. The upper limit for each range is shown in Table 2.

(*Label* **Table2**)

The last column indicates the limiting values which have been determined experimentally. *I do not understand the reason for this difference.* In view of the relatively poor sampling in the complex z-plane (essentially due to telemetry flux limitations), we interprete the telemetered values of z to correspond to values at the (geometric) centre of these ranges, as defined by eq. 54.

6 The Complete Calibration Model

(*Label* **CCS**)

The significance of the symbols used in the equations of this section and also elsewhere in this memorandum, is shown in Tables 3 and 4. For each symbol, successive columns indicate: [28]

- the type of variable (real or complex),
- the equation or section where it has been defined,
- its significance, and
- the equation or chapter which explains how its value is determined.

Note that during successive revisions of Version 3 of this document the calibration model was substantially modified by the introducton of the sum and difference functions $\mathcal{S}$ and $\mathcal{D}$ (eq. 23). A comparison of the present document with those prior to Version 3 (up to and including May 1995) can be found in Appendix 3.

The STAFF Spectrum Analyser does not actually measure any linear function of the sensor inputs, but only the power spectrum and the cross-spectrum. From eqs. (25) and (30), the cross-spectral matrix N_{ij} at the output of the the digital analyser before logarithmic compression is (*Label* **CCS1**)

$$N_{ij} = (H^n)^2 \, \mathcal{S}_i \mathcal{S}_j^* \, \left(< \overline{x}_i \overline{x}_j^* > \, + \Delta_{ij} \right) \quad \text{(no sum over } i, j) \tag{34}$$

Here $(H^n)^2$ is the "integrated response" of the digital filter, defined by eqs. 29 and 31. [3]

6.1 Separation of the Variables

6.1.1 The spin-plane functions

[2]

In the same way as the functions $F^m_{Bx}(f, A^m_{Bx})$ had their variables separated according to eq. 9, it is possible to separate the variables of the functions $\mathcal{S}$ and $\mathcal{D}$. [4] To simplify from eq. 41 onwards, we include H^n into these relations, thus (*Label* **defSSPs**)

$$\left.\begin{aligned} \mathcal{S}^m_i(f^n, A^m_i) &= \tfrac{1}{H^n} \, S^m_i(A^m_i) \times \tilde{S}^m_i(f^n) \\ \mathcal{D}^m_i(f^n, A^m_i) &= \tfrac{1}{H^n} \, D^m_i(A^m_i) \times \tilde{D}^m_i(f^n) \, . \end{aligned}\right\} \tag{35}$$

Note that:

- the functions S and D take account of the variation with ACG level, assumed to be the same for all frequencies within any given band.
- The functions $\tilde{S}$ and $\tilde{D}$ allow for the variation with frequency (channel number n) within each digital receiver input channel.
- The "sum" functions $\mathcal{S}$ are associated with the functions S and $\tilde{S}$, and
- the "difference" functions $\mathcal{D}$ are associated with the functions D and $\tilde{D}$.

6.1.2 The axial functions $\mathcal{S}_{Bx}$ S_{Bx} and $\tilde{S}_{Bx}$

It is convenient at this point to define, for the axial component, functions analogous to the S and $\tilde{S}$ of eq. 35 and 39: (*Label* **defSSPa**)

$$\begin{gathered} \mathcal{S}_{Bx} = F^m_{Bx}(f^n, A^m_{Bx}) \\ S_{Bx} = Q^m_{Bx}(A^m_{Bx}) \quad \tilde{S}_{Bx} = H^n P^m_{Bx}(f^n) \, . \end{gathered} \tag{36}$$

There are two reason for doing this:

- to combine the digital filter bandpass H^n with the analogue receiver bandpass characteristics $P^m_{Bx}(f^n)$, as in eq. 35.
- to homogenize the notation in the equations which follow: the index $p(i)$ may be used to represent indifferently B_x, B_s and E_s, thus (eq. 24), (*Label* **defpq**)

$$p(i) = B_x \ \text{ for } i = 1, \qquad p(i) = B_s \ \text{ for } i = 2 \text{ or } 3, \qquad p(i) = E_s \ \text{ for } i = 4 \text{ or } 5 \tag{37}$$

  with similar expressions for q in terms j.

Then we may generalise eqs. 35 and 36 to include all field components, (*Label* **defSSP**)

$$\left.\begin{aligned} \mathcal{S}^m_p(f^n, A^m_p) &= \tfrac{1}{H^n}\, S^m_p(A^m_p) \times \tilde{S}^m_p(f^n) \\ \mathcal{D}^m_p(f^n, A^m_p) &= \tfrac{1}{H^n}\, D^m_p(A^m_p) \times \tilde{D}^m_p(f^n)\ , \end{aligned}\right\} \tag{38}$$

although the second equation exists only for $p = 2$ or 3.

6.2 The Spin-plane functions $\mathcal{S}_{Bs}$, $\mathcal{S}_{Es}$, $\mathcal{D}_{Bs}$ and $\mathcal{D}_{Es}$

As in the case of eq. 9, the pairs of coefficients $S^m_p(A^m_p)$, $\tilde{S}^m_p(f^n)$ and $D^m_p(A^m_p)$, $\tilde{D}^m_p(f^n)$ are not uniquely defined. Therefore, as for eq. 10, we define $S^m_{Bs}(A^m_i)$ and $D^m_{Es}(A^m_i)$ so that when white noise of spectral density ρ_p (in $\mathrm{nT^2\,Hz^{-1}}$) in band m is applied simultaneously to the B_y and B_z sensors (or in $(\mathrm{V/m})^2\,\mathrm{Hz}^{-1}$ to the E_y and E_z sensors) (*Label* **defSQ**)

$$\left.\begin{aligned} \rho_{Bs} &= |S^m_{Bs}(A^m_{Bs})|^{-2} \\ \rho_{Es} &= |S^m_{Es}(A^m_{Es})|^{-2}\ . \end{aligned}\right\} \tag{39}$$

The magnitudes of the functions $S^m_i(A^m_i)$ and $\tilde{S}^m_i(f^n)$ are thus determined, but not their phases. They, and the functions D and $\tilde{D}$ must, of course, satisfy (eq. 23) (*Label* **defSP**)

$$\left.\begin{aligned} F_2(f^n, A_{Bs}) &= \mathcal{S}_{Bs} + \mathcal{D}_{Bs} = \tfrac{1}{H^n}\left[S^m_{Bs}(A^m_{Bs}) \times \tilde{S}^m_{Bs}(f^n) + D^m_{Bs}(A^m_{Bs}) \times \tilde{D}^m_{Bs}(f^n)\right] \\ F_3(f^n, A_{Bs}) &= \mathcal{S}_{Bs} - \mathcal{D}_{Bs} = \tfrac{1}{H^n}\left[S^m_{Bs}(A^m_{Bs}) \times \tilde{S}^m_{Bs}(f^n) - D^m_{Bs}(A^m_{Bs}) \times \tilde{D}^m_{Bs}(f^n)\right] \\ F_4(f^n, A_{Es}) &= \mathcal{S}_{Es} + \mathcal{D}_{Es} = \tfrac{1}{H^n}\left[S^m_{Es}(A^m_{Es}) \times \tilde{S}^m_{Es}(f^n) + D^m_{Es}(A^m_{Es}) \times \tilde{D}^m_{Es}(f^n)\right] \\ F_5(f^n, A_{Es}) &= \mathcal{S}_{Es} - \mathcal{D}_{Es} = \tfrac{1}{H^n}\left[S^m_{Es}(A^m_{Es}) \times \tilde{S}^m_{Es}(f^n) - D^m_{Es}(A^m_{Es}) \times \tilde{D}^m_{Es}(f^n)\right] \end{aligned}\right\} \tag{40}$$

where the functions F_2, F_3, F_4, and F_5 are, in principle, well-defined.

The use of these equations to determine the functions $D^m_p(A^m_p)$ and the parameters $\tilde{D}^m_p(f^n)$, and also the phases of $S^m_p(A^m_p)$ and $\tilde{S}^m_p(f^n)$, will be described fully in the report OBSPM–TN–0005.

By including H^n in eqs. 35, the coefficients $\tilde{S}^m_p(f^n)$ and $\tilde{D}^m_p(f^n)$ group together all the terms which depend upon f^n, *i.e.*, upon the channel number m, n, i but which are independent of the AGC. Thus there is one less table of calibration coefficients than if H^n were to be handled separately. Furthermore, we may further note:

- the $S^m_p(A^m_p)$ and $\tilde{D}^m_p(f^n)$ are the coefficients which are determined during the in-flight calibration cycle;
- the $\tilde{S}^m_p(f^n)$ and $D^m_p(A^m_p)$ are the coefficients which can be determined only by noise calibrations in the laboratory before launch;

6.3 The Physical Significance of $S_p^m(A_p^m)$ and $\tilde{S}_p^m(f^n)$

As shown by eqs. 10, 36, and 39 the parameters $S_p^m(A_p^m)$ characterise the analogue receivers; the mean spectral noise density in the overall pre-converter passband of analogue receiver m, as a function of the corresponding AGC output A_p^m (which is measured in telemetry counts) is

$$\rho_p^m = \frac{1}{\left[S_p^m(A_p^m)\right]^2} ;$$

the units of Q are $\left[\text{nT Hz}^{-\frac{1}{2}}\right]^{-1}$ (or $\left[\text{[V/m] Hz}^{-\frac{1}{2}}\right]^{-1}$ for the electric field). The parameters $S_p^m(A_p^m)$ are complex to allow for the phase of the transfer functions $\mathcal{S}_{Bx}$, $\mathcal{S}_{Bs}$, and $\mathcal{S}_{Es}$ to vary independently with their gains, as indicated by A_{Bx}^m, A_{Bs}^m or A_{Es}^m. Nevertheless, since the functions $\mathcal{D}_{Bs}$ and $\mathcal{D}_{Es}$ also contribute to relative phase differences, the functions $\mathcal{S}_{Bx}$, $\mathcal{S}_{Bs}$, and $\mathcal{S}_{Es}$ may each be defined to be real (*i.e.*, have zero phase) at one arbitrary level of gain (see Paper OBSPM-TN-0005, Section 3). [7]

The parameters $\tilde{S}_p^m(f^n)$ characterise the bandpass characteristics of the digital spectrum analyser, and also the variation with frequency of the analogue receivers. They allow independent auto and cross-spectral estimates to be obtained in both amplitude and phase at each of the nine frequencies f^n within each band m. When white noise of the spectral intensity ρ^{ref} required to produce the AGC output A^{ref} is applied to the input, the diagonal element N_{ii} of the cross-spectral matrix at frequency f^n of band m is given by $N_{ii}^{mn} = \left|S_p^m(A_p^m)\ \tilde{S}_p^m(f^n)\right|^2 \rho^{\text{ref}}$; the units of $\tilde{S}_p^m(f^n)$ are $\text{counts}^{\frac{1}{2}}$.

In the more general case, when measuring natural noise the mean spectral density of the field component p in the frequency passband f^n [2] of band m is given by

$$\rho_p(f^{mn}) = \frac{N_{ii}^{mn}}{\left|S_p^m(A_p^m)\ \tilde{S}_p^m(f^n)\right|^2} ,$$

where p is determined by eq. 37.

The above estimation for the spin plane components are valid only if the noise is isotropic in the spin plane. If this is not the case, the expressions for the spin plane field components are considerably more complicated, as will be seen in section 6.5.

6.4 The Complete Set of Calibration Coefficients

The sizes of the tables containing these different calibration data are:

$S_{Bx}^m(A_{Bx}^m)$		are each $m \times A = 3 \times 256 = 768$ point tables,
$S_{Bs}^m(A_{Bs}^m)$	$D_{Bs}^m(A_{Bs}^m)$	yielding a total of $5 \times 768 = 3840$ complex values
$S_{Es}^m(A_{Es}^m)$	$D_{Es}^m(A_{Es}^m)$	(*i.e.*, 7680 real values)
$\tilde{S}_{Bx}^m(f^n)$		are each $m \times n = 3 \times 9 = 27$ point tables,
$\tilde{S}_{Bs}^m(f^n)$	$\tilde{D}_{Bs}^m(f^n)$	yielding a total of $5 \times 27 = 135$ complex values
$\tilde{S}_{Es}^m(f^n)$	$\tilde{D}_{Es}^m(f^n)$	(*i.e.*, 270 real values)
$z_{ii}(p)$		is a 256 point table, or a mathematical expression, for the (real) diagonal elements
$z_{ij}(p)$		is a 256 point table, or a mathematical expression, for the (complex) non-diagonal elements.

[3]

If supplied entirely in tabular form, the total number of coefficients required for one calibration set (i.e., for one instrument at one time) is

$$7680 + 270 + 256 + 512 = 8718 \text{ real coefficients.}$$

6.5 The Correlator Output in Terms of the Natural Wave Field

From eqs. 34 and 35 (*Label* **CCS2**)

$$N_{ij}^{mn} \;=\; S_p^m(A_p^m)\; S_q^{m*}(A_q^m)\; \tilde{S}_p^m(f^n)\; \tilde{S}_q^{m*}(f^n)\left(< \overline{x}_i \overline{x}_j^* > + \Delta_{ij}^{mn}(A_{Bs}^m, A_{Es}^m)\right) \quad \text{(no sum over } p, q) \tag{41}$$

with $\Delta_{ij}^{mn}(A_{Bs}^m, A_{Es}^m)$ given by eq. 26 (page 18) for a spinning spacecraft. **These are the equations which must be solved to obtain $< \overline{x}_i \overline{x}_j^* >$ from the information in the telemetry data stream**. In this equation

- The function $S_p^m(A_p^m)$ describes the variation with AGC level A_p^m of the transfer function of receiver (or mean transfer function of the spin-plane receivers) of band m.
- The function $\tilde{S}_p^m(f^n)$ describes the variation with frequency f^n within the band m of the transfer function (or mean transfer function) of receiver(s) of that band.
- The subscripts $p(i)$ depend upon the input channels being considered, thus (eq. 37)) :

  $$p(1) = B_x, \qquad p(2) = B_s, \qquad p(3) = B_s, \qquad p(4) = E_s, \qquad p(5) = E_s,$$

  with a similar expression for $q(j)$.

The complete expression for Δ_{ij} is given by eq. 26 (page 18), [5] which is examined in detail in section 7.2 below. This equation uses the small quantities ϵ_i defined by eq. 27,

$$\begin{aligned} \epsilon_1 &= 0\ , \\ \epsilon_2 = +\mathcal{D}_{Bs}/\mathcal{S}_{Bs}\ , &\qquad \epsilon_3 = -\mathcal{D}_{Bs}/\mathcal{S}_{Bs}\ , \\ \epsilon_4 = +\mathcal{D}_{Es}/\mathcal{S}_{Es}\ , &\qquad \epsilon_5 = -\mathcal{D}_{Es}/\mathcal{S}_{Es}\ , \end{aligned}$$

and the m functions by eq. 85, [4]

$$\left.\begin{array}{rcccl} m_{2c} &=& \cos(\phi_2+\phi_1)\,\mathrm{sinc}\,(\phi_2-\phi_1) &=& \cos 2\varphi\ \mathrm{sinc}\,\delta\phi \\ m_{2s} &=& \sin(\phi_2+\phi_1)\,\mathrm{sinc}\,(\phi_2-\phi_1) &=& \sin 2\varphi\ \mathrm{sinc}\,\delta\phi \\ m_{4c} &=& \cos 2(\phi_2+\phi_1)\,\mathrm{sinc}\,2(\phi_2-\phi_1) &=& \cos 4\varphi\ \mathrm{sinc}\,2\delta\phi \\ m_{4s} &=& \sin 2(\phi_2+\phi_1)\,\mathrm{sinc}\,2(\phi_2-\phi_1) &=& \sin 4\varphi\ \mathrm{sinc}\,2\delta\phi \end{array}\right\} \tag{42}$$

with the function (eq. 87)

$$\mathrm{sinc}\ x = \frac{\sin x}{x}$$

and where φ and $\delta\phi$ are respectively the mean value and the range of the variation of the spin phase during the integration period,

$$\varphi = \frac{\phi_2 + \phi_1}{2} \qquad \text{and} \qquad \delta\phi = \phi_2 - \phi_1 \tag{43}$$

The indices k and ℓ used in eq. 26 are given by eq. 22; [6] [15] note that $(-)^{(k+\ell)}$ is positive/negative for i, j corresponding to sensors which are mutually parallel/perpendicular.

The parameters Δ_{ij} of eq. 26 are correction terms required only if it is found that the pairs of spin-plane analogue receivers are not well balanced, $\epsilon \neq 0$. In Appendix B we give explicit equations for each element of Δ_{ij}. Hopefully, except during experiment turn-on and commissioning, these correction terms will never be needed.

(*Label* **Table3a**)

(*Label* **Table3b**)

Symbol	Type	Defined	Represents	Determined	Units
$B^n(f)$	real	sect. 5.1	Bandpass characteristic of channel n of the digital receiver.	not required	Hz^{-1}
$\mathcal{D}_p^m(f^n, A_p^m)$	complex	eq. 23	Inbalance $\mathcal{D}_i = \frac{1}{2}(F_i - F_m)$, (& see eqs. 24)	sect. 4.4	none
$D_p^m(A_p^m)$	complex	23	Inbalance of $S_i^m(A_i^m)$		
$\tilde{D}_p^m(f^n)$	complex	35 or 36	Inbalance of $\tilde{S}_i^m(f^n)$		
$F_i^m(f, A)$	complex	eq. 20	The analogue transfer function for receiver i of band m.	eq. 9	none
H^n	real	eqs. 30	Integrated response of channel n of the digital analyser.	with $\tilde{S}_i^m(f^n)$	$\frac{(\mathrm{counts})^{\frac{1}{2}}}{\mathrm{nT\,Hz}^{-\frac{1}{2}}}$
$N_{ij}(p)$	complex	51 or 52	Decompression algorithm for the output from the digital analyser.	n/a	
$P_i^m(f^n)$	complex	eq. 9	Variation of the B_x analogue receiver transfer function with frequency.	with $\tilde{S}_i^m(f^n)$	$\mathrm{nT\,Hz}^{-\frac{1}{2}}$
$Q_1^m(A_1^m)$	complex	eq. 9	Variation of the B_x analogue receiver transfer function with AGC output.	sect. TN-05.1009	$\mathrm{nT}^{-1}\,\mathrm{Hz}^{\frac{1}{2}}$
$\mathcal{S}_p^m(f^n, A_p^m)$	complex	eq. 23	Mean, $\mathcal{S}_i = \frac{1}{2}(F_i + F_m)$, (& see eqs. 24)	sect. 4.4	none
$S_p^m(A_p^m)$	complex	35 or 36	($S_1 = Q_1^m(A_1^m)$) Variation of the analogue receiver transfer functions with AGC output.	Sect. TN-05.1008	$\mathrm{nT}^{-1}\,\mathrm{Hz}^{\frac{1}{2}}$
$\tilde{S}_p^m(f^n)$	complex	35 or 36	($\tilde{S}_1^m(f^n) = H^n P_1^m(f^n)$) The total frequency-channel-dependent (*i.e.*, everything except the AGC) transfer function for channel i, frequency n, of band m, including the effects of the analogue receiver, the A/D converter, de-spin and the digital analyser.	sect. TN–05.1003	$(\mathrm{counts})^{\frac{1}{2}}$
W^n	real	eq. 29	Equivalent bandwidth of channel n of the digital receiver.	not required	Hz
$\Delta_{ij}^{mn}(A_{Bs})$	complex	eq. 25	Functions needed to relate $< \overline{X}_i \overline{X}_j^* >$ to $< \overline{x}_i \overline{x}_j^* >$	sect. 7.2	none
$\epsilon_i^{mn}(A_{Bs})$	complex	eq. 27	the ratio $\epsilon_i = \mathcal{D}_i / \mathcal{S}_i$	eq. 27	none

Table 3: The symbols used to represent parameters describing the instrument

Symbol	Type	Defined	Represents	Determined	Units
A	real	eq. 6	The AGC signal	n/a	TM counts
$\overline{x}_i$	complex	eq. 73	Analytic signal of field component i in the ambient medium.	n/a	nT $\mathrm{Hz}^{-\frac{1}{2}}$
x_i	complex	eq. 20	Analytic signal as measured by the spinning sensor i.	n/a	nT $\mathrm{Hz}^{-\frac{1}{2}}$
X_i	complex	eq. 20	Analytic signal from receiver i at the input to the despin algorithm.	n/a	nT $\mathrm{Hz}^{-\frac{1}{2}}$
$\overline{X}_i$	complex	eq. 74	Analytic signal of field component i at the output of the despin algorithm.	n/a	nT $\mathrm{Hz}^{-\frac{1}{2}}$
$<\overline{x}_i\overline{x}_j^*>$	complex	eq. 84	Mean cross-spectral matrix in the inertial frame of the ambient plasma	chap. 9	$\mathrm{nT}^2\,\mathrm{Hz}^{-1}$
$<\overline{X}_i\overline{X}_j^*>$	complex	eq. 81	Mean cross-spectral matrix of the signal at the output from the despin.	sect. 9.1	$\mathrm{nT}^2\,\mathrm{Hz}^{-1}$
N_{ij}	complex	eq. 34	The digital analyser output (*i.e.*, the cross-correlation matrix) before logarithmic compression	sect. 9.1	counts
z_{ij}	complex	eq. 32	The normalised cross-spectral matrix.	sect. 9.1.2	none

For the E-field, replace the units nT by V/m
Counts are dimensionless: but the output from the spectrum analyser is always in counts, never $(\mathrm{counts})^{\frac{1}{2}}$

Table 4: The symbols used to represent physical variables

7 Discussion

7.1 Classification of the Terms Contributing to Δ_{ij}

Each element of the matrix Δ_{ij} is the sum of several terms (eq. 26). These different terms can be classified in at least two ways:

Magnitude. This classification is in terms of the order of magnitude (ϵ or ϵ^2) and the periodicity (constant, half or a quarter of the spin period) of the term. It is useful when computing the elements of the matrix Δ_{ij}, especially because it identifies the terms which are negligible and thus need not be computed.

Affinity: This classification is in terms of the relation of the given element to other elements of the matrix Δ_{ij}. This classification is helpful when using of the matrix Δ_{ij} to derive data in physical units, because it simplifies the inversion of eq. 41.

These two schemes of classification overlap: every term in eq. 26 has a magnitude and an affinity (the latter is the same for all terms contributing to the same element of the matrix Δ_{ij}). [15] In the following two subsections we examine these two classifications in more detail. []

7.1.1 Classification by order of magnitude & periodicity

The different terms contributing to Δ_{ij} can be conveniently classified according to their order of magnitude and their periodicity. This shows that in many standard modes of operation many of the terms disappear when the spacecraft spin rate is nominal. [3]

The terms of eq. 26 are divided into three groups, as follows:

1. **First order small terms**. The terms

$$\begin{aligned}\Delta_{ij} &= m_{2c}\left(\epsilon_j^* + \epsilon_i\right) < \overline{x}_i \overline{x}_j^* > \\ &- m_{2s}\left((-)^\ell \epsilon_j^* < \overline{x}_i \overline{x}_\ell^* > + (-)^k \epsilon_i < \overline{x}_k \overline{x}_j^* >\right)\end{aligned}$$

   disappear when integrated over an integral number of half-spin periods, $\delta\phi = n\pi$. This corresponds to an integration time which is a multiple of 2 s when the spacecraft is spinning at the nominal spin rate.

   These terms are written explicitly in Appendix B, section 1.

2. **Second order small terms which are independent of the spacecraft orientation**. The terms

$$\Delta_{ij} = \frac{1}{2}\,\epsilon_i \epsilon_j^* \left[< \overline{x}_i \overline{x}_j^* > + (-)^{(k+\ell)} < \overline{x}_k \overline{x}_\ell^* > \right]$$

   are independent of the spin phase and the integration time. [30]

   These terms were the only ones included in versions of this document up to and including Version 3. Subsequent developments involve changes to the existing computer code; these changes are detailed in Appendix D. [4] Note that the absence of any term $< \overline{x}_k \overline{x}_\ell^* >$ was a error which existed in this document prior to Version 4.

   These terms are written explicitly in Appendix B, section 2.

3. **Second order small terms modulated by spin phase**. The terms

$$\begin{aligned}\Delta_{ij} &= m_{4c}\,\frac{1}{2}\,\epsilon_i\epsilon_j^*\left(<\overline{x}_i\overline{x}_j^*> - (-)^{(k+\ell)}<\overline{x}_k\overline{x}_\ell^*>\right)\\ &- m_{4s}\,\frac{1}{2}\,\epsilon_i\epsilon_j^*\left((-)^{\ell}<\overline{x}_i\overline{x}_\ell^*> + (-)^{k}<\overline{x}_k\overline{x}_j^*>\right)\end{aligned}$$

disappear when integrated over an integral number of quarter-spin periods, $\delta\phi = n\pi/2$. This corresponds to an integration time which is a multiple of 1 s when the spacecraft is spinning at the nominal spin rate.

These terms are written explicitly in Appendix B, section 3.

Of the above three groups, the first is the most significant, both because of its magnitude, and because it seldom averages to zero; and the last is the least important, because it is small, and it averages to zero in normal mode.

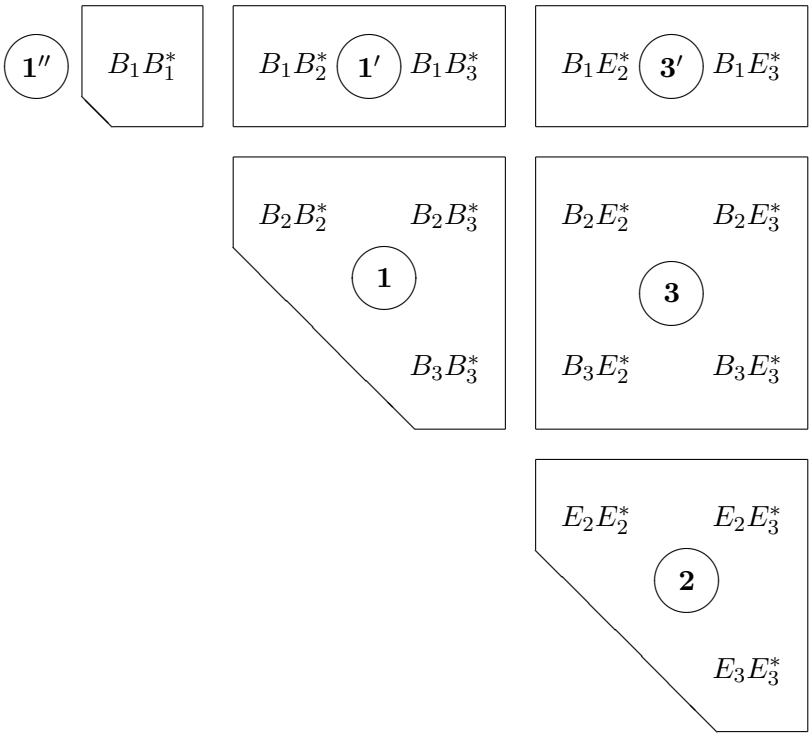

Figure 6: The six independent groups of STAFF-SA matrix elements

7.1.2 Classification by affinity

Examination of the equations of Appendix B shows that shows that the matrix elements can be grouped together so that the members of each group are totally independent of all the other groups. For the purposes of inversion of the matrix (see sections 9.3 and 9.4), these groups can be handled independently. There are six such groups, distributed as shown in Fig. 6. [6]

We choose to combine these six groups to form only three groups for the purpose of provision of logical instruments. The resulting correspondence between logical instrument and affinity group is shown in Table 5. [4]

Logical instrument	**aB**	**acB**	**aE**	**acE**	**cBE**
Affinity group	1	1	2	2	3
Relevant ϵ	ϵ_{Bs}	ϵ_{Bs}	ϵ_{Es}	ϵ_{Es}	ϵ_{Bs} and ϵ_{Es}

Table 5: The affinity groups required by the different logical instruments.

In summary, the various affinity groups are:

Group 1 concerns the purely magnetic logical instruments, **aB** and **acB**. Due to the absence of spin modulation of B_x, this group one has two sub-groups,

- $1'$ and
- $1''$, which is trivial: it concerns only one element which is identically zero, $\Delta_{11} = 0$. [8]

Group 2 concerns the purely electric logical instruments, **aE** and **acE**. Since no component of **E** is measured along the spin axis, this group not sub-divided.

Group 3 concerns the cross electric/magnetic logical instrument, **cEB**, and includes one sub-group,

- $3'$. [6]

7.1.3 Classification by position

It is also useful to separate each category of corrections into the diagonal and the off-diagonal elements of the spectral matrix, because they generally have different integration times. [16]

Diagonal elements

0. S_{11}. Both channels are along the spin-axis. As Cluster has only one spin axis sensor, measuring $x_1 \equiv B_x$, this concerns only one diagonal element, which is not modulated by the spin.

1. S_{ii} for $2 \leq i \leq 5$. The diagonal elements from the spin-plane sensors. These elements are modulated both at twice and at four times the spin frequency.

Off-diagonal elements

2. S_{1i} for $2 \leq i \leq 5$. x_i is along the spin-axis and and x_j is in the spin-plane. In this case the measured cross-spectral matrix is modulated at only twice the spin frequency.

3. S_{23} and S_{45}. x_i and x_j are both in the spin-plane and come from the same pair of sensors, that is, $|i - j| = 1$ and $i + j = 5$ or 9. In this case, the measured cross-spectral matrix is modulated both at twice and also at four times the spin frequency.

4. S_{24} and S_{35}. x_i and x_j are parallel but originate from different pairs of spin-plane sensors ($|i - j| = 2$, with $i + j = 6$ or 8).

5. S_{25} and S_{34}. x_i and x_j are orthogonal and originate from different pairs of spin-plane sensors ($i + j = 7$, with $|i - j| = 1$ or 3).

In addition, the different elements can be grouped according to whether they concern the magnetic field, the electric field, or both electric and magnetic field (for the cross-spectrum). [2]

The different contributions are indicated in Section 7.1.1, and in Appendix B we provide explicit expressions for all the elements of Δ_{ij}. The complete computation of the physical values involves the sum of all contributions. In reality, there are generally few terms which make a significant contribution. In the next section we discuss which contributions must computed for each mode of operation of the experiment. By computing only those contributions which are significant, it is possible to optimise the software execution speed. [7]

7.2 The Calculation of Δ_{ij}

In this section we indicate how to
- identify the elements of Δ_{ij} which must be calculated, and
- decide which terms contribute significantly to the identified elements.

The following procedure can be followed.

1. Decide whether any of the $\mathcal{D}$ are non-zero. This may be done when the calibration coeeficients are loaded from the calibration file when the N1→N2 programme is executed for the first time. If all the coeeficients $\mathcal{D}$ are zero (as is likely to often be the case), then a flag can be set to indicate that no further action is required (because all the $\epsilon_p^{mn}(A_p^m)$ are zero). [5]

2. If corrections are required, use Table 5 to identify the affinity group required for the particular logical instrument(s) being analysed. Note that groups 1 or 3 include all the associated sub-groups: that is, $1'$ and (the trivial) $1''$ with group 1, and $3'$ with group 3.

3. It may be worthwhile to use the last line of Table 5 to check whether there is any non-zero value of $\epsilon_p^{mn}(A_p^m)$ associated with the selected affinity group. It not, no further action is required. [14]

4. Determine whether the spin-rate is sufficiently close to nominal (spin period 4 s) for some of the terms to disappear. This is determined by a logical expression *(still TBD)* which depends upon the telemetered spin period and the magnitude of the largest (?) of the coefficients $\epsilon_p^{mn}(A_p^m)$. If this "near-nominal spin rate" condition is not satisfied, all terms associated with selected affinity group must be evaluated. [4]

5. If the spin rate is (nearly) nominal, many of the terms are (nearly) zero. The near-zero terms which need not be evaluated depend upon the instrument mode of operation, as indicated in Table 6. [11] [10]

7.2.1 Data acquired during a short interval of time

The correction to the approximation (*Label* **sincap**)

$$\operatorname{sinc} \delta\phi = 1 \tag{44}$$

for small values of $\delta\phi$ is less than 0.1%, 1% or 10% respectively for $\delta\phi < 4°$, $14°$ or $45°$. The terms which depend upon $4\delta\phi$ in the expression for Δ_{ij} (eq. 26) are all second order (proportional to $\epsilon_i \epsilon_j^*$) small quantitites and for angles less than about $22.5°$, that is, integration periods up to and including 0.25s, the approximation of eq. 44 is entirely adequate. [11]

Order of magnitude	ϵ	ϵ^2	
Periodicity (s/c rotations)	1/2	none	1/4
Group (of section 7.1.1)	1	2	3
Experiment mode			
normal 1	zero	non-zero	zero
normal 1'b	zero	non-zero	zero
normal 1'e	zero	non-zero	zero
normal 2b	non-zero	non-zero	non-zero
normal 2e	non-zero	non-zero	non-zero
special	zero	non-zero	non-zero
fast 1	non-zero	non-zero	non-zero
fast 2	non-zero	non-zero	non-zero
fast 3b	non-zero	non-zero	non-zero
fast 3e	non-zero	non-zero	non-zero
emergency	zero	non-zero	zero

Table 6: Identification of the terms which average to zero. For each experiment mode of operation, this table indicates the "magnitude" groups which are zero **when the spin rate is nearly nominal**.

8 Observations made with the Despin Algorithm OFF

The onboard digital despin algorithm can be commanded OFF. Then the spin phase, which is normally determined by the experiment via eq. 76, is set to (*Label* **oXOFF**)

$$\phi' \;=\; \text{constant} \;=\; \phi_c \; . \tag{45}$$

ϕ_c will normally be zero, but may be set to some other value *(this is still TBC)*. When $\phi_c = n\pi/2$ there is complete separation of the signals from the y-axis and the z-axis sensors. [7] This can be useful:

1. When one sensor is not functioning correctly, for example, when one of the electric dipoles is being used for Langmuir probe measurements;
2. When observing a source which is not in the inertial frame of reference, but is spinning with the spacecraft. In particular, this is the case for the internal calibration cycle, and also for laboratory tests. The spin OFF mode will also be useful for in-flight check-out, especially when searching for conducted interference.
3. When the instrument is given a high enough telemetry rate, it will be possible to observe the spin modulation of the outputs from the spectrum analyser. This will be useful for direction finding, and also for verification of the analysis performed numerically (in-flight and on the ground) when in the normal (despin ON) modes of operation. [15]

When the despin is OFF, eqs. 18 and 20 give (*c.f.* eq. 74) (*Label* **oC**)

$$\left.\begin{array}{rcl} \overline{X}_i & = & F_i x_i \cos\phi_c - (-)^k F_k x_k \sin\phi_c \\ \overline{X}_j & = & F_j x_j \sin\phi_c + (-)^\ell F_\ell x_\ell \cos\phi_c \end{array}\right\} \tag{46}$$

In the absence of despin this same equation also replaces eq. 77. Therefore, after being averaged, the spectrum analyser output is related directly to the correlation tensor of the field measured in the rotating spacecraft frame of reference, and eq. 84 is replaced by

$$\begin{array}{rcl} < \overline{X}_i \overline{X}_j^* > & = & \left[F_i F_j^* < x_i x_j^* >\right] \cos^2\phi_c \;+\; (-)^{(k+\ell)} \left[F_k^* F_\ell \;< x_k^* x_\ell >\right] \sin^2\phi_c \\ & + & \left[(-)^\ell F_i F_\ell^* < x_i x_\ell^* > + (-)^k F_j^* F_k < x_j^* x_k >\right] \cos\phi_c \, \sin\phi_c \; . \end{array} \tag{47}$$

In principle, this equation can be solved exactly and separately for the three groups 1, 2 and 3 of elements $< x_i x_j^* >$ shown in Fig. 6. But as the calibration model uses (for reasons explained in Section 4.4) the functions $\mathcal{S}_i$ and $\mathcal{D}_i$, we use eqs. 23 and 27 to obtain

$$F_i = \mathcal{S}_i + (-)^i \mathcal{D}_i = \mathcal{S}_i (1 + \epsilon_i) \; . \tag{48}$$

Then the correlator output N_{ij}^{mn} may be expressed in terms of $< x_i x_j^* >$ by eq. 41 (page 27) with $< \overline{x}_i \overline{x}_j^* >$ replaced by $< x_i x_j^* >$, (*Label* **CCS0**)

$$N_{ij}^{mn} \;=\; S_p^m(A_p^m)\; S_q^{m*}(A_q^m)\; \tilde{S}_p^m(f^n)\; \tilde{S}_q^{m*}(f^n) \left(< x_i x_j^* > + \Delta_{ij}^{mn}(A_{Bs}^m, A_{Es}^m) \right) \quad \text{(no sum over } p, q) \tag{49}$$

but with the (small) correction term Δ_{ij} given by the expression (*Label* **Deltaij0**)

$$\Delta_{ij}^{mn}(A_{Bs}^m, A_{Bs}^m) \;=\; TBD \; , \tag{50}$$

(which is totally different from eq. 26). (TBD= To Be Derived ; this expressed is not actually required until the day someone decides to freeze ϕ_c at some value $\phi_c \neq 0$). [2] The value of ϕ_c most likely to be used is the default value [25]

$$\phi_c \;=\; 0 \; ;$$

for which the expression 50 simplifies to

$$\Delta_{ij} \;=\; \left[\, \epsilon_i \;+\; \epsilon_j^* \;+\; \epsilon_i\, \epsilon_j^* \,\right] \;<\; x_i x_j^* \;>\;\; .$$

and eq. 49 is linear. [5]

Note that when the despin is ON the output of STAFF-SA is expressed in terms of the mean of the field components $< \overline{x}_i \overline{x}_j^* >$ measured in an inertial (despun satellite) frame of reference. When the despin is OFF, it is the mean of the field as measured in the spinning "satellite" coordinate system. This is seen by the replacement of $< \overline{x}_i \overline{x}_j^* >$ in eq. 41 by $< x_i x_j^* >$ in eq. 49.

During the period of measurement, the satellite rotates through an angle ϕ which increases continuously from ϕ_1 to ϕ_2 during the integration period.

- If $\delta\phi = \phi_2 - \phi_1$ is $\pi/2$ or greater, then the satellite rotates so much during the period of measurement that the cross-spectral matrix is nearly meaningless; this is precisely why the instrument normally operates with the despin ON. Nevertheless $B_x B_x^*$, $B_y B_y^* + B_z B_z^*$ and $E_y E_y^* + E_z E_z^*$ (the parallel [to the spin axis] and perpendicular magnetic power, and the perpendicular electric power) are invariant under rotation about the x-axis, and so these quantities are valid. [10]

- If $\delta\phi$ is small, say about $\pi/8$ or less, the resulting cross-spectral matrix in satellite coordinates does have some physical meaning; it is obtained in the instantaneous coordinate system of the spacecraft. The mean phase φ (eq. 43) is known, and so this matrix can be rotated about the satellite spin axis to transform it to the standard (despun satellite) coordinate system. [3] Now x_i and x_j are related to $\overline{x}_i$ and $\overline{x}_j$ by (*e.g.*, eq. 73)

$$\begin{aligned} x_i &= \;\; \overline{x}_i \cos\phi + \overline{x}_j \sin\phi \\ x_j &= -\overline{x}_i \sin\phi + \overline{x}_j \cos\phi \end{aligned} \quad ,$$

  as explained in sect. 9.5.3.

The expression 47 is so much simpler than expressions 49 and the complete expression for Δ_{ij} that it may be wondered why the change of variables of eq. 23 was introduced. The reason has already been given in section 4.4. When the despin is ON, the complete solution for $< \overline{X}_i \overline{X}_j^* >$ as a function of $< \overline{x}_i \overline{x}_j^* >$ is intractable when expressed in terms of F_y and F_z. Indeed, the complete expression for $< \overline{X}_i \overline{X}_j^* >$ in terms of $< \overline{x}_i \overline{x}_j^* >$ was never presented in versions of this document up to and including Issue 3, let alone a solution proposed. Apart from the physical support presented in Section 4.4, the introduction of the terms $\mathcal{S}_i$ and $\mathcal{D}_i$ (eq. 23) both simplifies the algebra and provides the small parameter, $\mathcal{D}_i$, in terms of which an iterative solution may be developed. [9]

Nevertheless, just as an exact solution exists for eq. 47 and therefore also for eq. 49, so an exact soluton exists for eqs. 25 and 26. This exact solution, which is algebraically complicated, is discussed in Section 9.4 and Appendix C *(which is still to be finished).* Unless the functions $\mathcal{D}_i$ are known not to be small (in the sense that ϵ_i is not small compared to unity), the iterative solution presented in Section 9.3 is rapid, adequate, and certainly easier to code. [5]

8.1 Signals from Sources Rotating with the Spacecraft

The only sources rotating with the spacecraft of any interest is the signal from the STAFF calibration signal generator used during the internal calibration cycle. There may also be interference generated aboard the spacecraft, but there it no requirement for scientific analysis of such signals.

As signals from sources aboard the spacecraft will not be analysed as part of the routine science data processing, it is possible to use the expressions 47 to determine the functions F_i, as explained in the document OBSPM–TN–0005. The F_i thus determined can be used, when necessary, to determine via eqs. 23 new functions $\mathcal{S}$ and $\mathcal{D}$ for the calibration tables used for the routine data processing.

Note that to determine the transfer functions F_i from either laboratory or in-flight measurements it is essential to run the experiment with despin OFF. [13]

9 Inversion of the Transfer Function

The problem can be stated thus:

- given that the telemetry output as a function of the characteristics of the ambient fields in an inertial coordinate system is given by eq. 102 and the logarithmic compression described in section 5.2,
- how can we calculate the cross-spectral matrix of the ambient fields in inertial coordinates as a function of the telemetry output ?

To study this problem, we treat the digital and analogue inversions separately.

9.1 Logarithmic Decompression of the Digital Output

(*Label* **LDDO**)

9.1.1 Elements on the leading diagonal

The power spectra, that is, the leading diagonal elements of the cross-spectral matrix, are compressed using 5 bits for the exponent e ($0 \leq e \leq 31$) and 3 bits for the mantissa m ($0 \leq m \leq 7$). The value N_{ii} of the analyser output is recovered via the expression (*Label* **Diag**)

$$N_{ii}(p) = 2^{(e-3)} \times (8+m) \quad \text{when} \quad i = j \; . \tag{51}$$

This logarithmic compression algorithm yields a good (± 0.2 dB) approximation to the output from the numerical analyser.

9.1.2 Off-diagonal elements

(*Label* **Ode**)

The non-diagonal elements are obtained by inversion of eq. 32, (*Label* **nonDiag1**)

$$N_{ij} = \sqrt{\overline{N}_{ii}\overline{N}_{jj}} \; z_{ij} \quad \text{when} \quad i \neq j \tag{52}$$

where $\overline{N}_{ii}$ (and similarly $\overline{N}_{jj}$) is the mean of all the values of N_{ii} (as given by eq. 51) acquired during the period of acquisition of the corresponding off-diagonal element; note that the mean values of the diagonal elements, although computed aboard the spacecraft for the purpose of normalisation, are not telemetered to the ground because they are also being telemetered at a higher rate. In eq. 52, (*Label* **nonDiag2**)

$$z_{ij} = x_{ij} + i y_{ij} \tag{53}$$

with x being determined from m_x and the sign bit s_x by (dropping the subscripts ij for simplicity) (*Label* **nonDiag3**)

$$\left.\begin{array}{rcl} x = (-)^{s_x}\, 2^{-9} & \text{for} & m_x = 0 \\ x = (-)^{s_x}\, 2^{-7} & \text{for} & m_x = 1 \\ x = (-)^{s_x}\, 2^{m_x - 7.5} & \text{for} & 2 \leq m_x \leq 7 \end{array}\right\} \tag{54}$$

and similar expressions for y in terms of m_y and s_y.

This compression algorithm for the phase yields a precision of about 5° near the real and imaginary axes, falling to about 10° for phases around ±45° and ±135°. Note that lines of separation between phase quantification bins do not lie exactly along the real and the imaginary axes (which would have been unfortunate), due to the phase shift introduced by the non-simultaneous sampling (section 4).

9.2 The Cross-Spectrum in the Ambient Medium

(*Label* **CSAM**)

The equations of the preceding section allow us to obtain from the telemetry the cross-spectral matrix X_{ij} (in channel n of band m) at the input to the A/D converter. This is related to the cross-spectral matrix of the fields in the ambient medium (in inertial co-ordinates) by eq. 41 (page 27),

$$N_{ij}^{mn} \;=\; S_p^m(A_p^m)\; S_q^{m*}(A_q^m)\; \tilde{S}_p^m(f^n)\; \tilde{S}_q^{m*}(f^n)\; \Big(< \overline{x}_i \overline{x}_j^* >^{mn} \; + \Delta_{ij}^{mn}(A_{Bs}^m) \Big) \quad \text{(no sum over } i,j)$$

where Δ_{ij} is given by eqs. 26 and 27.

The evaluation of Δ_{ij} uses the limits ϕ_1 and ϕ_2 of the range $\phi_1 \le \phi < \phi_2$ of values of ϕ used by STAFF-SA to despin the data aboard the spacecraft (see Appendix A). To calculate ϕ_1 and ϕ_2, the spacecraft spin phase ϕ_s at the corresponding times must be used; this is obtained from the telemetry (using Simon Walker's algorithm). The values be used to calculate the matrix Δ_{ij} are then

$$\phi_1 = \phi_s(t_1) + \phi_0 \quad \text{and} \quad \phi_2 = \phi_s(t_2) + \phi_0 \tag{55}$$

????? Equation **??** *has disappeared 2004/02/03 ?????*
where ϕ_0 is defined by eq. **??**. [9]

For each value of m and n, and using the corresponding value of A_{Bs}^m and the matrices N_{ij}^n, $S_i S_j^*$, $< \overline{x}_i \overline{x}_j^* >$ and Δ_{ij}, eq. 41 may be solved for $< \overline{x}_i \overline{x}_j^* >$ either exactly or iteratively.

The iterative solution (section 9.3) has perhaps the advantage that it is easier to code. It is probably adequate for most applications.

The exact solution (section 9.4) uses the properties of Δ_{ij} to split the matrix into small groups of elements which can be handled separately. [10]

9.2.1 The off-diagonal elements

It has already been noted (section 9.1.2) that for many instrument modes the off-diagonal elements are not sampled as frequently as the diagonal elements. Whatever method of solution is used, iterative or exact, this poses a problem for the inversion of eq. 41.

There is no way to increase the time resolution of the off-diagonal matrix elements to that of the diagonal elements. But it is not desirable to discard information by reducing the time resolution of the diagonal elements to that of the off-diagonal elements. [7]

It is proposed that the equations of Appendix B be used

1. for every value of the diagonal elements, using the values of the off-diagonal elements which were being sampled simultaneously. Thus the same off-diagonal elements may be used for several successive diagonal elements.

2. for every value of the off-diagonal elements, using the average of the values of the diagonal elements obtained during the concurrent period of time. This is analogous to the procedure used to re-normalise the off-diagonal elements. [8]

The validity of the results may be checked as follows. For every value of the diagonal elements obtained during step 1, a different physical value of the off-diagonal elements will be obtained. These values can be compared with the single value of the off-diagonal elements (for the same time interval) obtained obtained during step 2. The differences will be small if the values of ϵ are small. If the differences are not small, then the only conclusion which can be drawn is that the diagonal elements cannot be measured reliably with a time resolution higher than the off-diagonal elements of the cross-spectral matrix. [7]

9.3 The Iterative Solution

This was the first method tried. An attempt to find an exact solution is described in Section 9.4, [3] but in view of the incompleteness of the work it is probably better to use the iterative method. [2]

When Δ_{ij} is small, eqs. 25 and 26 may be solved iteratively, step by step, as follows:

1. The zero order solution neglects Δ_{ij} completely in eq. 25:

$$< \overline{x}_i \overline{x}_j^* >^0 = \frac{1}{\mathcal{S}_i \mathcal{S}_j^*} \; < \overline{X}_i \overline{X}_j^* > \tag{56}$$

2. The r^{th} order ($r \geq 0$) estimation of Δ_{ij}, which we denote by Δ_{ij}^r, is obtained by inserting the the r^{th} order solution $< \overline{x}_i \overline{x}_j^* >^r$ into eq. 26, as described in section 7.2. Note that this step in the iteration procedure introduces coupling between the diagonal and the off-diagonal terms in the cross-spectral matrix. [3]

3. The convergence test of Section 9.3.1 is applied. Note that for testing the zero order solution Δ_{ij}^0 must be derived from eq. 26 in conformity with step 2 of the iteration procedure (*i.e.*, use of the value $\Delta_{ij}^0 = 0$ would nullify the convergence test). [3]

4. The $(r+1)^{\text{th}}$ order solution is then obtained from eq. 25, thus:

$$< \overline{x}_i \overline{x}_j^* >^{(r+1)} = < \overline{x}_i \overline{x}_j^* >^0 - \Delta_{ij}^r \tag{57}$$

(N.B., it really is $< \overline{x}_i \overline{x}_j^* >^0$ which is used.)

5. If the convergence test was negative (*i.e.*, the procedure has not yet converged adequately), the process must be repeated starting from step 2 above; and so on, until adequate accuracy is achieved.

It is easy to show that the iteration process does converge. Suppose that the exact solution is $< \overline{x}_i \overline{x}_j^* >^s$, so that

$$< \overline{x}_i \overline{x}_j^* >^s = < \overline{x}_i \overline{x}_j^* >^0 - \Delta_{ij}^s \; .$$

Subtracting this from eq. 57, the error of the $(r+1)^{\text{th}}$ order solution is

$$< \overline{x}_i \overline{x}_j^* >^{(r+1)} - < \overline{x}_i \overline{x}_j^* >^s = - \left(\Delta_{ij}^r - \Delta_{ij}^s \right) = - \left(< \overline{x}_i \overline{x}_j^* >^{(r+1)} - < \overline{x}_i \overline{x}_j^* >^s \right) \frac{\partial \Delta_{ij}}{\partial < \overline{x}_i \overline{x}_j^* >} \; .$$

If

$$\frac{\partial \Delta_{ij}}{\partial < \overline{x}_i \overline{x}_j^* >} = \mathcal{O}(\epsilon) \; ,$$

then the error of the $(r+1)^{\text{th}}$ order solution is

$$< \overline{x}_i \overline{x}_j^* >^{(r+1)} - < \overline{x}_i \overline{x}_j^* >^s = \mathcal{O}(\epsilon^r) \; .$$

The process converges. [16]

9.3.1 Test for convergence

A criterion for "adequate accuracy" must be established. Comparison of each and every element of the matrix $\Delta_{ij}^{(r+1)} - \Delta_{ij}^{r}$ with the corresponding element of the matrix $< \overline{x}_i \overline{x}_j^* >^r$ is unsatisfactory, because if one (or more) of the elements $< \overline{x}_i \overline{x}_j^* >^r$ is zero convergence will be slow, and possibly non-existent. [4] From eq. 57

$$< \overline{x}_i \overline{x}_j^* >^{(r+1)} \; - \; < \overline{x}_i \overline{x}_j^* >^r = \; - \left(\Delta_{ij}^{r} - \Delta_{ij}^{(r-1)} \right) \; . \tag{58}$$

Thus the test for convergence is that $\left(\Delta_{ij}^{r} - \Delta_{ij}^{(r-1)} \right)$ be small compared with $< \overline{x}_i \overline{x}_j^* >^r$.

What exactly does "small compared with" mean for a tensor quantity ? Eq. 58 can be written

$$< \overline{x}_i \overline{x}_j^* >^{(r+1)} = < \overline{x}_i \overline{x}_k^* >^r \left\{ \delta_{kj} - [< \overline{x}_k \overline{x}_\ell^* >^r]^{-1} \left[\Delta_{\ell j}^{r} - \Delta_{\ell j}^{(r-1)} \right] \right\} \; .$$

The expression in curly brackets is an operator which should be as close to the identity operator δ_{kj} as possible. Introducing the matrix

$$T_{kj} \; = \; [< \overline{x}_k \overline{x}_\ell^* >^r]^{-1} \left[\Delta_{\ell j}^{r} - \Delta_{\ell j}^{(r-1)} \right]$$

Current version

each of the elements T_{kj} must separately satisfy

$$|T_{kj}| \; < \epsilon \; \ll \; 1 \quad \text{for all values of } k, j$$

where ϵ is some suitably small quantity. [6] This condition may be expressed in terms of the adjoint matrix of $< \overline{x}_k \overline{x}_\ell^* >^r$,

$$\left| \frac{\text{adj} \left\{ < \overline{x}_k \overline{x}_\ell^* >^r \right\} \left[\Delta_{\ell j}^{r} - \Delta_{\ell j}^{(r-1)} \right]}{\det \left(< \overline{x}_k \overline{x}_j^* >^r \right)} \right| \; < \; \epsilon \; \ll \; 1 \quad \text{for all values of } k, j \tag{59}$$

or, equivalently, because $\det \left(< \overline{x}_k \overline{x}_j^* >^r \right)$ is real,

$$-\epsilon \; \det \left(< \overline{x}_k \overline{x}_j^* >^r \right) \; < \; \text{adj} \left\{ < \overline{x}_k \overline{x}_\ell^* >^r \right\} \left[\Delta_{\ell j}^{r} - \Delta_{\ell j}^{(r-1)} \right] \; < \; \epsilon \; \det \left(< \overline{x}_k \overline{x}_j^* >^r \right) \quad \text{for all values of } k, j \tag{60}$$

The last three equations are not proper matrix equations because the limits are scalars, not matrices ; each equation applies separately for all allowable values of k and j. The moduli are the moduli of each of the individual elements k, j of the matrix. The condition is global in the sense that the same determinant $\det \left(< \overline{x}_k \overline{x}_j^* >^r \right)$ (which is independent of j and k) is used for testing all the matrix elements k, j.

Proposed new version *The following idea, first conceived in June 1999, has not been implemented as of November 25, 2004.*

the three (real) eigenvalues $\lambda^{(i)}$ of $\delta_{kj} - T_{kj}$ should each be nearly unity, $\left| 1 - \lambda^{(i)} \right| < \epsilon$. Since the eigenvalue equation $(\delta_{kj} - T_{kj})\, x_j = \lambda^{(i)}\, x_j$ may be written $T_{kj}\, x_j = (1 - \lambda^{(i)})\, x_j$, we deduce that the three eigenvalues of the matrix T_{ij} must each be less than ϵ.

The treatment of sub-matrices

We have already noted in Section 7.1.2 that different groups of matrix elements can be identified and treated independently. Therefore the problem of iteration may be considered separately for the elements of the different groups shown in Fig. 6 (page 32). [2]

The elements of groups 1, 2 and 3

These groups of elements form square sub-matrices ; that of group 3 is not Hermitian, but this is unimportant for what follows. [2] The adjoint of a completely general (complex, non-Hermitian) [2] matrix of rank 2 is rather simple,

$$\text{adj}\left\{\begin{pmatrix} a & b \\ c & d \end{pmatrix}\right\} = \begin{pmatrix} d & -b \\ -c & a \end{pmatrix} , \tag{61}$$

and thus we obtain a more rigourous and relatively simple convergence criterion for the elements of these three groups.

Note that, for groups 1, 2 and 3, eq. 59 represents four separate conditions which must all be satisfied, with $\det\left(< \overline{x}_k \overline{x}_j^* >^r\right)$ a determinant which need be evaluated only once. Eq. 59 implies [to understand the derivation of the following equation, it is useful to recall why a matrix of rank r and physical dimension L has an adjoint of dimension L^{r-1} and determinant of dimension L^r] that

$$-\epsilon \ \det\left(< \overline{x}_k \overline{x}_\ell^* >^r\right) \ < \ \det\left(\ \Delta_{\ell j}^r - \Delta_{\ell j}^{(r-1)} \ \right) \ < \ \epsilon \ \det\left(< \overline{x}_k \overline{x}_\ell^* >^r\right) \ .$$

This condition on the determinant $\det\left(\ \Delta_{\ell j}^r - \Delta_{\ell j}^{(r-1)} \ \right)$ is a necessary, but not a sufficient, condition for convergence. But the four conditions of eq. 59 are both necessary and sufficient. Therefore eqs. 61 and 59 (or 60) must be used as a test for convergence.

Can the determinant the matrix $< \overline{x}_k \overline{x}_j^* >^r$ be singular so that $\det\left(< \overline{x}_k \overline{x}_j^* >^r\right) = 0$? In theory it can, if the spin-plane signal is 100 % polarised. In practice, noise will ensure that this condition is unlikely to occur within the flight instrument; but, on the other hand, the rather course resolution of the digital telemetry will allow singularity to occur in the ground data. Therefore $\det\left(< \overline{x}_k \overline{x}_j^* >^r\right)$ must be tested for singularity; when detected, one further iteration should be enough to ensure that $\det\left(< \overline{x}_k \overline{x}_j^* >^r\right)$ is no longer zero. And if it is still zero, the iteration process may be considered to have converged.

It may appear curious that the number of iterations required depends upon the polarisation of the data; this may be explained by the fact that only coherent signals produce a coupling between the orthogonal spin-plane sensors. [15]

With respect to examining separately of each of the elements of $< \overline{x}_k \overline{x}_j^* >$, this method has the advantage of being "global", all elements are considered together. [2] But the criterion is not easy to use, the inversion of a Hermition matrix is computationally quite heavy; but it needs to be done only once, however many iterations are made. Furthermore, the process is simplified by the fact that the complete 5×5 cross- spectral matrix may be decomposed into smaller sub-matrices which may be inverted separately. [5]

Note that once Δ_{ij}^r has been evaluated, it may be used to evaluate $< \overline{x}_i \overline{x}_j^* >^{(r+1)}$ (step 4 of the iteration procedure) to obtain an even better approximation to the exact solution of eq. 25. [25]

The elements of groups 1′ and 3′

The preceding discussion for the square sub-matrices 1, 2 and 3 (see Fig. 6, page 32) must be modified for the elements of the vectors of groups $1'$ and $3'$.

We return to eq. 58 and ask the question : what exactly does "small compared with" mean for a vector quantity ? The answer is simple : the modulus of the correction vector must be small compared to the modulus of the vector being corrected,

$$\left|\Delta^r_{1j} - \Delta^{(r-1)}_{1j}\right| \; < \; \epsilon \left| < \overline{x}_1 \overline{x}^*_j >^r \right| \quad \text{with} \quad \epsilon \ll 1 \; . \tag{62}$$

This condition must be applied separately to group $1'$ ($2 \leq j \leq 3$) and group $3'$ ($4 \leq j \leq 5$). Note that the modulus of an arbitrary complex vector (a_2, a_3) is $\sqrt{a_2 a^*_2 + a_3 a^*_3}$. [10]

9.4 The Exact Solution

We have already noted in Section 7.1.2 that the elements of Δ_{ij} can be grouped together as shown in Fig. 6. Each group is totally independent of all other groups, and therefore eq. 41 can be solved independently for each separate group of elements. This is further discussed in Appendix C. [4]

9.5 Rotation to the Despun Satellite Co-ordinate System

As described in sect. 4.2, the data acquired by the STAFF spectrum analyser are despun digitally before being analysed. The resulting cross-spectral tensor $< \overline{X}_i \overline{X}^*_j >$ is obtained in the inertial co-ordinate system which has its x-axis parallel the O3 axis of the despun satellite system (*i.e.*, the satellite spin axis) and its y-axis at longitude ϕ_0 in the despun satellite system, where the offset ϕ_0 is defined by eq. **??**). *????? Equation* **??** *has disappeared 2004/02/03 ?????*

The despun satellite co-ordinate system is defined such that:

- the O3 axis is the satellite spin axis;
- the O1 axis lies orthogonal to the O3 axis in the plane defined by the O3 axis and the direction of the Sun; and
- the O2 axis is the third mutually orthogonal direction.

This is the quasi-inertial co-ordinate system closest to the satellite co-ordinate system, and is the co-ordinate system through which any satellite data must be transformed (at least in principle) before further transformation to any other inertial system. It is the natural co-ordinate system in which to present the cross-spectral tensor from the STAFF spectral analyser. [15]

It must be possible to represent a complete physical observable in any desired system of reference: in other words, it must be possible to transform the representation of a physical observable to any desired co-ordinate system. When this is possible, the representation of the observable (which we call the logical instrument) is said to be complete. The STAFF Spectrum Analyser produces several logical instruments; due to the absence of an axial component of the electric field, all execpt one of the STAFF-SA logical instruments are incomplete. [6]

9.5.1 Complete Logical Instrument

The logical instrument **acB** is the only complete STAFF-SA logical instrument. Its elements belong to affinity groups 1, $1'$ and $1''$ shown in Fig. 6. To transform from the co- ordinate system in which it is obtained to the co-ordinate system in which it is to be delivered, the cross-spectral tensor must first be rotated through the angle ϕ_0 about the x-axis. The required transformation is

$$< \overline{x}_i \overline{x}^*_j > \quad = \quad R_{ki} < \overline{x}_k \overline{x}^*_\ell > R_{\ell j}$$

[3] where the rotation matrix is (*Label* **rotmat1**)

$$R_{ij} = \begin{pmatrix} 1 & 0 & 0 \\ 0 & \cos\phi_0 & \sin\phi_0 \\ 0 & -\sin\phi_0 & \cos\phi_0 \end{pmatrix} \tag{63}$$

For almost every spinning spacecraft ever built, the O3 axis has been selected as the spin axis, and this convention is used by generic data analysis systems, including ISDAT which is to be used by the Cluster Wave Experiment Consortium. This is the reason why the despun satellite co-ordinate system is defined in the DDID (see reference in sect. 4.2) to have its O3 axis along the spin axis. Due to the orientation chosen for the Cluster spacecraft, this convention has the advantage of making the despun axis O3 aligned quite closely with the O3 axis of certain co-ordinate systems widely used to study magnetospheric phenomena, such as Geocentric Solar Ecliptic and Geocentric Solar Magnetic.

The permutation of axes is performed using the permutation matrix

$$P_{ij} = \begin{pmatrix} 0 & 1 & 0 \\ 0 & 0 & 1 \\ 1 & 0 & 0 \end{pmatrix}$$

It is convenient to combine this transformation with that of eq. 63. Then, the overall transformation to be performed is (*Label* **rot**)

$$< \overline{x}_i \overline{x}_j^* >_{\text{despun satellite}} \quad = \quad T_{ik} < \overline{x}_k \overline{x}_\ell^* > T_{j\ell}[30] \tag{64}$$

[3] [3] with the transformation matrix (*Label* **rotmat**)

$$T_{ij} \;=\; P_{ik} R_{kj} \;=\; \begin{pmatrix} 0 & \cos\phi_0 & \sin\phi_0 \\ 0 & -\sin\phi_0 & \cos\phi_0 \\ 1 & 0 & 0 \end{pmatrix} [6] \tag{65}$$

9.5.2 In-Complete Logical Instruments

In general, these logical instruments cannot be rotated to any other co-ordinate systems. There is, however, an exception: when the rotation is about the axis defined by the missing component.

The different incomplete STAFF-SA logical instruments are listed below, together with the treatment suggested for each of them.

acE: This logical instrument concerns the two-dimensional cross-spectral matrix

$$\begin{pmatrix} < \overline{x}_{Ey} \overline{x}_{Ey}^* > & < \overline{x}_{Ey} \overline{x}_{Ez}^* > \\ < \overline{x}_{Ez} \overline{x}_{Ey}^* > & < \overline{x}_{Ez} \overline{x}_{Ez}^* > \end{pmatrix} \quad ,$$

whose elements belong to the affinity group 2 shown in Fig. 6. This matrix can be rotated using eq. 64 by assigning arbitrary values to $< \overline{x}_{Ex} \overline{x}_{Ex}^* >$, $< \overline{x}_{Ex} \overline{x}_{Ey}^* >$, and $< \overline{x}_{Ex} \overline{x}_{Ez}^* >$. It is easy to show that after the transformation using eq. 64, the matrix elements

$$\begin{pmatrix} < \overline{x}_1 \overline{x}_1^* > & < \overline{x}_1 \overline{x}_2^* > \\ < \overline{x}_2 \overline{x}_1^* > & < \overline{x}_2 \overline{x}_2^* > \end{pmatrix}$$

are independent of the arbitrary values; all the other matrix elements must, of course, then be removed or otherwise invalidated.

Note that for the "arbitrary" values it is often convenient to use the elements with B_x in place of the missing (not measured) E_x; then all the elements of the matrix resulting from the rotation defined by eqs. 64 and 65 are valid, although the resulting matrix is **NOT** a complete logical instrument (see paragraph *e*-**mode** below). [4]

cEB: This logical instrument includes the elements

$$\begin{pmatrix} < \overline{x}_{Bx}\overline{x}^*_{Ey} > & < \overline{x}_{Bx}\overline{x}^*_{Ez} > \\ < \overline{x}_{By}\overline{x}^*_{Ey} > & < \overline{x}_{By}\overline{x}^*_{Ez} > \\ < \overline{x}_{Bz}\overline{x}^*_{Ey} > & < \overline{x}_{Bz}\overline{x}^*_{Ez} > \end{pmatrix} \quad .$$

Its elements belong to affinity groups 3 and $3'$ shown in Fig. 6. This logical instrument can be transformed using eq. 64 by assigning arbitrary values to $< \overline{x}_{Bx}\overline{x}^*_{Ex} >$, $< \overline{x}_{By}\overline{x}^*_{Ex} >$, and $< \overline{x}_{Bz}\overline{x}^*_{Ex} >$. The resulting matrix is correct, except for the elements $< \overline{x}_{B1}\overline{x}^*_{E3} >$, $< \overline{x}_{B2}\overline{x}^*_{E3} >$, and $< \overline{x}_{B3}\overline{x}^*_{E3} >$, that is, the last column of the matrix, which do not form part of the logical instrument.

As for the logical instrument (**acE**) discussed above, it is possible to use the elements with B_x in place of E_x (which is not measured); then the three "arbitrary" matrix elements are $< \overline{x}_{Bx}\overline{x}^*_{Bx} >$, $< \overline{x}_{By}\overline{x}^*_{Bx} >$, and $< \overline{x}_{Bz}\overline{x}^*_{Bx} >$. In this case all the elements of the transformed matrix are valid, including those of of the last row, $< \overline{B}_3\overline{B}^*_1 >$, $< \overline{B}_3\overline{B}^*_2 >$ and $< \overline{B}_3\overline{B}^*_3 >$. But the complete matrix is **not** a complete logical instrument.

(The image of the above elements with respect to the leading diagonal of the 5×5 cross spectral matrix of the magnetic and electric fields (*i.e.*, the complex conjugate of the transpose) contains physically equivalent information. If this matrix is transformed, the resulting matrix is correct except for its last column.)

aB: The auto-spectra $< \overline{x}_{Bx}\overline{x}^*_{Bx} >$, $< \overline{x}_{By}\overline{x}^*_{By} >$, and $< \overline{x}_{Bz}\overline{x}^*_{Bz} >$ of the leading diagonal of the **acB** logical instrument are measured with higher time resolution than the complete **acB** logical instrument. Owing to the absence of the matrix elements $< \overline{x}_{By}\overline{x}^*_{Bz} >$ (and its complex conjugate $< \overline{x}_{Bz}\overline{x}^*_{By} >$) with adequate time resolution, this logical instrument cannot be rotated. Nevertheless, the power densities parallel to and perpendicular to the satellite spin axis are invariant under the rotation of eq 64, and change their subscripts under the permutation of eq. 65, thus:

$$< \overline{x}_{B3}\overline{x}^*_{B3} > \;=\; < \overline{x}_{Bx}\overline{x}^*_{Bx} > \tag{66}$$

$$< \overline{x}_{B1}\overline{x}^*_{B1} > + < \overline{x}_{B2}\overline{x}^*_{B2} > \;=\; < \overline{x}_{By}\overline{x}^*_{By} > + < \overline{x}_{Bz}\overline{x}^*_{Bz} > \tag{67}$$

aE: The auto-spectra $< \overline{x}_{Ey}\overline{x}^*_{Ey} >$ and $< \overline{x}_{Ez}\overline{x}^*_{Ez} >$ of the leading diagonal of the **acE** logical instrument are also measured with higher time resolution than the complete **acE** logical instrument. As for **aB**, this logical instrument cannot be rotated, but the total power density perpendicauler to the spin axis is invariant:

$$< \overline{x}_{E1}\overline{x}^*_{E1} > + < \overline{x}_{E2}\overline{x}^*_{E2} > \;=\; < \overline{x}_{Ey}\overline{x}^*_{Ey} > + < \overline{x}_{Ez}\overline{x}^*_{Ez} > \tag{68}$$

e-**mode**: In the reduced "*e*-field" modes of operation, the entire cross-spectral matrix consists of only nine elements, belonging to affinity groups $1''$, 2 and $3'$, thus

$$\begin{pmatrix} < \overline{x}_{Bx}\overline{x}^*_{Bx} > & < \overline{x}_{Bx}\overline{x}^*_{Ey} > & < \overline{x}_{Bx}\overline{x}^*_{Ez} > \\ < \overline{x}_{Ey}\overline{x}^*_{Bx} > & < \overline{x}_{Ey}\overline{x}^*_{Ey} > & < \overline{x}_{Ey}\overline{x}^*_{Ez} > \\ < \overline{x}_{Ez}\overline{x}^*_{Bx} > & < \overline{x}_{Ez}\overline{x}^*_{Ey} > & < \overline{x}_{Ez}\overline{x}^*_{Ez} > \end{pmatrix} \quad .$$

This incomplete logical instrument has a very particular property: it undergoes the transformation of eq. 64 with matrix 65 as if it were a tensor quantity which, of course, it is not. The reason is that the transformation described by eq. 65 consists of:

- a rotation about the x-axis with the y and z components of the electric field both being measured (and the z component of the magnetic field remains unchanged);
- a permutation of axes.

After rotation by eqs. eq. 64 and 65 the tensor is

$$\begin{pmatrix} <\overline{E}_1\overline{E}_1^*> & <\overline{E}_1\overline{E}_2^*> & <\overline{E}_1\overline{B}_3^*> \\ <\overline{E}_2\overline{E}_1^*> & <\overline{E}_2\overline{E}_2^*> & <\overline{E}_2\overline{B}_3^*> \\ <\overline{B}_3\overline{E}_1^*> & <\overline{B}_3\overline{E}_2^*> & <\overline{B}_3\overline{B}_3^*> \end{pmatrix} \quad ;$$

all elements of this matrix are valid.

Note, however, that a rotation about any other axis is totally impossible for this mixed matrix, which therefore must **NEVER** be treated as one complete logical instrument, but rather as three separate incomplete ones. [24]

9.5.3 Despin OFF

As mentioned in sect. 8, the cross-specral matrix can be determined when the despin algorithm is OFF, and if the angle $\delta\phi$ through which the spacecraft spins during calculation of the cross-spectral matrix is not too large, say about $\pi/8$ or less, it is possible to relate the experimentally dtermined matrix to the matrix in an intertial system of reference.

In fact, all the equations of the preceding section can be used. However, to take account of the mean orientation of the spacecraft during the period of observation, it is necessary to replace everywhere (in sect. 9.5.2) the angle ϕ_0 by the angle $\phi_0 \pm \varphi$, where φ is defined by eq. 43. [10] *The sense (positive or negative) of the sign $\pm$ will be determined within the next few days.*

9.5.4 Methodology

The 5×5 spectral matrix

$$\begin{pmatrix} <\overline{B}_x\overline{B}_x^*> & <\overline{B}_x\overline{B}_y^*> & <\overline{B}_x\overline{B}_z^*> & - & <\overline{B}_x\overline{E}_y^*> & <\overline{B}_x\overline{E}_z^*> \\ <\overline{B}_y\overline{B}_x^*> & <\overline{B}_y\overline{B}_y^*> & <\overline{B}_y\overline{B}_z^*> & - & <\overline{B}_y\overline{E}_y^*> & <\overline{B}_y\overline{E}_z^*> \\ <\overline{B}_z\overline{B}_x^*> & <\overline{B}_z\overline{B}_y^*> & <\overline{B}_z\overline{B}_z^*> & - & <\overline{B}_z\overline{E}_y^*> & <\overline{B}_z\overline{E}_z^*> \\ & & & & & \\ - & - & - & - & - & - \\ <\overline{E}_y\overline{B}_x^*> & <\overline{E}_y\overline{B}_y^*> & <\overline{E}_y\overline{B}_z^*> & - & <\overline{E}_y\overline{E}_y^*> & <\overline{E}_y\overline{E}_z^*> \\ <\overline{E}_z\overline{B}_x^*> & <\overline{E}_z\overline{B}_y^*> & <\overline{E}_z\overline{B}_z^*> & - & <\overline{E}_z\overline{E}_y^*> & <\overline{E}_y\overline{E}_z^*> \end{pmatrix} \tag{69}$$

contains the complete output from one frequency channel of the spectrun analyser. The dashes indicate elements which would complete the matrix if the E_x component were measured. After despin and permutation of axes, this matrix becomes, in despun satellite co-ordinates,

$$\begin{pmatrix} <\overline{B}_1\overline{B}_1^*> & <\overline{B}_1\overline{B}_2^*> & <\overline{B}_1\overline{B}_3^*> & <\overline{B}_1\overline{E}_1^*> & <\overline{B}_1\overline{E}_2^*> & - \\ <\overline{B}_2\overline{B}_1^*> & <\overline{B}_2\overline{B}_2^*> & <\overline{B}_2\overline{B}_3^*> & <\overline{B}_2\overline{E}_1^*> & <\overline{B}_2\overline{E}_2^*> & - \\ <\overline{B}_3\overline{B}_1^*> & <\overline{B}_3\overline{B}_2^*> & <\overline{B}_3\overline{B}_3^*> & <\overline{B}_3\overline{E}_1^*> & <\overline{B}_3\overline{E}_2^*> & - \\ & & & & & \\ <\overline{E}_1\overline{B}_1^*> & <\overline{E}_1\overline{B}_2^*> & <\overline{E}_1\overline{B}_3^*> & <\overline{E}_1\overline{E}_1^*> & <\overline{E}_1\overline{E}_2^*> & - \\ <\overline{E}_2\overline{B}_1^*> & <\overline{E}_2\overline{B}_2^*> & <\overline{E}_2\overline{B}_3^*> & <\overline{E}_2\overline{E}_1^*> & <\overline{E}_2\overline{E}_2^*> & - \\ - & - & - & - & - & - \end{pmatrix} . \tag{70}$$

Note that the component $< \overline{B}_x \overline{B}_x^* > = < \overline{B}_3 \overline{B}_3^* >$ is along the spin-axis; it is the only component whose value is not affected by rotation about the spin axis; but its position in the matrix is changed by the permutation of axes.

The rotation of the different logical instruments discussed in the preceding section can be handled simultaneously if the "missing" row and column (represented by dashes) in matrix 69 are replaced respectively by the first row and the first column, thus

$$\begin{pmatrix} < \overline{B}_x \overline{B}_x^* > & < \overline{B}_x \overline{B}_y^* > & < \overline{B}_x \overline{B}_z^* > & < \overline{B}_x \overline{B}_x^* > & < \overline{B}_x \overline{E}_y^* > & < \overline{B}_x \overline{E}_z^* > \\ < \overline{B}_y \overline{B}_x^* > & < \overline{B}_y \overline{B}_y^* > & < \overline{B}_y \overline{B}_z^* > & < \overline{B}_y \overline{B}_x^* > & < \overline{B}_y \overline{E}_y^* > & < \overline{B}_y \overline{E}_z^* > \\ < \overline{B}_z \overline{B}_x^* > & < \overline{B}_z \overline{B}_y^* > & < \overline{B}_z \overline{B}_z^* > & < \overline{B}_z \overline{B}_x^* > & < \overline{B}_z \overline{E}_y^* > & < \overline{B}_z \overline{E}_z^* > \\ & & & & & \\ < \overline{B}_x \overline{B}_x^* > & < \overline{B}_x \overline{B}_y^* > & < \overline{B}_x \overline{B}_z^* > & < \overline{B}_x \overline{B}_x^* > & < \overline{B}_x \overline{E}_y^* > & < \overline{B}_x \overline{E}_z^* > \\ < \overline{E}_y \overline{B}_x^* > & < \overline{E}_y \overline{B}_y^* > & < \overline{E}_y \overline{B}_z^* > & < \overline{E}_y \overline{B}_x^* > & < \overline{E}_y \overline{E}_y^* > & < \overline{E}_y \overline{E}_z^* > \\ < \overline{E}_z \overline{B}_x^* > & < \overline{E}_z \overline{B}_y^* > & < \overline{E}_z \overline{B}_z^* > & < \overline{E}_z \overline{B}_x^* > & < \overline{E}_z \overline{E}_y^* > & < \overline{E}_y \overline{E}_z^* > \end{pmatrix} . \quad (71)$$

Three of the four sub-matrices are inhomogeneous (B_x replaces E_x in some elements) but nevertheless, because it represents a rotation about the x-axis (plus a permutation of the axes), the transformation represented by eq. 65 can be applied separately to the four 3×3 sub-matrices. The result is the 6×6 matrix

$$\begin{pmatrix} < \overline{B}_1 \overline{B}_1^* > & < \overline{B}_1 \overline{B}_2^* > & < \overline{B}_1 \overline{B}_3^* > & < \overline{B}_1 \overline{E}_1^* > & < \overline{B}_1 \overline{E}_2^* > & < \overline{B}_1 \overline{B}_3^* > \\ < \overline{B}_2 \overline{B}_1^* > & < \overline{B}_2 \overline{B}_2^* > & < \overline{B}_2 \overline{B}_3^* > & < \overline{B}_2 \overline{E}_1^* > & < \overline{B}_2 \overline{E}_2^* > & < \overline{B}_2 \overline{B}_3^* > \\ < \overline{B}_3 \overline{B}_1^* > & < \overline{B}_3 \overline{B}_2^* > & < \overline{B}_3 \overline{B}_3^* > & < \overline{B}_3 \overline{E}_1^* > & < \overline{B}_3 \overline{E}_2^* > & < \overline{B}_3 \overline{B}_3^* > \\ & & & & & \\ < \overline{E}_1 \overline{B}_1^* > & < \overline{E}_1 \overline{B}_2^* > & < \overline{E}_1 \overline{B}_3^* > & < \overline{E}_1 \overline{E}_1^* > & < \overline{E}_1 \overline{E}_2^* > & < \overline{E}_1 \overline{B}_3^* > \\ < \overline{E}_2 \overline{B}_1^* > & < \overline{E}_2 \overline{B}_2^* > & < \overline{E}_2 \overline{B}_3^* > & < \overline{E}_2 \overline{E}_1^* > & < \overline{B}_2 \overline{E}_2^* > & < \overline{E}_2 \overline{B}_3^* > \\ < \overline{B}_3 \overline{B}_1^* > & < \overline{B}_3 \overline{B}_2^* > & < \overline{B}_3 \overline{B}_3^* > & < \overline{B}_3 \overline{E}_1^* > & < \overline{B}_3 \overline{E}_2^* > & < \overline{B}_3 \overline{B}_3^* > \end{pmatrix} . \quad (72)$$

All elements are correct. The last row and the last column are respectively equal to the third row and the third column.

This transformations is equivalent to rotating matrix 71 using a 6×6 rotation matrix which has the 3×3 matrix of eq. 65 at each of its four corners. It is even possible to modify such a 6×6 rotation matrix to allow transformation of magnetic fields into electric fields if the rotation becomes relativistic. But the Cluster spacecraft will disintegrate first !

10 Application of the Transfer Function

This section summarises the procedure which will apply the equations and coefficients described in the preceding sections to the conversion of the data from level 1 (telemetry units) to level 2 (physical units). It describes step-by-step the algorithm which must be coded to realise the procedure.

1. Acquire one packet of STAFF-SA data.
2. Decompress the elements of the leading diagonal of the cross-spectral matrix using the expression 51 or, equivalently, use a 256-point look-up table.
3. Decompress the off-diagonal elements of the cross-spectral matrix, using eq. 54 for the decompression, then eq. 53 to assemble the complex value; alternatively (and probably better), a look-up table can be used to determine the corresponding 256 complex values..
4. Compute the average values of the diagonal elements of the cross-spectral matrix during the period of acquistion of the off-diagonal elements.
5. Renormalize the off-diagonal elements, using eq. 52, where N_{ii} and N_{jj} are the average values just calculated. (See section 9.1.2 for an explanation.)

We now have the numerical output from the digital analyser as it was before being compressed for the telemetry, that is, the matrix elements $< \overline{X}_i \overline{X}_j^* >$. In addition, we have the diagonal elements $< \overline{X}_i \overline{X}_i^* >$ (the power spectra) which are telemetered at higher time resolution.

6. Assemble the data into the different logical instruments. Note that the diagonal elements of the cross-spectral matrix are the average values calculated at step 4 above; the telemetered of the diagonal elements are sampled more rapidly, and form a separate logical instrument.

We now convert the data in each of these logical instruments into physical units, solving eq. 41. But before doint this, it is necessary to test the appliction (on-board) of the despin algorithm.

7. Verify that the flag indicates that the onboard despin algorithm is ON; if not, proceed to step 16.
8. Compute the phase angles ϕ_1 and ϕ_2 at the beginning and end of the integration interval, using eq. 55. [2]
9. Identify which of the elements of $\mathcal{S}_i \mathcal{S}_j^*$ and Δ_{ij} are involved (*i.e.*, decide for which values of i and j the calculations are to be performed), as described in section 7.2.

For each value of m and of n,

10. Use eqs. 27, 35, and the tables of calibration coefficients (see section 6.4) to compute the $\epsilon_i^{mn}(A_p^m)$ for the required values of i (the parameter H^n disappears from the ratio).
11. Use the procedure of section 7.2 and, if necessary, Table 6 to compute the different elements of $\Delta_{ij}^{mn}(A_{Bs}^m)$. [2]
12. For all the elements of the logical instrument being processed, use $< \overline{X}_i \overline{X}_j^* >$ and the equations of sect. 9.3 or method of sect. 9.4 to derive $< \overline{x}_i \overline{x}_j^* >$ in physical units in an inertial (non-spinning) reference system.

Repeat steps 9 through 11 for all values of m and n. Then:

13. Rotate (for all values of m and n) the resulting tensors $< \overline{x}_i \overline{x}_j^* >$ through an angle of ϕ_0 about the spin axis to bring them to the despun spacecraft reference frame, [2] and permute the axes as explained in sect. 9.5. [2]

14. Output the results as one record for the logical instruments being processed.

For the AGC logical instrument,

15. the spectral power density is determined from eqs. 10 and 39.

The following sequence is used when the on-board despin algorithm is OFF. The fields are then evaluated in the (spinning) spacecraft coordinate system (see section 9.5.3). [2]

16. When the despin is OFF, the fields are ?????

11 Calibration Procedures

The section concerns the interface to the WEC data processing system. *It has not been revised for Versions 4.*

11.1 Routine Processing

Input : the necessary AGC words and the corresponding n digital analyser data telemetry words.

Output: the number of values of the spectral density in physical units corresponding to the logical instrument required.

The calibration procedure will be applied when processing the data from level 1 to level 2. The processing the data from level 1 to level 2 includes two important operations: conversion into physical units, and complete separation into logical instruments. Exactly how these operations will be performed is still *TBD*.

11.2 Insertion of New Calibration Tables

Input : The tables of STAFF calibration coefficients. These tables will be received in a standard format as specified in the *TBD* document, and implanted in the STAFF server using a standard procedure described in the *TBD* document. These tables will be produced by the CSPI and distributed by the CTM.

Output: none.

11.3 Determination of the Calibration Updates

This will be performed in the CSPI.

12 References

1. "WEC Timing", ref. CL–DWP–TN–0002, Issue 0, Rev. 3, dated 1998 December 01
2. "WEC/ISDAT Coordinate Transformations", ref. CWD–OBSPM–DD–002, the Issue 1, Rev. 1, dated 1995 March 24.
3. "Data Delivery Interface Document" (DDID), CL–ESC–ID–2001, Issue 3, dated 2000 May 19.

APPENDIX 1

Cross-References to Technical Notes TN-0005, TN–0006 and TN–0007

This document is one of a series, which includes

TN–0001 STAFF Spectrum Analyser : Conversion of the Science Data to Physical Units, by C.C. Harvey, M. Belkacemi, R. Manning, F. Wouters and Y. de Conchy. This paper. The description of the calibration model.

TN–0005 STAFF Spectrum Analyser : Derivation of the Calibration Coefficients, by C.C. Harvey, Y. de Conchy, F. Wouters and L. Sitruk. The description of a procedure to determine the calibration coefficients introduced in the model of TN–0001.

TN–0006 STAFF Spectrum Analyser : Laboratory Measurements to Determine the Calibration Coefficients, by Y. de Conchy and C.C. Harvey. Laboratory measurements performed on the flight units and the subsequent analysis leading to the calibration coefficients as supplied at the time of launch.

TN–0007 STAFF Spectrum Analyser : In-flight validation of the Calibration Coefficients, by Y. de Conchy, R. Manning and C.C. Harvey. Description of the in-flight calibration cycle, its analysis, and the resulting corrected values of the calibration coefficients used during the mission.

There are frequent cross-references between these four documents. To handle these cross-references automatically and reliably (although not in the most convenient way for the reader) without making too large an investment in LaTeX programming, the following procedure has been adopted. A list has been produced of all inter-paper cross-references. This file is processed separately by each of the four LaTeX source codes in a list-making environment ; thus, Appendix 1 of each paper contains a numbered list of the cross-references, the numbering being identical. Using this and the other information provided in the appendices, it is possible to trace the appropriate cross-reference.

The reference numbers below, as well as the descriptions of the items, are common to this appendix and the corresponding appendices of papers OBSPM–TN–0005, OBSPM–TN–0006 and OBSPM–TN–0007.

Note that equations or sections with **reference number ¿1000** are simply equations or sections which occur in other papers of the series, but which **are not cited** in this paper. [2]

Ref 1. X_i is expressed in terms of x_i by eq. 6 of this paper

Ref 2. The separation of variables $F_i^m(f^n, A_i^m) = P_i^m(f^n) \times Q_i^m(A_i^m)$ is introduced by eq. 9 of this paper

Ref 3. The despin algorithm and its consequences are described in Sect. 4 of this paper

Ref 4. The sum and difference functions $\mathcal{S}_i^m(f^n, A_i^m)$ and $\mathcal{D}_i^m(f^n, A_i^m)$ are defined by eq. 23 of this paper

Ref 5. The axial function F_{Bx}^m, P_{Bx}^m and Q_{Bx}^m are expressed in terms of $\mathcal{S}_{Bx}$, S_{Bx} and $\tilde{S}_{Bx}$ by eq. 36 of this paper

Ref 6. The separation of the spin-plane variables is described in Sect. 6.1.1 of this paper

Ref 7. In particular, the separation of the variables

$$\mathcal{S}_i^m(f^n, A_i^m) = \frac{1}{H^n}\, S_i^m(A_i^m) \times \tilde{S}_i^m(f^n) \quad \text{and} \quad \mathcal{D}_i^m(f^n, A_i^m) = \frac{1}{H^n}\, D_i^m(A_i^m) \times \tilde{D}_i^m(f^n)$$

is defined by eq. 38 of this paper

Ref 8. The overall (analogue+digital) receiver response is given by eq. 41 of this paper

Ref 9. The matrix Δ_{ij} is defined by eq. 26 of this paper

Ref 10. The small parameters ϵ_p^m are defined by eq. 27 of this paper

Ref 11. The indices p and q are determined by eq. 37 of this paper

Ref 12. The Physical Significance of $S_p^m(A_p^m)$ and $\tilde{S}_p^m(f^n)$ is described in Sect. 6.3 of this paper

Ref 13. The Complete Set of Calibration Coefficients is described in Sect. 6.4 of this paper

Ref 14. The value of $|Q_{Bx}^m(A_{Bx}^m)|$ is determined by eq. 10 of this paper

Ref 15. The relation between N_{ij}^n and $< \overline{X}_i \overline{X}_j^* >$ is eq. 30 of this paper

Ref 16. The expression for $< \overline{X}_i \overline{X}_j^* >$ when the despin is OFF is eq. 47 of this paper

Ref 17. The non-diagonal elements are normalised in eq. 53 of this paper

Ref 18. The two options for separating the variables are compared in Appendix D of this paper

Ref 19. The computation of Δ_{ij} is detailed in Appendix B of this paper

Ref 20. The digital receiver spectral passband characteristic is introduced in Sect. 5.1 of this paper

Ref 21. A method (*now [November 25, 2004] replaced by method of TN–0005)* to determine $Q_{Bx}^m(A_{Bx}^m)$ is proposed in eq. 16 of this paper

Ref 22. The phase of the Q_i^m functions is discussed in Sect. 2.5.1 of this paper

Ref 23. The logarithmic decompression of the digital output is described in Sect. 9.1 of this paper

Ref 24. The expression for N_{ij} in terms of $< \overline{x}_i \overline{x}_j^* >$ is given by eq. 34 of this paper

Ref 25. The Complete Calibration Model is described in Sect. 6 of this paper

Ref 26. The analysis of the cross-spectral matrix is described in Sect. 1001 as explained in Paper TN–0005

Ref 27. A determination of S_{Bx}^m and S_{Bs}^m is provided by eq. 1002 as explained in Paper TN–0005

Ref 28. Determination of the Variation with Frequency is described in Sect. 1003 as explained in Paper TN–0005

Ref 29. $\mathcal{I}m\{S^m_{Bs}(A^m_{Bs\,\mathrm{ref}})\}$ is put equal to zero by eq. 1004 as explained in Paper TN–0005

Ref 30. $\tilde{S}^m_{Bx}(f_n)$ is determined via eq. 1005 as explained in Paper TN–0005

Ref 31. The function $\tilde{S}^m_{Bx}(f_n)$ is defined to be real in Sect. 1006 as explained in Paper TN–0005

Ref 32. $\tilde{S}^m_{Bs}(f^n)$ and $\tilde{D}^m_{Bs}(f_n)$ are determined via eq. 1007 as explained in Paper TN–0005

Ref 33. Determination of the Variation with AGC level is described in Sect. 1008 as explained in Paper TN–0005

Ref 34. The coefficients V^m_{Bx}, V^m_{Bs} and V^m_{Es} are defined by eq. 1010 as explained in Paper TN–0005

Ref 35. The "sensor modified" $S'^m_p(A^m_p)$ is given by eq. 1011 as explained in Paper TN–0005

Ref 36. The "sensor modified" $D'^m_p(A^m_p)$ is given by eq. 1012 as explained in Paper TN–0005

Ref 37. The "sensor modified" $\tilde{S}'^n_{Bx}$ is given by eq. 1013 as explained in Paper TN–0005

Ref 38. The "sensor modified" $\tilde{S}'^n_p$ and $\tilde{D}'^n_p$ are given by eq. 1014 as explained in Paper TN–0005

Ref 39. The in-flight calibration cycle is documented in Sect. 1015 as explained in Paper TN–0007

Ref 40. The in-flight determination of the calibration coefficients is explained in Chap. 1009 as explained in Paper TN–0007

A The Effects of the Spin on the Cross-Spectral Matrix

Let $\overline{x}_i$ and $\overline{x}_j$ denote the two spin-plane field components in the despun satellite coordinate system, which is an inertial system with O1 along the spin axis (which, incidentally, is close to the **south** ecliptic pole), and O2 axis in the plane containing O1 and the direction of the Sun. The spinning antenna measures the fields (*Label* **ox**)

$$\left.\begin{array}{rcl} x_i &=& \overline{x}_i \cos\phi'' + \overline{x}_j \sin\phi'' \\ x_j &=& -\overline{x}_i \sin\phi'' + \overline{x}_j \cos\phi'' \end{array}\right\} \tag{73}$$

where $\phi'' = \phi + 45°$ is the phase angle of the E_y antenna, ϕ being the spin phase as defined in Issue 3 of the DDID (see Section 4.3), and 45° the offset between the WEC E_y-axis and the spacecraft y-axis (see Fig. 4, page 15). In eq. 73, $i = 2$ or 4, and $j = i + 1$.

After de-spin, the inputs to the digital part of the STAFF spectrum analyser are, from eqs. 18 and 20, (*Label* **oX**)

$$\left.\begin{array}{rcl} \overline{X}_i &=& F_i x_i \cos\phi' - F_j x_j \sin\phi' \\ \overline{X}_j &=& F_i x_i \sin\phi' + F_j x_j \cos\phi' \end{array}\right\} \tag{74}$$

where ϕ' is the angle through which the spacecraft has rotated since the time $T_{\rm SRP}$ of the Sun Reference Pulse. Combining with eqs. 73,

$$\begin{array}{rcl} \overline{X}_i &=& (\overline{x}_i \cos\phi'' + \overline{x}_j \sin\phi'')F_i \cos\phi' + (\overline{x}_i \sin\phi'' - \overline{x}_j \cos\phi'')F_j \sin\phi' \\ \overline{X}_j &=& (\overline{x}_i \cos\phi'' + \overline{x}_j \sin\phi'')F_i \sin\phi' - (\overline{x}_i \sin\phi'' - \overline{x}_j \cos\phi'')F_j \cos\phi'. \end{array}$$

Re-arranging, we obtain the following expressions for the (despun) spin-plane signals at the input to the digital analyser in terms of the ambient spin-plane field components in inertial co-ordinates:

$$\begin{array}{rcllcl} \overline{X}_i &=& \overline{x}_i(F_i \cos\phi'' \cos\phi' + F_j \sin\phi'' \sin\phi') &+& \overline{x}_j(F_i \sin\phi'' \cos\phi' F_j \cos\phi'' \sin\phi') \\ \overline{X}_j &=& \overline{x}_j(F_i \sin\phi'' \sin\phi' + F_j \cos\phi'' \cos\phi') &+& \overline{x}_i(F_i \cos\phi'' \sin\phi' F_j \sin\phi'' \cos\phi') \end{array} \tag{75}$$

The value of ϕ' determined from eq. 19 is $\phi' = \phi - \phi_{\rm SRP}$, so that (*Label* **spnclk**)

$$\phi'' - \phi' = \phi_0 = \phi_{\rm SRP} + 45° = 18.8° \; . \tag{76}$$

where we have used the value $\phi_{\rm SRP} = 333.8°$ mentioned in Section 4.3.

Point reached 2004/02/03 ; continue from here

For convenience, we put $\phi_0 = 0$: this causes the derived cross-spectral matrix (eqs. 80, 81, and 83, 84) to be in a coordinate system rotated by ϕ_0 with respect to the despun satellite coordinate system (section 4.2). With $\phi' = \phi$, eqs. 75 simplify to (*Label* **XxX**)

$$\left.\begin{array}{rcllcl} \overline{X}_i &=& \frac{1}{2}(F_i + F_j)\,\overline{x}_i &+& \frac{1}{2}(F_i - F_j)\,(\overline{x}_i \cos 2\phi + \overline{x}_j \sin 2\phi) \\ \overline{X}_j &=& \frac{1}{2}(F_i + F_j)\,\overline{x}_j &-& \frac{1}{2}(F_i - F_j)\,(\overline{x}_j \cos 2\phi - \overline{x}_i \sin 2\phi) \end{array}\right\} \tag{77}$$

(remember, $i = 2$ or 4 and $j = i + 1$). We note that if $F_j = F_i$ these expressions reduce to $\overline{X}_i = \overline{x}_i F_i$ and $\overline{X}_j = \overline{x}_j F_i$ for all ϕ. However, when $F_j \neq F_i$, as is generally the case, they give

$$\begin{array}{rcccl} \overline{X}_i = \overline{x}_i F_i & \text{and} & \overline{X}_j = \overline{x}_j F_j & \text{for} & \phi = 0 \\ \text{and } \overline{X}_i = \overline{x}_i F_j & \text{and} & \overline{X}_j = \overline{x}_j F_i & \text{for} & \phi = \pi/2 \;\; ; \end{array}$$

every quarter of a revolution the analogue transfer functions are completely interchanged between pairs of spin-plane components. Furthermore, when $\phi = 45°$,

$$\begin{aligned} \overline{X}_i &= \overline{x}_i \frac{1}{2}(F_i + F_j) + \overline{x}_j \frac{1}{2}(F_i - F_j) \\ \overline{X}_j &= \overline{x}_j \frac{1}{2}(F_i + F_j) + \overline{x}_i \frac{1}{2}(F_i - F_j) \; . \end{aligned}$$

Any difference $F_i - F_j$ in gain causes each of the despun spin-plane signals to be "contaminated" by the mutually orthogonal spin-plane component. It is this coupling of the spin-plane components which is responsible for the complexity of the equations which follow.

The cross-spectral matrix elements are computed using signals coming either from the same pair of spin-plane sensors (magnetic/magnetic or electric/electric), or from different pairs of spin-plane sensors (magnetic/electric). In the latter case four different analogue receivers are used simultaneously to determine one cross-spectral matrix element. To take account of this, we re-write eqs. 77 as (*Label* **XixXj**)

$$\left.\begin{aligned} \overline{X}_i &= \mathcal{S}_i\, \overline{x}_i + \mathcal{D}_i \left(\overline{x}_i \cos 2\phi - (-)^k \overline{x}_k \sin 2\phi \right) \\ \overline{X}_j &= \mathcal{S}_j\, \overline{x}_j + \mathcal{D}_j \left(\overline{x}_j \cos 2\phi - (-)^\ell\, \overline{x}_\ell \sin 2\phi \right) \end{aligned}\right\} \tag{78}$$

where (eq. 23)

$$\begin{aligned} \mathcal{S}_i &= \tfrac{1}{2}\,(F_i + F_k) \quad \text{and} \quad \mathcal{D}_i = \tfrac{1}{2}\,(F_i - F_k) \\ \mathcal{S}_j &= \tfrac{1}{2}\,(F_j + F_\ell) \quad \text{and} \quad \mathcal{D}_j = \tfrac{1}{2}\,(F_j - F_\ell) \quad , \end{aligned} \tag{79}$$

with k and ℓ defined by (eq. 22)

$$\begin{aligned} &k = 5 - i \quad \text{and} \quad \ell = 5 - j \quad \text{for} \quad 2 \le i, j \le 3 \quad \text{(magnetic sensors)} \\ &k = 9 - i \quad \text{and} \quad \ell = 9 - j \quad \text{for} \quad 4 \le i, j \le 5 \quad \text{(electric sensors)} \; . \end{aligned}$$

The first of eqs. 78 corresponds to **both** of eqs. 77. The second equation is entirely equivalent to the first and will be used whenever a second field component is required to construct the cross-spectral matrix.

From eqs. 78 we obtain the following expressions for the instantaneous cross-spectral matrix: (*Label* **Corr5**) (*Label* **Corr6**)

$$\overline{X}_1 \overline{X}_i^* = \mathcal{S}_1 \mathcal{S}_i^*\, \overline{x}_1 \overline{x}_i^* + \mathcal{S}_1 \mathcal{D}_i^* \left[\overline{x}_1 \overline{x}_i^* \cos 2\phi - (-)^k\, \overline{x}_1 \overline{x}_k^* \sin 2\phi \right] \tag{80}$$

$$\begin{aligned} \overline{X}_i \overline{X}_j^* &= \mathcal{S}_i \mathcal{S}_j^*\, \overline{x}_i \overline{x}_j^* + \frac{1}{2}\, \mathcal{D}_i \mathcal{D}_j^* \left[\overline{x}_i \overline{x}_j^* + (-)^{(k+\ell)}\, \overline{x}_k \overline{x}_\ell^* \right] \\ &+ \left(\mathcal{S}_i \mathcal{D}_j^* + \mathcal{D}_i \mathcal{S}_j^* \right) \overline{x}_i \overline{x}_j^* \cos 2\phi - \left((-)^\ell \mathcal{S}_i \mathcal{D}_j^*\, \overline{x}_i \overline{x}_\ell^* + (-)^k \mathcal{D}_i \mathcal{S}_j^*\, \overline{x}_k \overline{x}_j^* \right) \sin 2\phi \\ &+ \frac{1}{2}\, \mathcal{D}_i \mathcal{D}_j^* \left[\left(\overline{x}_i \overline{x}_j^* - (-)^{(k+\ell)} \overline{x}_k \overline{x}_\ell^* \right) \cos 4\phi - \left((-)^\ell \overline{x}_i \overline{x}_\ell^* + (-)^k \overline{x}_k \overline{x}_j^* \right) \sin 4\phi \right] \end{aligned} \tag{81}$$

We note that:

1. In view of eq. 23, namely

$$\begin{aligned} \mathcal{S}_2 &= \mathcal{S}_3 = \mathcal{S}_{Bs} \\ \mathcal{D}_2 &= -\mathcal{D}_3 = \mathcal{D}_{Bs} \end{aligned} \quad \text{and} \quad \begin{aligned} \mathcal{S}_4 &= \mathcal{S}_5 = \mathcal{S}_{Es} \\ \mathcal{D}_4 &= -\mathcal{D}_5 = \mathcal{D}_{Es} \; , \end{aligned} \tag{82}$$

the eight functions $\mathcal{S}_i$ and $\mathcal{D}_j$ for $2 \le i \le 5$ are equivalent to only four independent functions $\mathcal{S}_{Bs}$, $\mathcal{D}_{Bs}$, $\mathcal{S}_{Es}$ and $\mathcal{D}_{Es}$, which are in turn equivalent to the four functions F_i for $2 \le i \le 5$).

2. A multiplicative factor of $(-)^k$ is associated with every occurrence of $\overline{x}_k$; and similarly, a factor $(-)^\ell$ for every occurrence of $\overline{x}_\ell$.

3. The ratio $\epsilon_i = \mathcal{D}_i/\mathcal{S}_i$ defined by eq. 27 is very small unless there is non-negligeable experiment aging.

4. During ground data processing it is generally necessary (see section 9.2) to calculate ϕ in order to derive the cross-spectral matrix in physical units.

5. Putting $\phi' = \phi$ to derive equation 77 has for consequence that the equations of this appendix cannot be applied to observations obtained when the spin is OFF.

6. They can, however, be used for a vanishingly short integration period (see below, eq. **??**); in this particular case the result is the same as with despin OFF.

7. When this is done, all terms involving $(-)^k$ and $(-)^\ell$ disappear. *On November 25, 2004, this still needs to be checked.*

A.1 The Integrated Cross-Spectral Matrix

Let us assume that during the time interval required to accumulate one cross-spectral matrix, the spacecraft rotates so that ϕ varies in the range of eq. 21

$$\phi_1 \leq \phi \ < \phi_2 \ .$$

The experiment uses the value of ϕ which it computes (aboard the spacecraft) from the Sun Reference Pulse (see section 4.2); $\phi = 0$ coincides with the SRP. (See also section 9.2.)

The values of the cross-spectral matrix elements derived by the digital spectrum analyser are obtained by assuming that during the integration period the signal in the ambient plasma is statistically homogeneous, and that the AGC level does not fluctuate appreciably; this assumption is reasonable because:

- for any component, variations on a time-scale shorter than the telemetry read-out rate cannot be handled in any case, and
- for the spin-plane components, the receivers AGCs are strapped together in pairs, so that the AGC varies very little with changing spin phase.

Averaging $\overline{X}_i\overline{X}_j^*$ as given by eqs. 80 and 81 over the range of ϕ of eq. 21, we obtain the mean value $< \overline{X}_i\overline{X}_j^* >$: (*Label* **X1Xi**) (*Label* **XiXj**)

$$< \overline{X}_1\overline{X}_i^* > \ = \ \mathcal{S}_1\mathcal{S}_i^* \ < \overline{x}_1\overline{x}_i^* > \ + \mathcal{S}_1\mathcal{D}_i^* \Big[\, m_{2c} < \overline{x}_1\overline{x}_i^* > - \, (-)^k \, m_{2s} < \overline{x}_1\overline{x}_k^* > \Big] \qquad (83)$$

$$\begin{aligned} < \overline{X}_i\overline{X}_j^* > \ &= \ \mathcal{S}_i\mathcal{S}_j^* \ < \overline{x}_i\overline{x}_j^* > \ + \frac{1}{2} \, \mathcal{D}_i\mathcal{D}_j^* \Big[< \overline{x}_i\overline{x}_j^* > + (-)^{(k+\ell)} < \overline{x}_k\overline{x}_\ell^* > \Big] \\ &+ \ m_{2c} \Big(\mathcal{S}_i\mathcal{D}_j^* + \mathcal{D}_i\mathcal{S}_j^* \Big) < \overline{x}_i\overline{x}_j^* > \\ &- \ m_{2s} \Big((-)^\ell \mathcal{S}_i\mathcal{D}_j^* \ < \overline{x}_i\overline{x}_\ell^* > + (-)^k \mathcal{D}_i\mathcal{S}_j^* \ < \overline{x}_k\overline{x}_j^* > \Big) \\ &+ \ m_{4c} \, \frac{1}{2} \, \mathcal{D}_i\mathcal{D}_j^* \Big(< \overline{x}_i\overline{x}_j^* > - \, (-)^{(k+\ell)} < \overline{x}_k\overline{x}_\ell^* > \Big) \\ &- \ m_{4s} \, \frac{1}{2} \, \mathcal{D}_i\mathcal{D}_j^* \Big((-)^\ell < \overline{x}_i\overline{x}_\ell^* > + (-)^k < \overline{x}_k\overline{x}_j^* > \Big) \end{aligned} \qquad (84)$$

where (*Label* **mcs**)

$$\left.\begin{array}{rcccccl} m_{2c} & = & \frac{1}{\phi_2-\phi_1}\int_{\phi_1}^{\phi_2}\cos 2\phi\; d\phi & = & \frac{1}{2}\frac{\sin 2\phi_2-\sin 2\phi_1}{\phi_2-\phi_1} & = & \cos 2\varphi\,\mathrm{sinc}\,\delta\phi \\ m_{2s} & = & \frac{1}{\phi_2-\phi_1}\int_{\phi_1}^{\phi_2}\sin 2\phi\; d\phi & = & -\frac{1}{2}\frac{\cos 2\phi_2-\cos 2\phi_1}{\phi_2-\phi_1} & = & \sin 2\varphi\,\mathrm{sinc}\,\delta\phi \\ m_{4c} & = & \frac{1}{\phi_2-\phi_1}\int_{\phi_1}^{\phi_2}\cos 4\phi\; d\phi & = & \frac{1}{4}\frac{\sin 4\phi_2-\sin 4\phi_1}{\phi_2-\phi_1} & = & \cos 4\varphi\,\mathrm{sinc}\,2\delta\phi \\ m_{4s} & = & \frac{1}{\phi_2-\phi_1}\int_{\phi_1}^{\phi_2}\sin 4\phi\; d\phi & = & -\frac{1}{4}\frac{\cos 4\phi_2-\cos 4\phi_1}{\phi_2-\phi_1} & = & \sin 4\varphi\,\mathrm{sinc}\,2\delta\phi\;, \end{array}\right\} \tag{85}$$

where (eq. 43)

$$\varphi = \frac{\phi_2+\phi_1}{2} \qquad \text{and} \qquad \delta\phi = \phi_2-\phi_1 \tag{86}$$

and the function $\mathrm{sinc}\,x$ is defined by (*Label* **defsinc**)

$$\mathrm{sinc}\,x \;=\; \frac{\sin x}{x}\;.[16] \tag{87}$$

Note that (*Label* **mcs1**)

$$\lim_{\phi_2\to\phi_1}\mathrm{sinc}\,\phi = 1-\frac{\phi^2}{6}+\mathcal{O}(\phi^4) \qquad \text{and} \qquad \lim_{\phi_2\to\phi_1+n\pi}\mathrm{sinc}\,\phi = 0[4] \tag{88}$$

so that (*Label* **mcs0**)

$$\left.\begin{array}{lll} m_{2c}=m_{2s}=0 & \text{when} & \phi_2-\phi_1=n\pi\;, \\ m_{4c}=m_{4s}=0 & \text{when} & \phi_2-\phi_1=n\pi/2\;. \end{array}\right\} \tag{89}$$

Different methods of performing the averaging required to obtain the mean value $<\overline{X}_i\overline{X}_j^*>$ are employed in bands A and B, and in band C (see Fig. 5); this has no impact upon the validity of eqs. 83 and 84. But, for the receivers of band A, the spacecraft spins through an appreciable angle during the determination of a single elementary cross-spectral estimate, and the present equations are not strictly valid. Nevertheless, nothing better is available is the absence of waveform data. *This point was discussed in April 1993 by Bob Manning and Chris Harvey in an exchange of e-mail, which could usefully be summarised here.*

Each equation represented by the general expressions 83 and 84 involves two (F_i and F_m), three (F_1, F_i and F_k), or four (F_i, F_j, F_k and F_ℓ transfer functions. We note that:

1. Eqs. 85 and 88 show that the m_x functions satisfy $-1 \le m_x \le +1$.

2. In the special case of the integration period equal to an integral number of half spin periods, the m functions are zero (eq. 89) and the only contributions come from the first line of eq. 84 (and each of equations **??** through **??**).

3. As already mentioned, the difference functions $\mathcal{D}_i$ are expected to be small with respect to the mean values $\mathcal{S}_i$; then products of the type $\mathcal{S}_i\mathcal{D}_j$ are first order small quantities (with respect to $\mathcal{S}_i\mathcal{S}_j$), and the products of the type $\mathcal{D}_i\mathcal{D}_j$ are second order small quantities.

Eqs. 83 and 84 show that $\overline{X}_i\overline{X}_j^*$ is Hermitian. For every term in eq. 81, the interchange of i and j (and the corresponding interchange of m and n) yields the complex conjugate. This is evident for the first and fourth lines of eq. 84, but less obvious for the other lines; it may be verfied more easily using eqs. **??** through **??** below. Eq. 78 may be used to demonstrate the same behavior for the elements $\overline{X}_1\overline{X}_i^*$. Therefore$\overline{X}_i\overline{X}_j^*$ is Hermitian.

The relation between the matrices $< \overline{X}_i \overline{X}_j^* >$ and $< \overline{x}_i \overline{x}_j^* >$ is not linear: it cannot be represented by a matrix equation. From a formal point of view this considerably complicates the inversion of eqs. 83 ans 84. However, examination of the individual elements of these equations shows (section **??** below) that the equations can, in principle, be inverted by treating different groups of elements separately, as discussed in section 9.4.

A.2 Dimensionless Variables

In view of

- the complexity of the exact inversion eqs. 83 and 84;
- the fact that most of the terms in are very small, and
- some are exactly zero in important experiment operational modes,

it is interesting to approximate the solution by an expansion in terms of the small parameters $\epsilon_i = \mathcal{D}_i/\mathcal{S}_i$ defined by eq. 27. For this, we rewrite eqs. 83 and 84 in terms of ϵ_i, which yields eq. 25:

$$< \overline{X}_i \overline{X}_j^* >= \mathcal{S}_i \mathcal{S}_j^* \left(< \overline{x}_i \overline{x}_j^* > \ + \Delta_{ij} \right)$$

where

$$\begin{aligned}
\Delta_{ij} &= \frac{1}{2}\,\epsilon_i \epsilon_j^* \left[< \overline{x}_i \overline{x}_j^* > + (-)^{(k+\ell)} < \overline{x}_k \overline{x}_\ell^* > \right] \\
&+ m_{2c} \left(\epsilon_j^* + \epsilon_i \right) < \overline{x}_i \overline{x}_j^* > \\
&- m_{2s} \left((-)^\ell \epsilon_j^* \ < \overline{x}_i \overline{x}_\ell^* > + (-)^k \epsilon_i \ < \overline{x}_k \overline{x}_j^* > \right) \\
&+ m_{4c}\,\frac{1}{2}\,\epsilon_i \epsilon_j^* \left(< \overline{x}_i \overline{x}_j^* > - (-)^{(k+\ell)} < \overline{x}_k \overline{x}_\ell^* > \right) \\
&- m_{4s}\,\frac{1}{2}\,\epsilon_i \epsilon_j^* \left((-)^\ell < \overline{x}_i \overline{x}_\ell^* > + (-)^k < \overline{x}_k \overline{x}_j^* > \right)
\end{aligned} \tag{90}$$

This is the equation 26, which is fundamental to the calibration model (see pages 27, 18, 28, 28, 31, 31, 31, 34, 36, 37, 40, 41, 41). [2]

B The Computation of Δ_{ij}

(*Label* **CDelta**)

In this appendix we list all the equatons required to compute Δ, ordered in such a way that, following the logic of section 7.2, it is easy to select the terms required as a function of:

- the order (in ϵ) of the correction;
- the period of integration (terms often average to zero);
- the logical instrument (diagonal, non-diagonal, magnetic, electric.

In these equations, φ and $\delta\phi$ are the mean value and the range of variation of the spin phase during the period of integration, given by eq. 43,

$$\varphi = \frac{\phi_2 + \phi_1}{2} \qquad \text{and} \qquad \delta\phi = \phi_2 - \phi_1 \ ,$$

and ϵ is defined by eq. 27

$$\epsilon_{Bs} = \mathcal{D}_{Bs}/\mathcal{S}_{Bs} \qquad\qquad \epsilon_{Es} = \mathcal{D}_{Es}/\mathcal{S}_{Es} \ .$$

1 – First order terms which disappear for $\delta\phi = n\pi$

1.1 – Diagonal elements

1.1.1 *Magnetic*

$$\Delta_{11} = 0$$

$$\Delta_{22} = +\left[(\epsilon^*_{Bs}+\epsilon_{Bs}) < \overline{x}_2\overline{x}^*_2 > \cos 2\varphi + (\epsilon^*_{Bs} < \overline{x}_2\overline{x}^*_3 > +\epsilon_{Bs} < \overline{x}_3\overline{x}^*_2 >) \sin 2\varphi\right] \mathrm{sinc}\, \delta\phi$$
$$\Delta_{33} = +\left[(\epsilon^*_{Bs}+\epsilon_{Bs}) < \overline{x}_3\overline{x}^*_3 > \cos 2\varphi - (\epsilon^*_{Bs} < \overline{x}_3\overline{x}^*_2 > +\epsilon_{Bs} < \overline{x}_2\overline{x}^*_3 >) \sin 2\varphi\right] \mathrm{sinc}\, \delta\phi$$

1.1.2 *Electric*

$$\Delta_{44} = +\left[(\epsilon^*_{Es}+\epsilon_{Es}) < \overline{x}_4\overline{x}^*_4 > \cos 2\varphi + (\epsilon^*_{Bs} < \overline{x}_4\overline{x}^*_5 > +\epsilon_{Bs} < \overline{x}_5\overline{x}^*_4 >) \sin 2\varphi\right] \mathrm{sinc}\, \delta\phi$$
$$\Delta_{55} = +\left[(\epsilon^*_{Es}+\epsilon_{Es}) < \overline{x}_5\overline{x}^*_5 > \cos 2\varphi - (\epsilon^*_{Bs} < \overline{x}_5\overline{x}^*_4 > +\epsilon_{Bs} < \overline{x}_4\overline{x}^*_5 >) \sin 2\varphi\right] \mathrm{sinc}\, \delta\phi$$

1.2 – Off-diagonal elements

1.2.1 *Magnetic*

$$\Delta_{12} = +\epsilon^*_{Bs}\left[< \overline{x}_1\overline{x}^*_2 > \cos 2\varphi + < \overline{x}_1\overline{x}^*_3 > \sin 2\varphi\right] \mathrm{sinc}\, \delta\phi$$
$$\Delta_{13} = -\epsilon^*_{Bs}\left[< \overline{x}_1\overline{x}^*_3 > \cos 2\varphi - < \overline{x}_1\overline{x}^*_2 > \sin 2\varphi\right] \mathrm{sinc}\, \delta\phi$$
$$\Delta_{23} = \left[(\epsilon_{Bs}-\epsilon^*_{Bs}) < \overline{x}_2\overline{x}^*_3 > \cos 2\varphi + (\epsilon^*_{Bs} < \overline{x}_2\overline{x}^*_2 > + \epsilon_{Bs} < \overline{x}_3\overline{x}^*_3 >) \sin 2\varphi\right] \mathrm{sinc}\, \delta\phi$$

1.2.2 *Electric*

$$\Delta_{45} = \left[(\epsilon_{Es}-\epsilon^*_{Es}) < \overline{x}_4\overline{x}^*_5 > \cos 2\varphi + (\epsilon^*_{Es} < \overline{x}_4\overline{x}^*_4 > + \epsilon_{Es} < \overline{x}_5\overline{x}^*_5 >) \sin 2\varphi\right] \mathrm{sinc}\, \delta\phi$$

1.2.3 *Electromagnetic*

$$\Delta_{14} = +\epsilon^*_{Es}\left[< \overline{x}_1\overline{x}^*_4 > \cos 2\varphi + < \overline{x}_1\overline{x}^*_5 > \sin 2\varphi\right] \mathrm{sinc}\, \delta\phi$$
$$\Delta_{15} = -\epsilon^*_{Es}\left[< \overline{x}_1\overline{x}^*_5 > \cos 2\varphi - < \overline{x}_1\overline{x}^*_4 > \sin 2\varphi\right] \mathrm{sinc}\, \delta\phi$$
$$\Delta_{24} = +\left[(\epsilon^*_{Es}+\epsilon_{Bs}) < \overline{x}_2\overline{x}^*_4 > \cos 2\varphi + (\epsilon^*_{Es} < \overline{x}_2\overline{x}^*_5 > +\epsilon_{Bs} < \overline{x}_3\overline{x}^*_4 >) \sin 2\varphi\right] \mathrm{sinc}\, \delta\phi$$
$$\Delta_{25} = -\left[(\epsilon^*_{Es}-\epsilon_{Bs}) < \overline{x}_2\overline{x}^*_5 > \cos 2\varphi + (\epsilon^*_{Es} < \overline{x}_2\overline{x}^*_4 > +\epsilon_{Bs} < \overline{x}_3\overline{x}^*_5 >) \sin 2\varphi\right] \mathrm{sinc}\, \delta\phi$$
$$\Delta_{34} = +\left[(\epsilon^*_{Es}-\epsilon_{Bs}) < \overline{x}_3\overline{x}^*_4 > \cos 2\varphi + (\epsilon^*_{Es} < \overline{x}_3\overline{x}^*_5 > +\epsilon_{Bs} < \overline{x}_2\overline{x}^*_4 >) \sin 2\varphi\right] \mathrm{sinc}\, \delta\phi$$
$$\Delta_{35} = -\left[(\epsilon^*_{Es}+\epsilon_{Bs}) < \overline{x}_3\overline{x}^*_5 > \cos 2\varphi + (\epsilon^*_{Es} < \overline{x}_3\overline{x}^*_4 > +\epsilon_{Bs} < \overline{x}_2\overline{x}^*_5 >) \sin 2\varphi\right] \mathrm{sinc}\, \delta\phi$$

2 – Second order terms independent of spin phase

2.1 – Diagonal elements

2.1.1 *Magnetic*

$$\Delta_{11} = 0$$
$$\Delta_{22} = \frac{1}{2}\,\epsilon_{Bs}\epsilon^*_{Bs}\left[< \overline{x}_2\overline{x}^*_2 > + < \overline{x}_3\overline{x}^*_3 >\right]$$
$$\Delta_{33} = \frac{1}{2}\,\epsilon_{Bs}\epsilon^*_{Bs}\left[< \overline{x}_3\overline{x}^*_3 > + < \overline{x}_2\overline{x}^*_2 >\right]$$

2.1.2 *Electric*

$$\Delta_{44} = \frac{1}{2}\,\epsilon_{Es}\epsilon^*_{Es}\,[<\overline{x}_4\overline{x}^*_4> + <\overline{x}_5\overline{x}^*_5>]$$
$$\Delta_{55} = \frac{1}{2}\,\epsilon_{Es}\epsilon^*_{Es}\,[<\overline{x}_5\overline{x}^*_5> + <\overline{x}_4\overline{x}^*_4>]$$

2.2 – Off-diagonal elements

2.2.1 *Magnetic*

$$\Delta_{12} = \Delta_{13} = 0$$
$$\Delta_{23} = -\frac{1}{2}\,\epsilon_{Bs}\epsilon^*_{Bs}\,[<\overline{x}_2\overline{x}^*_3> - <\overline{x}_3\overline{x}^*_2>]$$

2.2.2 *Electric*

$$\Delta_{45} = -\frac{1}{2}\,\epsilon_{Es}\epsilon^*_{Es}\,[<\overline{x}_4\overline{x}^*_5> - <\overline{x}_5\overline{x}^*_4>]$$

2.2.3 *Electromagnetic*

$$\Delta_{14} = \Delta_{15} = 0$$
$$\Delta_{24} = +\frac{1}{2}\,\epsilon_{Bs}\epsilon^*_{Es}\,[<\overline{x}_2\overline{x}^*_4> + <\overline{x}_3\overline{x}^*_5>]$$
$$\Delta_{25} = -\frac{1}{2}\,\epsilon_{Bs}\epsilon^*_{Es}\,[<\overline{x}_2\overline{x}^*_5> - <\overline{x}_3\overline{x}^*_4>]$$
$$\Delta_{34} = -\frac{1}{2}\,\epsilon_{Bs}\epsilon^*_{Es}\,[<\overline{x}_3\overline{x}^*_4> - <\overline{x}_2\overline{x}^*_5>]$$
$$\Delta_{35} = +\frac{1}{2}\,\epsilon_{Bs}\epsilon^*_{Es}\,[<\overline{x}_3\overline{x}^*_5> + <\overline{x}_2\overline{x}^*_4>]$$

3 – Second order terms which disappear for $\delta\phi = n\pi/2$

3.1 – Diagonal elements

3.1.1 *Magnetic*

$$\Delta_{11} = 0$$
$$\Delta_{22} = \frac{1}{2}\,\epsilon_{Bs}\epsilon^*_{Bs}\,[(<\overline{x}_2\overline{x}^*_2> - <\overline{x}_3\overline{x}^*_3>)\cos 4\varphi + (<\overline{x}_2\overline{x}^*_3> + <\overline{x}_3\overline{x}^*_2>)\sin 4\varphi]\,\mathrm{sinc}\,2\delta\phi$$
$$\Delta_{33} = \frac{1}{2}\,\epsilon_{Bs}\epsilon^*_{Bs}\,[(<\overline{x}_3\overline{x}^*_3> - <\overline{x}_2\overline{x}^*_2>)\cos 4\varphi - (<\overline{x}_3\overline{x}^*_2> + <\overline{x}_2\overline{x}^*_3>)\sin 4\varphi]\,\mathrm{sinc}\,2\delta\phi$$

3.1.2 *Electric*

$$\Delta_{44} = \frac{1}{2}\,\epsilon_{Es}\epsilon^*_{Es}\,[(<\overline{x}_4\overline{x}^*_4> - <\overline{x}_5\overline{x}^*_5>)\cos 4\varphi + (<\overline{x}_4\overline{x}^*_5> + <\overline{x}_5\overline{x}^*_4>)\sin 4\varphi]\,\mathrm{sinc}\,2\delta\phi$$

$$\Delta_{55} = \frac{1}{2}\,\epsilon_{Es}\epsilon^*_{Es}\,[(<\overline{x}_5\overline{x}^*_5> - <\overline{x}_4\overline{x}^*_4>)\cos 4\varphi - (<\overline{x}_5\overline{x}^*_4> + <\overline{x}_4\overline{x}^*_5>)\sin 4\varphi]\,\mathrm{sinc}\,2\delta\phi$$

3.2 – Off-diagonal elements

3.2.1 *Magnetic*

$$\Delta_{12} = \Delta_{13} = 0$$

$$\Delta_{23} = -\frac{1}{2}\,\epsilon_{Bs}\epsilon^*_{Bs}\,[(<\overline{x}_2\overline{x}^*_3> + <\overline{x}_3\overline{x}^*_2>)\cos 4\varphi + (<\overline{x}_2\overline{x}^*_2> - <\overline{x}_3\overline{x}^*_3>)\sin 4\varphi]\,\mathrm{sinc}\,2\delta\phi$$

3.2.2 *Electric*

$$\Delta_{45} = -\frac{1}{2}\,\epsilon_{Es}\epsilon^*_{Es}\,[(<\overline{x}_4\overline{x}^*_5> + <\overline{x}_5\overline{x}^*_4>)\cos 4\varphi + (<\overline{x}_4\overline{x}^*_4> - <\overline{x}_5\overline{x}^*_5>)\sin 4\varphi]\,\mathrm{sinc}\,2\delta\phi$$

3.2.3 *Electromagnetic*

$$\Delta_{14} = \Delta_{15} = 0$$

$$\Delta_{24} = +\frac{1}{2}\,\epsilon_{Bs}\epsilon^*_{Es}\,[(<\overline{x}_2\overline{x}^*_4> - <\overline{x}_3\overline{x}^*_5>)\cos 4\varphi + (<\overline{x}_2\overline{x}^*_5> + <\overline{x}_3\overline{x}^*_4>)\sin 4\varphi]\,\mathrm{sinc}\,2\delta\phi$$

$$\Delta_{25} = -\frac{1}{2}\,\epsilon_{Bs}\epsilon^*_{Es}\,[(<\overline{x}_2\overline{x}^*_5> + <\overline{x}_3\overline{x}^*_4>)\cos 4\varphi - (<\overline{x}_2\overline{x}^*_4> - <\overline{x}_3\overline{x}^*_5>)\sin 4\varphi]\,\mathrm{sinc}\,2\delta\phi$$

$$\Delta_{34} = -\frac{1}{2}\,\epsilon_{Bs}\epsilon^*_{Es}\,[(<\overline{x}_3\overline{x}^*_4> + <\overline{x}_2\overline{x}^*_5>)\cos 4\varphi + (<\overline{x}_3\overline{x}^*_5> - <\overline{x}_2\overline{x}^*_4>)\sin 4\varphi]\,\mathrm{sinc}\,2\delta\phi$$

$$\Delta_{35} = +\frac{1}{2}\,\epsilon_{Bs}\epsilon^*_{Es}\,[(<\overline{x}_3\overline{x}^*_5> - <\overline{x}_2\overline{x}^*_4>)\cos 4\varphi - (<\overline{x}_3\overline{x}^*_4> + <\overline{x}_2\overline{x}^*_5>)\sin 4\varphi]\,\mathrm{sinc}\,2\delta\phi$$

C The Exact Solution

To obtain $< x_i x_j^* >$ in terms of $< X_i X_j^* >$, equations 25 and 26 must be inverted. The equations of the preceding section show that this can be performed by taking the elements in small groups, as follows.

Spin-plane Magnetic Field

Consider the simplest field components, spin-plane magnetic field components, which involve only two analogue receivers. Eqs. 25, 26 and 27 may be written

$$\begin{pmatrix} < X_2 X_2^* > \\ < X_2 X_3^* > \\ < X_3 X_2^* > \\ < X_3 X_3^* > \end{pmatrix} = |\mathcal{S}_{Bs}|^2 \times (\mathbf{I} + \mathbf{M}) \times \begin{pmatrix} < x_2 x_2^* > \\ < x_2 x_3^* > \\ < x_3 x_2^* > \\ < x_3 x_3^* > \end{pmatrix} \tag{91}$$

where $\mathbf{M}$ contains contributions from the equations of Sections C.1.1.1, C.1.2.1, C.2.1.1, and C.2.2.1, C.3.1.1 and C.3.2.1, which may be grouped as follows :

$$\mathbf{M} = \mathbf{M}_0 + \mathbf{M}_{2c} \cos 2\varphi + \mathbf{M}_{2s} \sin 2\varphi + \mathbf{M}_{4c} \cos 4\varphi + \mathbf{M}_{4s} \sin 4\varphi \tag{92}$$

this equation, hurriedly typed on June 7 1998, needs to be checked where [8]

$$\mathbf{M}_0 = \frac{1}{2} |\epsilon_{Bs}|^2 \begin{pmatrix} 1 & 0 & 0 & 1 \\ 0 & -1 & +1 & 0 \\ 0 & +1 & -1 & 0 \\ 1 & 0 & 0 & 1 \end{pmatrix} \tag{93}$$

$$\mathbf{M}_{2c} = (\epsilon_{Bs})^* + \epsilon_{Bs})^*) \begin{pmatrix} 1 & 0 & 0 & 0 \\ 0 & -1 & 0 & 0 \\ 0 & 0 & 1 & 0 \\ 0 & 0 & 0 & -1 \end{pmatrix} \tag{94}$$

$$\mathbf{M}_{2s} = \begin{pmatrix} 0 & +\epsilon Bs^* & +\epsilon_{Bs} & 0 \\ +\epsilon Bs^* & 0 & 0 & +\epsilon_{Bs} \\ -\epsilon_{Bs} & 0 & 0 & -\epsilon Bs^* \\ 0 & +\epsilon_{Bs} & +\epsilon Bs^* & 0 \end{pmatrix} \tag{95}$$

$$\mathbf{M}_{4c} = \frac{1}{2} |\epsilon_{Bs}|^2 \begin{pmatrix} +1 & 0 & 0 & -1 \\ 0 & -1 & -1 & 0 \\ 0 & -1 & -1 & 0 \\ -1 & 0 & 0 & +1 \end{pmatrix} \tag{96}$$

$$\mathbf{M}_{4s} = \frac{1}{2} |\epsilon_{Bs}|^2 \begin{pmatrix} 0 & +1 & +1 & 0 \\ +1 & 0 & 0 & -1 \\ -1 & 0 & 0 & +1 \\ 0 & -1 & -1 & 0 \end{pmatrix} \tag{97}$$

Eq. 91 can be solved by inverting the matrix $(\mathbf{I}+\mathbf{M})$. This is tedious and, computationally, it is a time-consuming operation; but it is not impossible.

Spin-plane Electric Field

The calculation of the spin-plane electric field matrix elements $< x_4 x_4^* >$, $< x_4 x_5^* >$, $< x_5 x_4^* >$, $< x_5 x_5^* >$ is handled in an exactly analogous manner.

Cross-correlations with the Axial Field

These are the elements of the first line (or, equivalently, the first column) of the matrix $< x_i x_j^* >$. Their determination involves three transfer functions. Nevertheless, once the diagonal elements have been determined as described above, it is easy to apply eq. **??** to compute these elements.

Magnetic/Electric Correlations in the Spin Plane

The only remaining matrix elements are $< x_2 x_4^* >$, $< x_2 x_5^* >$, $< x_3 x_4^* >$, $< x_3 x_5^* >$, and their complex conjugates. To determine these elements, eqs. **??** and **??** must be used.

D Comparison of Equations with those of Versions up to 3.0

(*Label* **SCSMo**)

The major change in Version 4 of this document is the replacement of the functions

$$G_2(A,f) = \frac{1}{H^n} Q_2(A) R_2(f) \quad \text{and} \quad G_3(A,f) = \frac{1}{H^n} Q_3(A) R_3(f) \tag{98}$$

by the functions of eq. 35, namely

$$\mathcal{S}_p(A,f) = \frac{1}{H^n} S_p(A) \tilde{S}_p(f) \quad \text{and} \quad \mathcal{D}_p(A,f) = \frac{1}{H^n} D_p(A) \tilde{D}_p(f) \tag{99}$$

Using eq. 23 we obtain, for example, for the spin-plane magnetic field,

$$\begin{aligned} S_{Bs}(A)\tilde{S}_{Bs}(f) &= \frac{1}{2}\left[Q_2(A)R_2(f) + Q_3(A)R_3(f)\right] , \\ D_{Bs}(A)\tilde{D}_{Bs}(f) &= \frac{1}{2}\left[Q_2(A)R_2(f) - Q_3(A)R_3(f)\right] . \end{aligned}$$

It is immediately clear that there is no exact relation between $S_{Bs}(A)$, $D_{Bs}(A)$ and $Q_2(A)$, $Q_3(A)$, or between $\tilde{S}_{Bs}(f)$, $\tilde{D}_{Bs}(f)$ and $R_2(f)$, $R_3(f)$; in general,

$$S_{Bs}(A) \neq \frac{1}{2}\left[Q_2(A) + Q_3(A)\right] , \qquad D_{Bs}(A) \neq \frac{1}{2}\left[Q_2(A) - Q_3(A)\right] , \tag{100}$$

$$\tilde{S}_{Bs}(f) \neq \frac{1}{2}\left[R_2(f) + R_3(f)\right] , \qquad \tilde{D}_{Bs}(f) \neq \frac{1}{2}\left[R_2(f) - R_3(f)\right] . \tag{101}$$

This is due to the fact that eqs. 99 are approximations to the true functions $\mathcal{S}(A,f)$ and $\mathcal{D}(A,f)$, just as eqs. 98 are approximations to $G_2(A,f)$ and $G_3(A,f)$. There is no reason to believe that eq. 98 is a better approximation than eq. 99, it is merely a different approximation. Note that eqs. 100 become true equalities if $R_2(f) = R_3(f)$, and that eqs. 101 become equalities if $Q_2(A) = Q_3(A)$. [28]

Finally, the equations used to derive the tables of new calibration coefficients from the old coefficients are:

$$\begin{array}{ll} S_{Bx}(A) = Q_1(A) & D_{Bx}(A) = \text{ n}'\text{existe pas} \\ \tilde{S}_{Bx}(f) = R_1(f) & \tilde{D}_{Bx}(f) = \text{ n}'\text{existe pas} \\ \\ S_{Bs}(A) = \frac{1}{2}\left[Q_2(A) + Q_3(A)\right] & D_{Bs}(A) = \frac{1}{2}\left[Q_2(A) - Q_3(A)\right] \\ \tilde{S}_{Bs}(f) = \frac{1}{2}\left[R_2(f) + R_3(f)\right] & \tilde{D}_{Bs}(f) = \frac{1}{2}\left[R_2(f) - R_3(f)\right] \\ \\ S_{Es}(A) = \frac{1}{2}\left[Q_4(A) + Q_5(A)\right] & D_{Es}(A) = \frac{1}{2}\left[Q_4(A) - Q_5(A)\right] \\ \tilde{S}_{Es}(f) = \frac{1}{2}\left[R_4(f) + R_5(f)\right] & \tilde{D}_{Es}(f) = \frac{1}{2}\left[R_4(f) - R_5(f)\right] \end{array}$$

We now compare the equations of section 41 with the equations as they were before introducing the functions $\mathcal{S}_i$ and $\mathcal{D}_i$ defined by eqs. 23: that is, in all versions up to and including May 1995. Table 7 shows the various symbols used in earlier versions of this report, and the corresponding symbols in the present version.

(*Label* **Table4**)

Previously equation 34 was

$$N_{ij}^n = (H^n)^2 \left[S_{ij} < \overline{x}_i \overline{x}_j^* > + S'_{ij} < \overline{x}_i^* \overline{x}_j > \right] \quad \text{(no sum over } i,j\text{)[5]}$$

New	Old	Defined	Represents	Determined	
unchanged	$B^n(f)$	sect. 5.1	Bandpass characteristic of channel n of the digital receiver.	not required	
unchanged	$F_i^m(f,A)$	eq. 20	The analogue transfer function for receiver i of band m.	eq. 9	
not used	$G_i^m(f,A)$	eq. **??**	$H^n \times F_i^m(f,A)$	see sect. 6	(c n
unchanged	H^n	eqs. 30	Integrated response of channel n of the digital analyser.	within R_i^{mn}	(c n
unchanged	$N_{ij}(p)$	51 or 52	Decompression algorithm for the output from the digital analyser.	n/a	
unchanged	P_i^{mn}	eq. 9	Variation of the analogue receiver transfer function with frequency.	within R_i^{mn}	nT
unchanged	$Q_i^m(A_i^m)$	eq. 9	Variation of the analogue receiver transfer function with AGC output.	sect. ref. 1009 of Appendix 1	nT
$\tilde{S}_p^m(f^n)$	R_i^{mn}	eq. **??**	$R_i^{mn} = H^n P_i^{mn}$ The total frequency-channel-dependent (*i.e.*, everything except the AGC) transfer function for channel i, frequency n, of band m, including the effects of the analogue receiver, the A/D converter, de-spin and the digital analyser.	sect. ref. 1003 of Appendix 1	(c
not used	S_{ij}	eq. 102	The relation between $< \overline{X}_i \overline{X}_j^* >$ and $< \overline{x}_i \overline{x}_j^* >$	sect. 41	
not used	T_{ij}	eq. **??**	Inverse of S_{ij}	eq. **??**	
unchanged	W^n	eq. 29	Equivalent bandwidth of channel n of the digital receiver.	not required	
unchanged	A	eq. 6	The AGC signal	n/a	TM
unchanged	$\overline{x}_i$	eq. 73	Analytic signal of field component i in the ambient medium.	n/a	nT
unchanged	x_i	eq. 20	Analytic signal as measured by the spinning sensor i.	n/a	nT
unchanged	X_i	eq. 20	Analytic signal from receiver i at the input to the despin algorithm.	n/a	nT
unchanged	$\overline{X}_i$	eq. 74	Analytic signal of field component i at the output of the despin algorithm.	n/a	nT
unchanged	$< \overline{x}_i \overline{x}_j^* >$	eq. 80	Mean cross-spectral matrix in the inertial frame of the ambient plasma	eq. **??**	nT
unchanged	$< \overline{X}_i \overline{X}_j^* >$	eq. 81	Mean cross-spectral matrix of the signal at the output from the despin algorithm.	sect. 9.1	nT
unchanged	N_{ij}	eq. 34	The digital analyser output (*i.e.*, the cross-correlation matrix) before logarithmic compression	sect. 9.1	c
unchanged	z_{ij}	eq. 32	The normalised cross-spectral matrix.	sect. 9.1.2	

N.B., for the E-field, replace the units nT by V/m

Counts are dimensionless. Nevertheless, the output from the spectrum analyser is always in $\left(\frac{\quad}{\quad}\right)^1$

The basic equation used in earlier versions (up to and including version 3) is the following equation which occurred in section 4.4: (*Label* **SCSM1**)

$$< \overline{X}_i \overline{X}_j^* > = \; S_{ij} \times < \overline{x}_i \overline{x}_j^* > \; + \; S'_{ij} \times < \overline{x}_i^* \overline{x}_j > \quad \text{(no sum over } i, j), \tag{102}$$

where the values of $S_{ij}(f, A)$ and $S'_{ij}(f, A)$ were expressed in terms of from one to four of the different functions $F_i(f, A)$. Eq. 102 has now been replaced by eq. 25:

$$< \overline{X}_i \overline{X}_j^* > = \mathcal{S}_i \mathcal{S}_j^* \left(< \overline{x}_i \overline{x}_j^* > \; + \Delta_{ij} \right)$$

The text needs to be checked from here ... In versions of this document prior to Issue 3, these equations where given as (*Label* **X1Xio**) (*Label* **XiXjo**)

$$< \overline{X}_1 \overline{X}_i^* > \;\; = \;\; < \overline{x}_1 \overline{x}_i^* > \; F_1 (F_i^* + F_m^*) \; / \; 2 \tag{103}$$

$$\begin{aligned} < \overline{X}_i \overline{X}_j^* > \;\; &= \;\; < \overline{x}_i \overline{x}_j^* > \Big(F_i F_n^* + F_m F_j^* + 3 (F_i F_j^* + F_m^* F_n) \Big) \; / \; 8 \\ &\pm \;\; < \overline{x}_m \overline{x}_n^* > \; (F_i - F_m)(F_j^* - F_n^*) \; / \; 8 \; , \end{aligned} \tag{104}$$

where (*Label* **sign**)

- the upper sign is to be used if X_j, like X_i, is parallel to $\theta = 0$, or
- the lower sign is to be used if X_j is orthogonal to the reference direction $\theta = 0$. (105)

These expressions are equivalent to the expressions **??** and **??**, except for the sign $\pm$ replacing $(-)^{i+j}$. The effect of this error appears in the equations corresponding (in earlier issues) to the actual eq. **??**; but since the calibration coefficients used until now have always had the difference functions $\mathcal{D}_i$ (eq. 23) identically equal to zero, the consequences of this error have not been apparent in any of the numerical tests. ..... *needs to be checked to here*

When the expressions 80 and 81 are averaged over a complete spin period, the relation between $< \overline{x}_i \overline{x}_j^* >$ and $< \overline{X}_i \overline{X}_j^* >$ becomes somewhat more simple. The following expressions are all derived in the Appendix, but we express the results in terms of the matrices S_{ij} and S'_{ij} defined by eq. 102. Throughout this section, m and n are given by eq. 22.

The different elements of the cross-spectral matrix must be treated separately; there are six different cases to consider:

1. S_{11}. Both channels are along the spin-axis. The equations are effectively unchanged, being previously (*Label* **11so**)

$$\left.\begin{aligned} S_{11} &= |F_1|^2 \\ S'_{11} &= 0. \end{aligned}\right\} \tag{106}$$

   This is entirely equivalent to eqs. 25 and **??**.

2. S_{1i} for $2 \leq i \leq 5$. x_i is along the spin-axis and and x_j is in the spin-plane. The previous expression (*Label* **1iso**)

$$\left.\begin{aligned} S_{1i} &= F_1 (F_i^* + F_m^*) \; / \; 2 \\ S'_{1i} &= 0. \end{aligned}\right\} \tag{107}$$

   is entirely equivalent to the expressions 25 and **??**.

3. S_{ii} for $2 \leq i \leq 5$. The diagonal elements from the spin-plane sensors. The expression obtained previously was (*Label* **iiso**)

$$\left.\begin{aligned} S_{ii} &= (F_i F_m^* + F_m F_i^* + 3(|F_i|^2 + |F_m|^2)) \; / \; 8 \\ S'_{ii} &= 0. \end{aligned}\right\} \tag{108}$$

   We note that the (second order small) contribution from $< x_m x_m^* >$ is new, whilst the contribution from $< x_i x_i^* >$ is unchanged.

4. S_{23} and S_{45}. x_i and x_j are both in the spin-plane and come from the same pair of sensors, that is, $|i-j| = 1$ and $i+j = 5$ or 9. In this case, the measured cross-spectral matrix is modulated both at twice and also at four times the spin frequency. Its value averaged over an integral number of half spin-periods is related to the "true" cross-spectral matrix by (*Label* **ijsameso**)

$$\left.\begin{array}{rcl} S_{ij} & = & \Big(|F_i|^2 + |F_j|^2 + 3(F_i F_j^* + F_i^* F_j)\Big) \ / \ 8 \\ S'_{ij} & = & \Big((F_i - F_j)(F_i^* - F_j^*)\Big) \ / \ 8 \ . \end{array}\right\} \tag{109}$$

5. S_{24} and S_{35}. x_i and x_j are parallel but originate from different pairs of spin-plane sensors ($|i-j| = 2$, with $i+j = 6$ or 8); (*Label* **ijparaso**)

$$\left.\begin{array}{rcl} S_{ij} & = & \Big(F_i F_n^* + F_m F_j^* + 3(F_i F_j^* + F_m F_n^*)\Big) \ / \ 8 \\ S'_{ij} & = & + \Big((F_i - F_m)(F_j^* - F_n^*)\Big) \ / \ 8 \ . \end{array}\right\} \tag{110}$$

6. S_{25} and S_{34}. x_i and x_j are orthogonal and originate from different pairs of spin-plane sensors ($i+j = 7$, with $|i-j| = 1$ or 3); (*Label* **ijdiffso**)

$$\left.\begin{array}{rcl} S_{ij} & = & \Big(F_i F_n^* + F_m F_j^* + 3(F_i F_j^* + F_m F_n^*)\Big) \ / \ 8 \\ S'_{ij} & = & - \Big((F_i - F_m)(F_j^* - F_n^*)\Big) \ / \ 8 \ . \end{array}\right\} \tag{111}$$

All the above expressions are obtained from equations **??** through **??** of the Appendix.

D.1 Data Acquired during one Quarter of a Spin Period

This case is complicated: the angular terms do not average to zero, so the spin phase enters into the resulting expressions.

D.2 Spacecraft not Spinning

This is the configuration which will be used during the calibration cycle to determine the transfer functions F_i. It is essential to disable the digital de-spin algorithm for both laboratory and inflight calibrations (for which the stimuli are applied in a frame at rest with respect to the spacecraft).

If we take the spacecraft orientation to have $\phi = 0$, then only the first term of eq. 80 and eq. 81 need to be taken into account, and the result is rather simple: (*Label* **SCSM2o**)

$$S_{ij} = |F_i|^2 \quad \text{and} \quad S'_{ij} = 0 \ . \tag{112}$$

Cross References to LaTeX named files

File	From Section	To Section
tn01sb	Title	Docstatus
tn01sc	Introduction	**??**
tn01sd	3	Discussion
tn01se	5	6.5
tn01sf	7	8.1
tn01sg	9	Determination of the Calibration Updates
tn01sh	Cross-References to Technical Note TN–0005	
tn01si	A	B
tn01sj	C	
tn01sk	D	Spacecraft not Spinning
tn01sl	Material which has been removed	

Equations not cited in this paper

The following is a list references which figure in Appendix A but are not cited in this Technical Note. Their inclusion here is merely to suppress needless (correct but confusing) LaTeX information messages.

This is the last page of the printed Technical Note ; it should be discarded.

1001.

1002.

1003.

1004.

1005.

1006.

1007.

1008.

1009.

1010.

1011.

1012.

1013.

1014.

1015.